UNIVERSITY OF SOUTHAMPTON

Faculty of Engineering, Science and Mathematics

School of Mathematics

Mathematical Modelling For a Non-invasive Method of Monitoring Intracranial Pressure

by

Jonathan Peter Moles

Submitted for the degree course of Doctor of Philosophy

December 2009

UNIVERSITY OF SOUTHAMPTON

ABSTRACT

Faculty of Engineering, Science and Mathematics

School of Mathematics

Doctor of Philosophy

Mathematical Modelling for a Non-invasive Method of Monitoring Intracranial Pressure

by Jonathan Peter Moles

The central focus of this work is the interpretation of Tympanic Membrane Displacement (TMD) data in order to infer behaviour of Intracranial Pressure (ICP). This is conducted by developing a mathematical model of the physiology, collecting experimental data and then conducting optimisation of the mathematical model using the experimental data.

Passive TMD techniques monitor volume displacements in the external ear canal; from these measurements information about Inner Ear Pressure (IEP) changes can be inferred. In many patients IEP is in communication with ICP and information about ICP can also be inferred from TMD measurements. However, the TMD waveform also contains contributions from other sources (respiration and cardiovascular waves) which must also be analysed.

To recreate the physical mechanisms affecting TMD measurements the mathematical modelling of TMD is broken into four main components: IEP driven by ICP, ABP, and two respiration related effects. The IEP component of the TMD model includes nonlinear mechanisms which are believed to be important in the communication between ICP and TMD.

This work shows that an accurate TMD model contains substantial contributions from three main sources: IEP driven by ICP (42.4%), ABP (20.1%), and the two respiration related components (37.5%).

Contents

List of Figures

List of Tables

Declaration Of Authorship

I, Jonathan Peter Moles, declare that the thesis entitled "Mathematical Modelling for a Non-invasive Method of Monitoring Intracranial Pressure" and the work presented in the thesis are both my own, and have been generated by me as the result of my own original research. I confirm that:

1. this work was done wholly or mainly while in candidature for a research degree at this University;
2. where any part of this thesis has previously been submitted for a degree or any other qualification at this University or any other institution, this has been clearly stated;
3. where I have consulted the published work of others, this is always clearly attributed;
4. where I have quoted from the work of others, the source is always given. With the exception of such quotations, this thesis is entirely my own work;
5. I have acknowledged all main sources of help;
6. where the thesis is based on work done by myself jointly with others, I have made clear exactly what was done by others and what I have contributed myself;
7. none of this work has been published before submission;

Signed: .....

Date: .....

Acknowledgements

I would like to make specific mention of a number of people to whom I am very grateful; without them, producing this thesis may never have been possible.

Firstly, my supervisor, Professor Colin Please (Applied Mathematics Group, School of Mathematics, University of Southampton, UK), who I wish to thank for the many hours of help and guidance he gave me throughout my research, and particularly in the preparation of my thesis. His patience was limitless and his comments were always constructive and clear. Thank you for your help.

My industrial partners, Dr Robert Marchbanks, (Marchbanks Measurement Systems Ltd, Lymington, UK) and Dr Anthony Birch (Department of Medical Physics & Bioengineering, Southampton General Hospital, Southampton, UK), who I hope both understand how grateful I am for their help throughout this project; as without their many contributions none of this research would have been possible.

I wish to thank the Neuro Intensive Care Unit team (Southampton General Hospital, Southampton, UK) for collaborating with our research group and aiding us in the recruitment of suitable patients for our data acquisition.

I am grateful to Dr F. H. Linthicum, Jr., M.D. (Head, Department of Histopathology Director, Temporal Bone Histopathology Lab, House Ear Institute, Los Angeles, U.S.A.) for providing the temporal bone slices which were analysed and the results of which strengthened the foundation of this work.

I am grateful to all the School of Mathematics staff for assisting me with the

administrative tasks necessary for completing my doctoral program: in particular Frances Hubbold.

I wish to thank all my friends and family for their kind support, patience and encouragement throughout my work; especially my parents Andrea and Peter, my loving partner Claire, and my close friends Alex Hamilton and Laura Ward.

Finally, I wish to acknowledge the direct and indirect financial support provided by the Engineering and Physical Science Research Council, Marchbanks Measurements Systems Ltd., Southampton University Hospitals NHS Trust and the University of Southampton, without this it would not have been possible for me to do this work.

Jonathan Moles

December, 2009.

Preface

Research Objective

This research is primarily concerned with forming and testing a mathematical model of a potential technique for non-surgically monitoring intracranial pressure (ICP, brain pressure). The technique measures movements of the ear drum, in terms of volume displacement, and is called passive tympanic membrane displacement (TMD) measurement; it is one of the transcranial and cerebral sonography (TCCS) techniques. This movement of the eardrum is thought to be caused by brain pressure waves entering the inner ear and acting on the mechanisms which normally allow a person to detect sound waves which enter the external ear canal. However, TMD measurements may not be driven solely by brain pressure waves, they may also be directly affected by cardiovascular and respiratory waves; investigation of these additional factors forms is a significant part of this research.

A sample of the data collected during this research project is presented as four plots of the normalised waveforms, these data streams were measured simultaneously from one intensive care patient. TMD, ICP, Arterial Blood Pressure (ABP) and respiration pressure (ventilator-driven airway pressure - VAP) are shown in figures 1 to 4 respectively.

The long-term goal of this research is to understand how TMD measurements are affected by ICP, arterial blood pressure and respiratory variations in order to infer

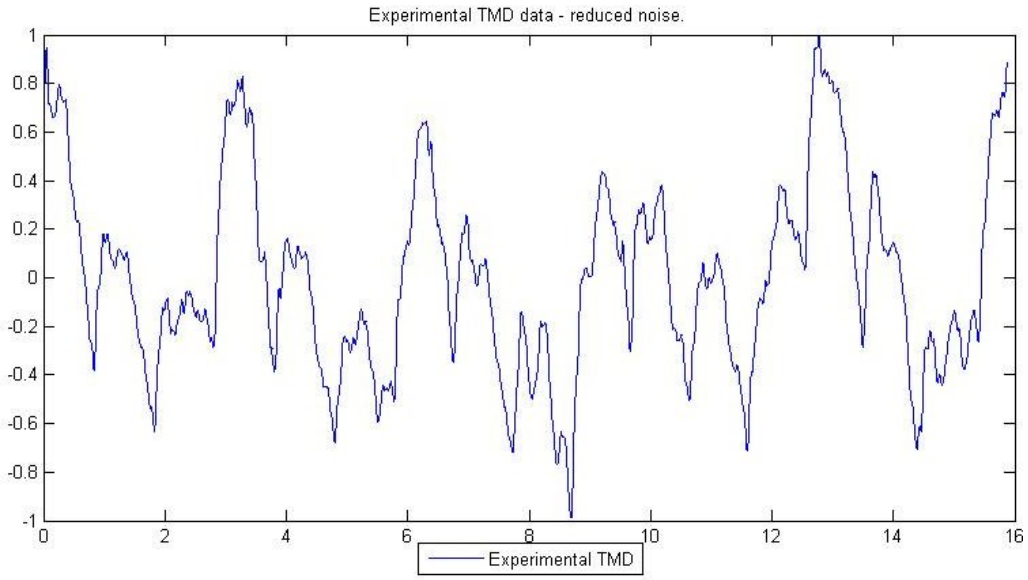

Figure 1: Normalised TMD data sample.(The horizontal scale is in seconds.)

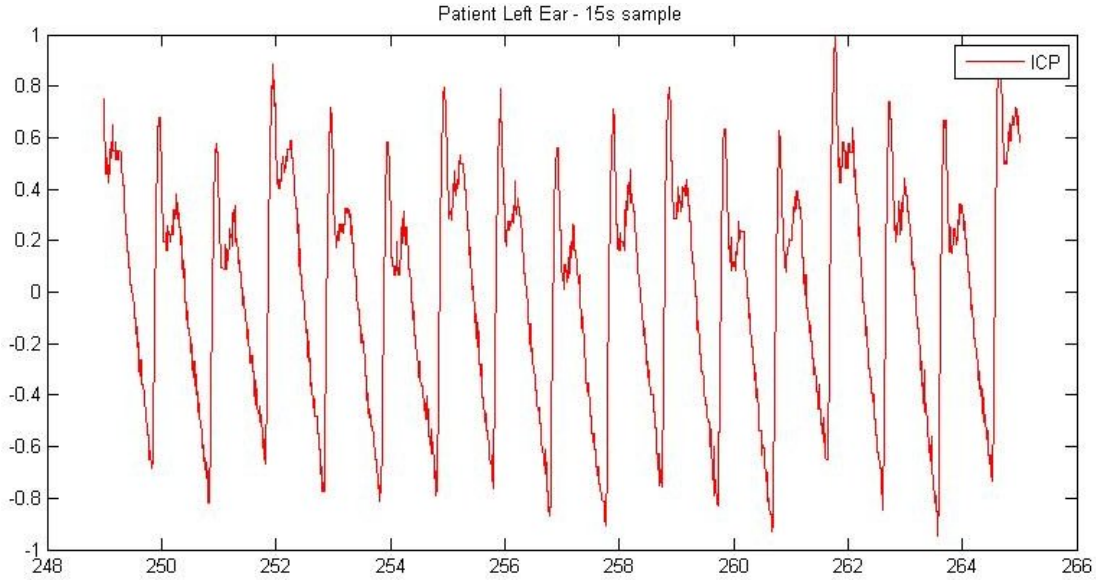

Figure 2: Normalised ICP data sample.(The horizontal scale is in seconds.)

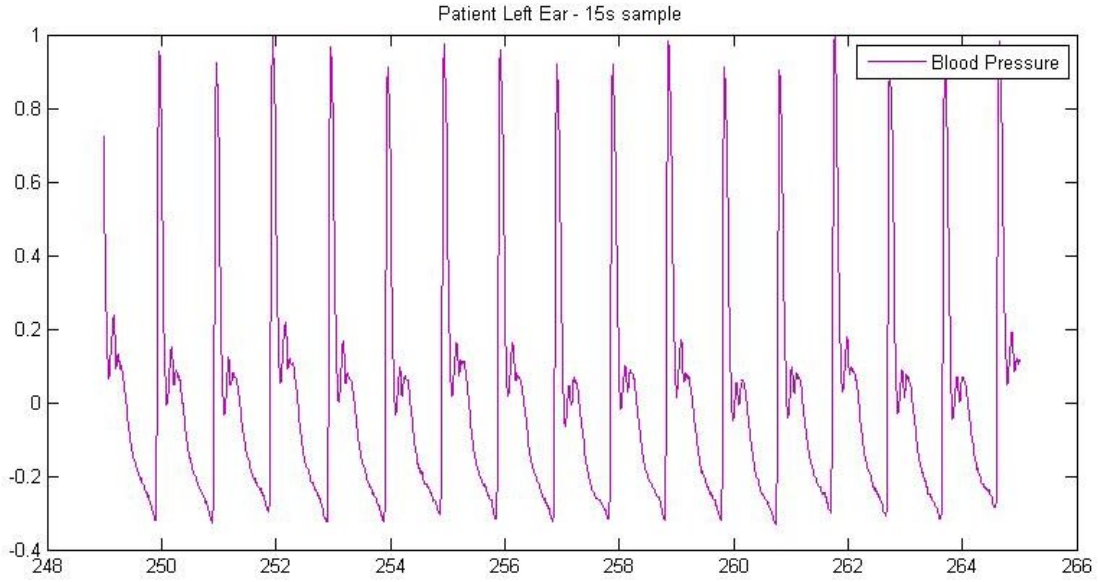

Figure 3: Normalised arterial blood pressure ABP data sample.
(The horizontal scale is in seconds.)

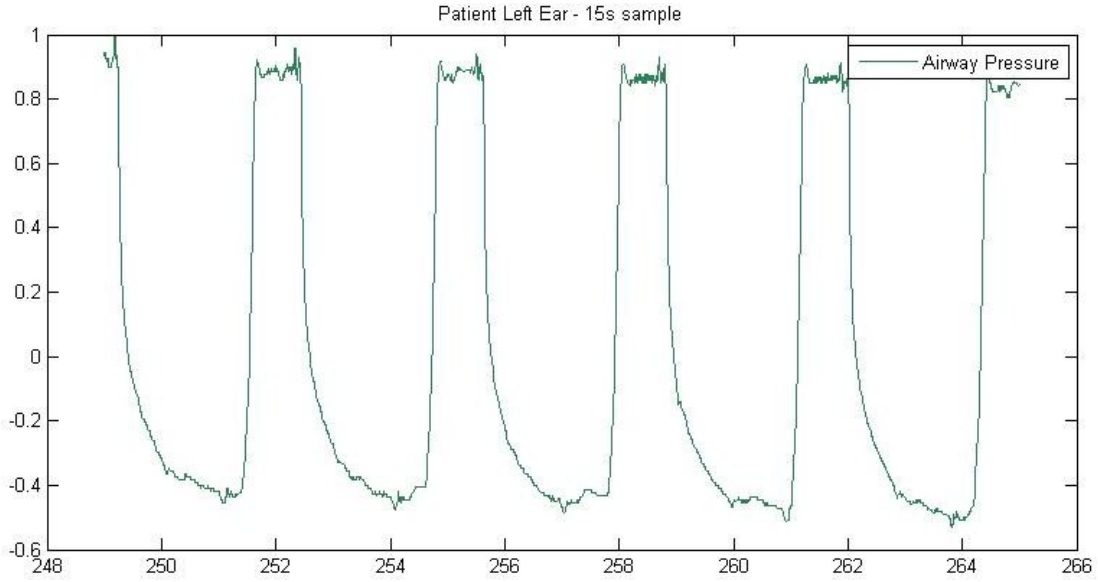

Figure 4: Normalised ventilator-driven airway pressure data sample.
(The horizontal scale is in seconds.)

the ICP from the TMD. From such understanding it is hoped that the non-invasive TMD technique can be used in situations where it is not appropriate to use an invasive ICP measurement to determine brain pressure.

Summary of Thesis

Below is a summary of the information contained within each chapter of this thesis; within these the chapters each aspect of the research process is explained.

Chapter 1 provides general introduction to the material on which this research is based; including a significant portion of the non-mathematical information required for this research. Within the chapter the motivation for the research is outlined, along with a summary of the anatomical information as considered within the context of this work, and an introduction to the family of TMD techniques; the passive TMD technique is used for experimental data acquisition in this study. The chapter finishes by providing evidence of possible nonlinear mechanisms that may affect the TMD techniques; the most likely of which are modelled in this work.

Chapter 2 presents the formulation of the mathematical model for passive TMD measurements. The physiological system generating TMD measurements is formed of a collection of complex biological components and within chapter 2 a model component is developed to represent the significant effects of each component and how they affect each other. The modelling is divided into different sections each dealing with a component, group of components or interfaces in the physical system before being drawn together to form the complete TMD model at the end of the chapter.

Chapter 3 analyses the complete TMD model and components of the model. Initially the system is non-dimensionalised and analytical solutions of special cases are considered. Then numerical approximations are established for all model components, such that the model can be driven by sample data and the output compared

to the appropriate sample TMD data.

Chapter 4 outlines the setup of the clinical research study and data acquisition process conducted as part of this reseach to produced the experimental data required for the TMD modelling process. This chapter includes summaries of work conducted by Dr A.A. Birch, Dr R.J. Marchbanks and myself, and my own work on the data preparation process required for the project.

Chapter 5 outlines the parameter estimation process. This involves fitting the complete TMD model to experimental TMD data using optimisation techniques. This is required because within the complete TMD model there are a number of parameters for which values are unknown for any specific patient and thus an optimisation process is required to estimate reasonable parameter values.

In chapter 6 the results of the parameter estimation process are presented. In order to aid in the understanding and interpretation of the results a short explanation of the waveforms used and produced in the modelling process, along with an informal "by eye" evaluation of their importance and relevance, is included. Many of the results were affected by noise on the TMD data signal and this is discussed here.

The final chapter, Conclusions, draws together the keys results of this research and discusses them. This discussion is broken into five sections - the first discusses conclusions relating to the complete model, followed by one section for each of the three main sources contributing to TMD and a final section discussing future work.

Chapter 1

Introduction

The first chapter of this thesis provides a general introduction to the material on which the research presented here is based. Because some of the information considered in this research is very subject specific, a substantial amount of anatomical information must be covered to fully understand the system being researched.

Much of the non-mathematical information required to understand this research is provided within this chapter and it is broken down in the following way. The first section is concerned with the motivation and long term goals of the research area as a whole. The second section provides a general introduction to some of the anatomy of the system being considered. The third section provides a brief account of the relevant historical steps taken in this subject area. The fourth section provides further information related to the anatomy and pressure-volume interactions of the fluid surrounding the brain. The fifth section introduces the techniques used in the experimental data acquisition process used within this study; specifically, the passive tympanic membrane displacement (tympanic membrane displacement (TMD)) technique which is the primary focus of all modelling in this work. The final section provides evidence of possible nonlinear mechanisms which may affect the techniques being used and modelled in this work.

1.1 Motivation

Within the skull cerebral spinal fluid (CSF) baths and supports the brain. It also provides basic mechanical and immunological protection for the brain "cushioning" it inside the skull [34]. The pressure of the CSF within the skull is called the intracranial pressure (ICP); ICP is carefully self-regulated because raised ICP is a life threatening condition. Headaches, vomiting, papilloedema and reduced levels of consciousness are all symptoms of increased levels of ICP, but these are non-specific symptoms which can make abnormal levels of ICP hard to diagnose. In many instances raised ICP, if untreated, will lead to lethal levels of brain damage [34]. Because of this ICP is an important factor when treating many brain injuries.

Monitoring ICP is not a straightforward procedure. It is possible to monitoring CSF pressure during lumbar puncture, but this method is of limited value for monitoring ICP as an isolated pressure reading does not indicate trend or detect pressure waves, additionally it is contraindicative in the presence of an intracranial mass - such as a brain tumour. Continuous monitoring via lumbar puncture is also possible, but is still an invasive procedure and carries similar risks to other invasive techniques which many clinicians consider to produce better results [38].

Other techniques use a pressure transducer placed progressively further into the brain. The meninges is the membrane which surrounds the central nervous system. It consists of three layers; the dura matter, the arachnoid matter, and the pia matter (see figure 1.1). When the pressure transducer is placed against the outer surface of the dura, the outermost layer of the meninges, it is referred to as epidural ICP monitoring. While when the transducer is placed inside the dura the resulting pressure measurement is called subdural ICP monitoring. In the cases where the pressure transducer is positioned within the arachnoid space it is referred to as subarachnoid ICP monitoring; and Parenchymal ICP monitoring occurs when all layers of the meninges are pierced and the pressure transducer placed within the brain tissue. However, the 'gold' standard by which other methods are compared

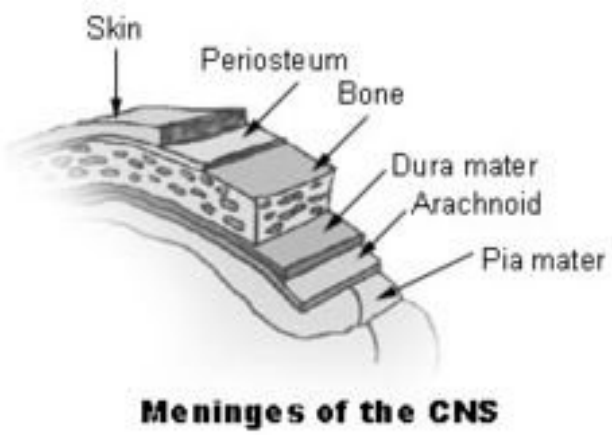

Figure 1.1: Schematic diagram of the meninges of the Central Nervous System (brain and spinal cord). Reproduced from [58].

is intraventricular ICP monitoring: this uses a pressure transducer tipped catheter placed in the lateral ventrical [34]. All these current ICP monitoring techniques are invasive and carry risks of infection and complications that are inherent in such procedures, particularly as they usually require a general anaesthetic.

There are at least 1.4 million traumatic brain injuries (TBI) in the United States each year. Of them, about 50,000 die, 235,000 are hospitalized, and 1.1 million are treated and released from Emergency departments [32]. Those who are treated and released from Emergency departments without being admitted are not suitable for invasive procedures and therefore have had no ICP measurements taken. Thus a non-invasive ICP measurements would be of particular use with this patient group as well as others.

Non-invasive measurements of ICP carry little to no risk of infection, and impose none of limitations on frequency or duration of monitoring normally associated with the current surgical procedures. If such methods can be reliably developed then their use could facilitate the earlier diagnosis of various diseases and improved clinical management for many patients. These benefits have motivated the

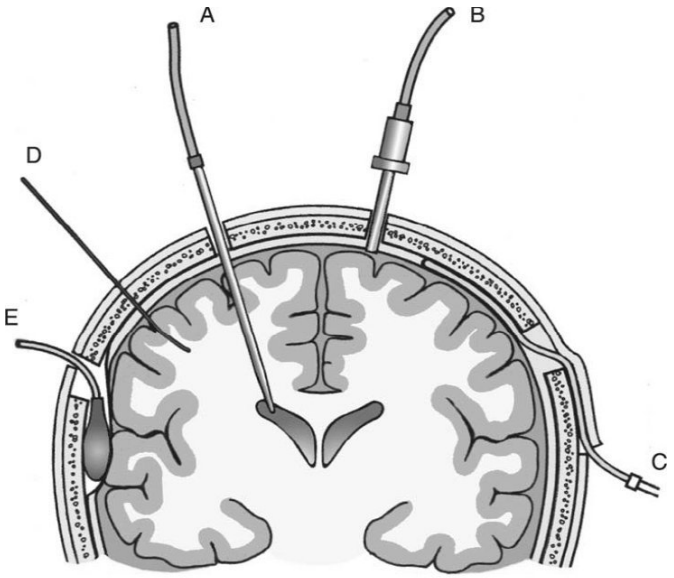

Figure 1.2: Location of pressure transducer placement for direct ICP monitoring: (A) Intraventricular, (B) Subarachnoid, (C) Subdural, (D) Parenchymal, and (E) Epidural. Reproduced from [41].

development and investigation of several non-invasive techniques. Most patented techniques use ultrasound to measure physiological properties such as the internal diameter of the cranium; intracranial or intraocular blood flow, the acoustic properties of the cranium, or pulsations of the cerebral ventricles. These techniques all have complexities, some of which are specific to each technique, but these will not be covered here as this work focuses on the family of Transcranial and Cerebral Sonography (TCCS) techniques. These techniques use tympanic membrane displacement (TMD) measurements to infer information about inner ear pressure (IEP) and are covered in more detail in section 1.5 of this chapter.

1.2 Anatomy of the Ear

This section provides a brief introduction to the general anatomy of the inner, middle, and outer ear. Only a general overview of the main anatomical components

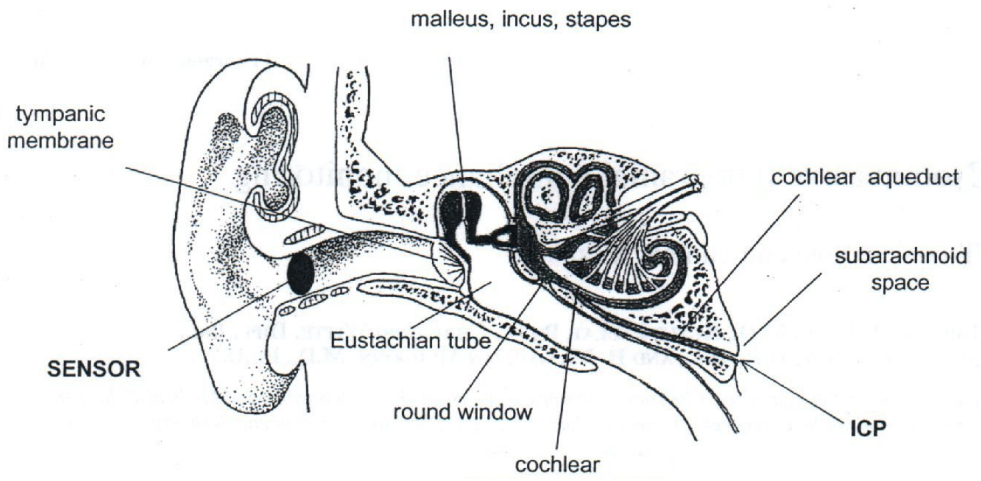

Figure 1.3: schematic anatomy of the outer, middle and inner ear also showing the location of TMD sensor. Reproduced from [30].

and their functions are given here, as more detailed information is provided in later chapters when necessary.

The structure of the ear is generally divided into three main compartments; the outer ear, middle ear and inner ear. The outer ear is the external ear canal which is lined with skin and blood vessels; the external ear canal is separated from the middle ear by the tympanic membrane (ear drum). Within the middle ear are three small bones called the ossicles (commonly called the hammer, anvil and stirrup). The malleus (the hammer), the outermost ossicle, is attached to the internal surface of the tympanic membrane and to the incus (the anvil). The incus is attached to the stapes (stirrup), and the stapes footplate rests against the oval window membrane (OWM) that forms part of the interface between the middle and inner ear. The stapes footplate is held in place by the annular ligament, and the stapedial muscle is attached to the head of the stapes. These three bones provide a mechanical link between the tympanic membrane and the inner ear, and are the route by which sound waves are transmitted from the external ear canal to the inner ear.

The inner ear is a complex structure formed of a series of channels and hollows

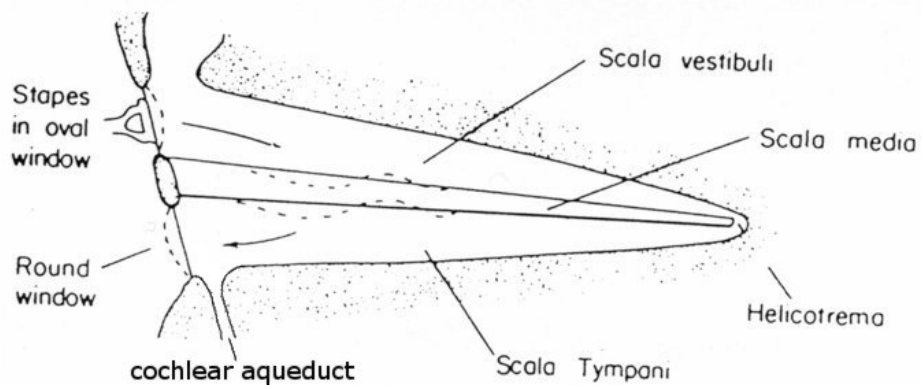

Figure 1.4: A schematic of the cochlea uncoiled (with cochlear aqueduct labelled). The dashed lines indicate the membranes that deform within the inner-ear when sound waves are communicated to from the external ear canal (via the stapes). Reproduced and modified from [51].

within the bone (the bony labyrinth) and within which a membranous labyrinth is suspended. The bony labyrinth is filled with perilymph (a fluid much very similar to CSF) and the membranous labyrinth is filled with endolymph (an unusual fluid with high levels of potassium). The vestibular organ is part of these bony and membranous labyrinths; it detects head movement and orientation so that humans can maintain balance.

The cochlea (or cochlea chamber; CC), another part of the labyrinths, is a tapering tube curled into a tight spiral (much like a snail's shell); it detects pressure variations in the inner ear generated by sound waves incident on the tympanic membrane and transmitted through the ossicles to the cochlea. This project is concerned with both the cochlear aqueduct (CA; which will be the main focus later in this work) and the cochlea. To prevent confusion between the cochlear aqueduct and the cochlea, the cochlea will be referred to as the CC throughout the remainder of this work (or simply as the inner ear inner ear for the purpose of model derivation).

The CC is divided into three compartments: The scala vestibuli, the scala media

and the scala tympani. It is divided into these sections by two parts of membranous labyrinth running up its centre: These membranes are involved in the process of converting sound waves into electrical impulses which are sent to the brain. The first of the three sections, the scala vestibuli, is filled with perilymph and contains the oval window within it. The second, the scala media, is filled with endolymph and runs up the centre separating the scala vestibular from the scala tympani - except at the very tip where the scala vestibuli and the scala tympani are in direct fluid communication with each other. The third section, the scala tympani, is also filled with perilymph and contains within it the round window membrane (RWM), which forms the second part of the interface between the inner and middle ear. (See fig 1.4 for a schematic of the anatomy.) Also contained within the scala tympani is an entrance to the cochlear aqueduct (CA), which forms one of the links to the intracranial space and is focus point of much work in this research.

The inner ear is linked to the CSF spaces by both the CA and the endolymphatic sac. The endolymphatic sac is located within the cerebrospinal space and is connected to the bony labyrinth of the inner ear via the endolymphatic duct (vestibular aqueduct). Fluid pressure transfer through the endolymphatic duct is considered to be limited compared to that of the CA because the endolymph fluid is not in direct communication with CSF.

The cochlear aqueduct (CA) is a tubular hollow in the skull which runs from the subarachnoid space (just below the brain) to the CC, its entrance into the CC is adjacent to the round window membrane. The course of the CA is typically a gentle 'S' curve and its width tapers in from either end giving it a slight 'hour glass' like shape. In many individuals the CA is lined with connective tissue which, in some cases, appears to be so dense that it renders the aqueduct un-patents or occluded (blocked). The degree to which the CA is blocked (either by bone or tissue) is referred to as its patency; with patents being fully open (such that fluid pressure transfer is possible) and un-patents being blocked (such that fluid pressure communication is either highly limited or impossible).

The tissue lining the CA varies in form and quantity between patients and its precise nature and structure has yet to be fully understood. It is believed that the CA is patents at birth and slowly occludes with age [61, 43, 4], although some studies do not agree [24]. The fluid which fills the CA is a combination of CSF and perilymph, which are very similar in constitution and for the purpose of this research they are considered identical.

Figure 2.6 (in chapter 2) shows three slice of human temporal bone tissue which clearly show the point where the CA enters the CC (provided by [35]). The proximity of the opening of the CA to the round window membrane (RWM) can be seen clearly in these slices along with various other structures. The possible effects of structures shown in these slices form the basis for components of the model developed in this research and are discussed later in this work.

1.3 Background Research

The measurement of inner ear pressure (IEP) is of particular interest with regard to non-invasive methods of monitoring ICP. This is because in most humans there is a direct link between the intracranial and intralabyrinthine fluid-filled spaces (the inner ear); this link transmits fluid pressures between the two compartments [47]. However, the relationship between these two pressure waves is still relatively unknown and is the main subject of this work.

There are two main routes of communication between the inner ear and cerebrospinal spaces; the CA and the endolymphatic sac and duct. Although fluid pressure communication might be possible via the endolymphatic sac it is likely that this would be limited in comparison to the CA, this is because no direct fluid exchange can take place between the endolymphatic sac and the cerebrospinal space [31]. The CA is the more promising route of fluid communication, although in some individuals it contains loose connective tissue which, if excessively present,

may block the CA and reduce or prevent pressure transfer via this route.

Early research into the relationship between ICP and perilymphatic pressure was first conducted on cats [5]. Perilymphatic and ICP were measured simultaneously and then analysed. When the CA was patents respiratory and cardiovascular pressure waves could be identified within the perilymphatic pressure. In 4 of the 5 cats studied these same waves were no longer exhibited when the cochlear aqueduct was surgically blocked. It was concluded that in the cat perilymphatic and CSF pressure waves were related.

Further studies conducted on cats used more accurate techniques to monitor perilymph, CSF, middle ear, venous and arterial pressures, with CA patents and surgically blocked [12]. The perilymphatic pressure mirrored that of the CSF pressure when the CA was patents, but with a certain time lag. In contrast to the earlier work, perilymphatic pressure was found to change with CSF pressure even when the CA was blocked, although the amplitude of this was significantly less. (See Fig. 1.5.)

These experiments showed the perilymph and CSF compartments to be linked by the CA as well as in partial communication via the endolymphatic sac and duct. It was concluded that CA patency is the single most important factor relating the pressure transfer from the CSF to the perilymph in cats [11, 10].

Originally the research conducted on cats was not believed to extend to humans and the CA was presumed to be closed in humans until, in 1978, a histological study of more than 100 temporal bones of humans found the CA to be patents in most samples. Patency was observed to decrease as the age of subjects increased [61]. The view that patency decreases as age increases has been challenged in some work [24], but is generally accepted and has been endorsed by others [43, 4].

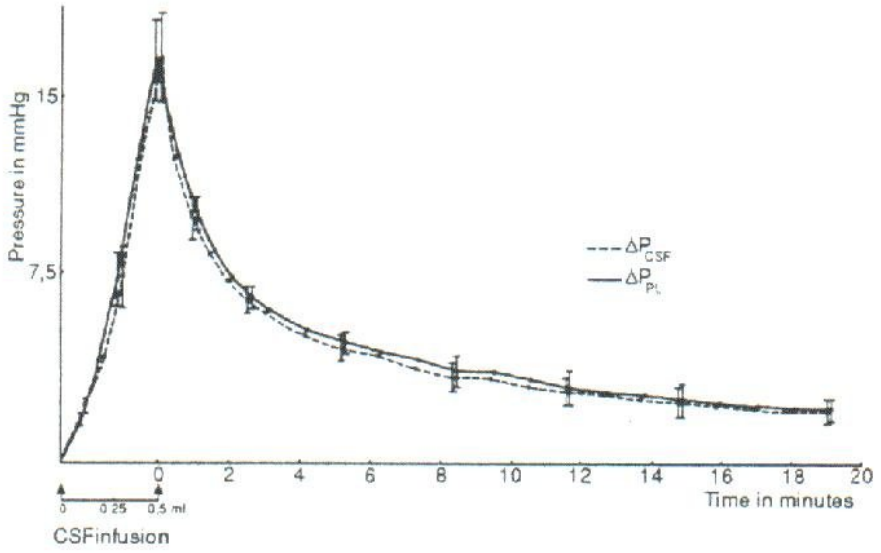

A - Effects of intracranial infusion (*arrows*) of artificial CSF in ten cats with the cochlear aqueduct patent. Mean values ± SEM are given for changes in PPL and PCSF.

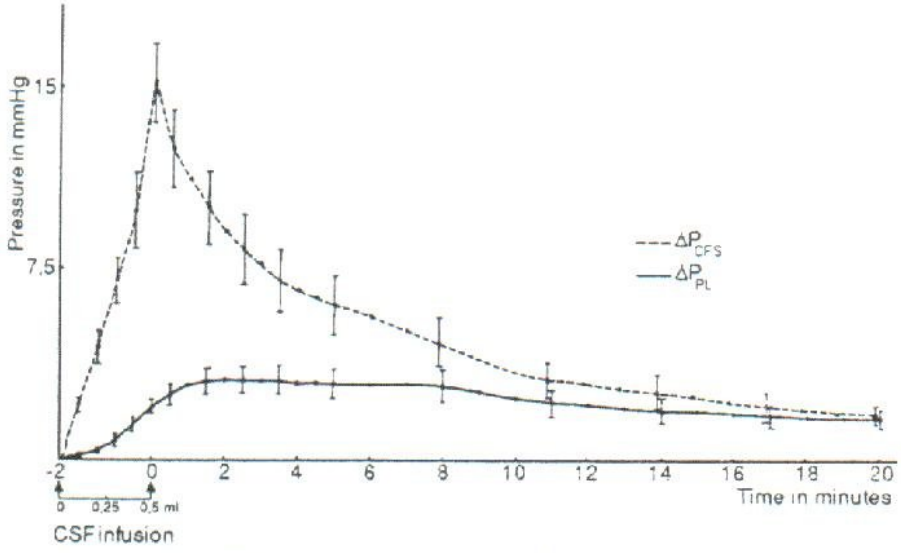

B - Effects of intracranial infusion (*arrows*) in ten cats with the CA blocked. Mean values ± SEM are given for changes in PPL and PCSF.

Figure 1.5: Results showing ICP and IEP (reproduced from [12]). Note the difference in the IEP when the CA is blocked compared to when the CA is patents.

1.4 Intracranial Pressure-Volume Relationships.

To understand much of the research relating ICP to IEP it is beneficial to have an understanding of the interactions between pressure and volume within the skull. This section provides a basic introductions to this topic and introduces important mechanisms such as the measure of "give" in the system which is known as compliances.

When a child is born its skull is not fused into one shell that completely surrounds the brain as in adults: Sutural fusion is the process by which the skull forms a complete shell around the brain and then fuses solid. Once sutural fusion takes place in babies the skull is assumed to behave like a rigid box with little capacity for expansion. The interchanging volumes of CSF and intracranial blood are believed to be the main mechanism for maintaining ICP [18, 48]. It has been shown that pressure and volume within the skull have an exponential relationship [39, 3]. The compliances of a chamber is defined to be the rate of change of volume (ΔV) per unit change in pressure (ΔP). The ratio $\frac{\Delta V}{\Delta P}$ is equivalent to the gradient of the volume versus pressure curve, obtained by slowly injecting known amounts of fluid into the craniospinal space and recording the pressure. It is conceptually easier to deal with the pressure versus volume curve. In this case compliances is the inverse of the gradient ($\frac{\Delta P}{\Delta V}$) and thus the steeper the curve the lower the compliances at that point. Compliance is a measure of the 'give' of a space and, clinically, it suggests how well the intracranial space is compensating for additional volume. Figure 1.6 shows the pressure volume curve and the numbers 1 through to 4 illustrate the regions where the different clinical behaviours associated with decreasing compliances are exhibited. The typical interpretation in the medical literature is that the region 1 - 2 shows a highly compliant environment where an increase in volume produces only a small increase in pressure; The region 2 - 3 is believed to represent an environment where the transition from "low" compliances to "high" compliances occurs; The final section 3 - 4 show a highly noncompliant

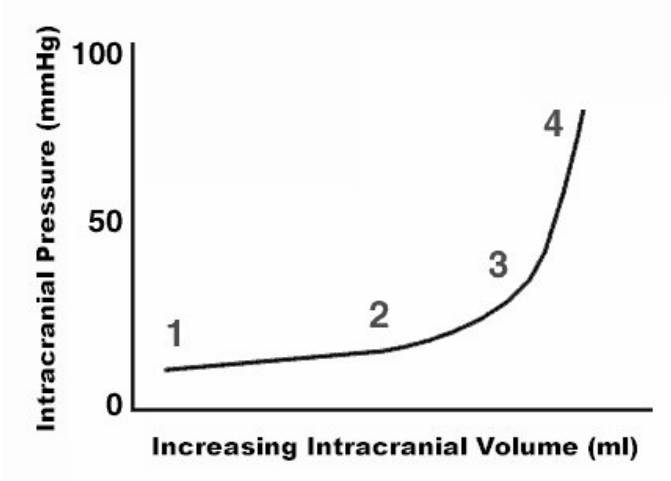

Figure 1.6: Pressure volume curve. 1 - Highly compliant, 2 - Medium compliance, 3 - Low compliances (loss of 'give' within tissue), 4 - Very Low compliances (any 'give' in the system is forced by very high pressures changes). Reproduced from [7].

environment where any increase in volume causes large increases in pressure, this is what most clinicians wish to avoid.

ICP waves are induced by the cardiovascular pulse and respiration. Each heartbeat adds a certain volume of blood to the cerebrospinal space, which induces an intracranial pressure wave, the blood is then removed via venous blood flow. Respiration affects ICP, causing it to fall with each inspiration and rise with expiration. Because respiration occurs at a lower frequency than the cardiovascular pulse the position on the pressure volume curve, and compliances, can be inferred by monitoring the change in the amplitude of the cardiovascular component of ICP waves with respiration. Figure 1.7 shows how amplitude of ICP waves change at different levels of compliances, as are caused by variations in cardiovascular and respiration waves. These changes can be observed both with invasive ICP monitoring and passive TMD measurement. The cardiovascular pulse is generated as the heart beats, normally at around 1-2Hz which corresponds to a heart rate of

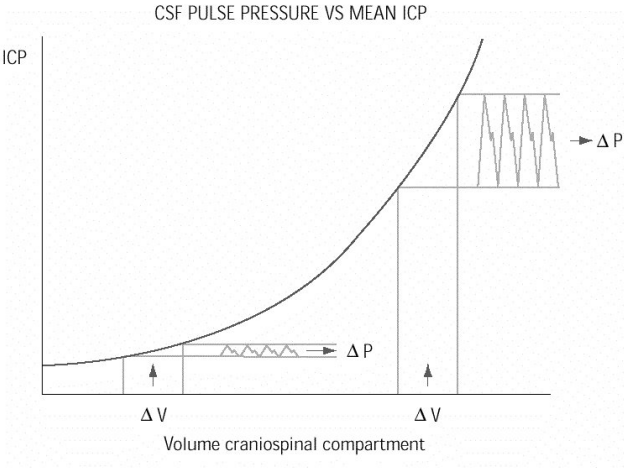

Figure 1.7: Pressure volume curve, illustrating the different compliances. Reproduced from [7].

60-120 beats per minute [28].

1.5 Tympanic Membrane Displacement

The tympanic membrane (ear drum) is linked to the inner ear by the ossicles. Normally sound waves in the air enter the external ear canal and when they reach the tympanic membrane they cause it to move. The force due to these sound waves is then transmitted to the oval window, via the ossicles, and into the inner ear. Thus sound waves are transmitted to the cochlea (inner ear) which converts them into nervous impulses that finally reach the brain.

Conversely, if there are variations in IEP, then these can be transmitted in the opposite direction along the chain by acting on the oval window, which in turn transmits to the tympanic membrane via the ossicles. Since the CSF is in communication with the inner ear, in principle a change in ICP will therefore be reflected in terms of movement of the tympanic membrane. It was shown by Ernst and Marchbanks [49] that displacement of the tympanic membrane reflects changes in

perilymphatic pressure (one measure of IEP) and this was shown using a method of measuring TMD which used a short tone stimulus.

TMD techniques involve having an earplug positioned in the ear canal of the outer ear such that an airtight seal is formed. An airflow sensor is then used to detect the movement of the tympanic membrane by measuring the resulting volume displacements of the air [36].

The technique can be used either passively, by "listening" to TMD, or actively, by measuring TMD in response to an auditory stimulus [47]. This work focuses on the results of passive TMD measurements, but for completeness an introduction to the active TMD measurement is presented first.

The purpose of the stimulus in the active TMD technique is to acoustically invoke the stapedial reflex - this is when the stapedial muscle pulls on the stapes footplate which in turn pulls on the TM. This only occurs in response to a tone burst of sufficient intensity; a short tone pulse (0.3 s, 1000 Hz) elicits the reflex that displaces the TM. The stapedial reflex response was then defined to be the volume displaced over a period of 1.0 seconds in response to the stimulus pulse [50]. The critical observation that was made in these studies was that when perilymphatic pressure is high the stapedial reflex tends to cause the TM to be pulled medially (inwards), and when it is low the stapedial reflex tends to cause the TM to be pulled laterally (outwards). This is illustrated in Figure 1.8. For normal levels of IEP the movement of the TM tended to be a combination of medial followed by lateral - inward then outward (this is not shown in the Figure 1.8).

To establish whether TMD measurements might reflect ICP the patency of the CA must be established. ICP varies with posture, therefore a change from sitting to supine (laying flat) will increase ICP. It then follows that if the CA is patents then an increase in perilymphatic pressure will be observed. Consequently if a change in TMD measurements is observed between sitting and supine, and the middle ear pressure remains constant, the CA can be taken to be patents. To quantify the

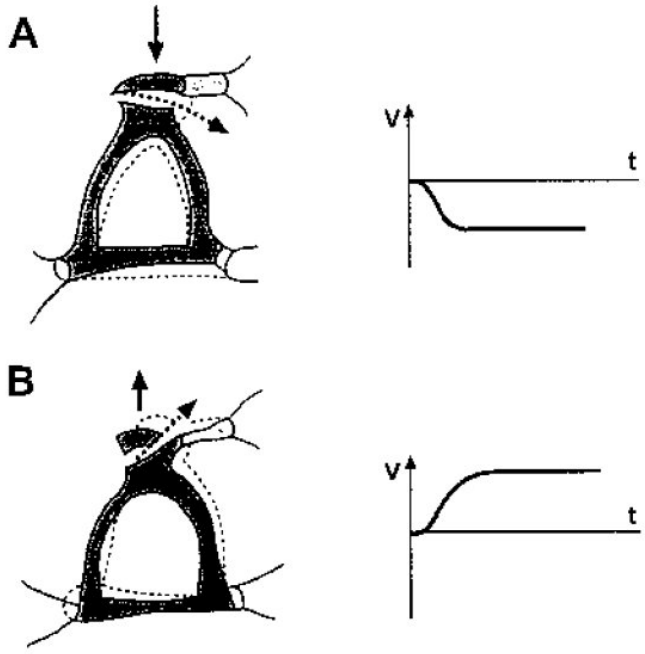

Figure 1.8: A - the position of the stapes with high IEP. B - the position of the stapes with low IEP. The dotted lines show the position of the stapes at normal pressure and the dotted arrows show the direction of movement caused by the stapedial reflex. Reproduced from [59].

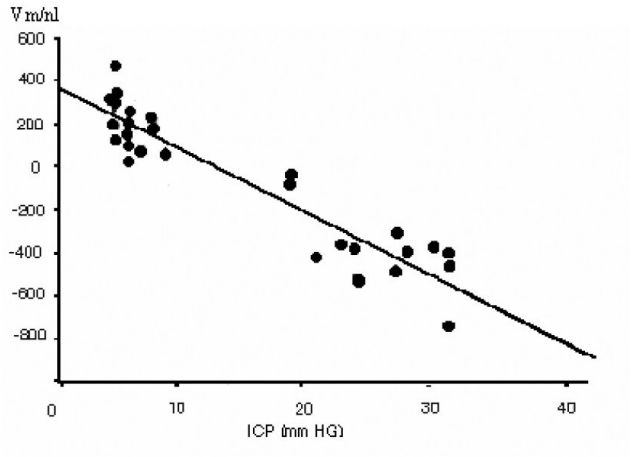

Figure 1.9: Correlation between ICP and Active TMD measurements - correlation coefficient = 0.94. Reproduced from [50].

difference between the TMD measurements the mean displacement when sitting is divided by the same value when supine. If this fraction is greater than 0.1 the CA is assumed to be patents [47].

The accuracy and repeatability of the TMD volume change during a stapedial reflex has been evaluated under more controlled conditions in a prospective study [50] which compared serial TMD tests with direct ICP measurements. A strong correlation was found between TMD and ICP (shown in Figure 1.9), and the relationship between TMD and ICP was firmly established. Although the TMD stapedial reflex test is reproducible in detecting changes in ICP, the technique does not measure absolute levels of ICP mainly due to large intersubject variations [50].

Passive observation of TMD, where no stimulus is used, shows continuous dynamic pressure waves that contain pulses and pressure waves from many origins; This is referred to as spontaneous activity. There are a variety of different pressure waves within the TMD, with varying periodicity; Four of the waveforms present within the continuous dynamic pressure wave have been identified; a cardiovascular wave,

a respiratory wave, a cardiovascular modulated with respiratory wave and an M wave. M waves are a particular type of ICP waveform, the detailed study of which is not required in the work presented here. The cardiovascular wave is present in most ears [37]. The pressure waves measured with the TMD analyser may contain components from many sources, including vasculature of the outer ear as well as from the intracranial fluid. In general their origins are from vasculature throughout the ear, although a significant proportion are believed to be intracranial [37].

One study using the TMD analyser examined the cardiovascular wave in relation to posture, intra-cochlear fluid pressure, middle ear compliances and pressure, and cerebral to labyrinth fluid pressure transfer [28]. The study included 10 normal subjects and looked at the variation in TMD over a 6 second period. Peak to trough amplitude was measured, the periodicity of which was checked against the radial pulse. Intersubject variability was high at 13.5%, however intrasubject variation was much smaller than intersubject variation suggesting a real trend. The most significant positive findings of this study were changes in cardiovascular amplitude with posture and with peak compliances of the middle ear ($p=0.001$).

TMD contains a cardiovascular component; this could be driven by the cardiovascular component of ICP or vasculature in the middle or inner ear. Tympanic membrane peak compliances and cardiovascular amplitude show strong correlation ($r=0.61$); the higher the compliances, the higher the amplitude of the pressure waves recorded. This supports the idea that measurements of TMD that show characteristics of the cardiovascular pulse are of intracranial origin [28].

1.6 Nonlinear Mechanisms

Although pressure waveforms from the inner ear are believed to have components of intracranial origin they still display some characteristics of their own. One possible cause of this would be nonlinear mechanisms in the communication of pressures

between the intracranial and inner ear spaces. The main route for pressure transfer is the CA and little is known about its dynamic properties in humans. It is likely that some of the nonlinear mechanisms that affect pressure propagation properties are related to the anatomy of the CA and or the anatomical structures around it.

Several studies have been conducted on guinea pigs, these involved manipulation of the ICP and/or detailed investigation of the anatomy of the CA and the surrounding structures. The first studies used square wave and short pulses in ICP while measuring IEP and found that pressure equalization process was nonlinear, thus implying that the propagation properties of the CA are nonlinear, and depended on direction of fluid propagation [56]. Later research then examined in more detail the properties of the local anatomy, and their possible effects, and this research indicated that flow resistance through the CA was a nonlinear function of the flow rate but did not appear to be dependent on the direction of fluid motion through the CA [57, 60]. It was hypothesised that nonlinearities in the pressure transfer properties were dependent not just on a combination of pressure difference and compliances, but on the position of the round window membrane [57, 33]. Further research studied the anatomical structures in the fluid pressure communication route, such as the round window membrane, and provided additional evidence that this structure is key to determining the propagation properties between the intracranial spaces and the inner ear [19, 27]. However, these findings are not based on human material and thus they must be combined with other research/data to form a reasonable basis from which potential nonlinear mechanisms can be hypothesised. This is discussed in more detail in Section 2.3.

Another mechanism that must be considered is the conversion of pressure changes in the inner ear into volume displacements in the external ear canal. Some research indicates that the ossicles may not transmit displacement in a linear manner and thus they may be an additional source of nonlinear propagation properties. In some instances readings of TMD have shown that the pressure wave (thought to be driven by ICP) is inverted [30]. The body of work concerning the movement of

the ossicles, although diverse, is of limited relevance to the work presented here for two reasons. The first and main reason is that the majority of the work focuses on high-frequency oscillations caused by sound waves incident on the tympanic membrane - opposed to the low frequency oscillations produced by ICP, arterial blood pressure (ABP) and respiration waves. The second reason is that the work is primarily concerned with the movement of the ossicles driven by pressure changes in the external ear canal acting on the tympanic membrane. This is the opposite to what occurs in this research, where pressure changes within the inner ear act on the stapes foot-plate and move the ossicles. However, some relevant information can be inferred from this work. A study using both the intact and the reconstructed ossicular chain to research the effects of static pressure changes in the external ear canal showed that the lateral to medial (outward to inward) movement of the malleus was converted into predominantly superior to inferior (up to down) movement of the incus [40]. This is shown in Figure 1.10.

It should be noted that it is unclear how these behaviours might change when the pressure-change is applied via the inner ear - opposed to the external ear canal - as is the case in this research. Although there may be nonlinear mechanisms affecting the motion of the ossicles, there is currently more evidence indicating that the CA, and its interactions with the RWM, are the source of nonlinear behaviours observed in passive TMD measurements.

1.7 Chapter Summary

Within this chapter the background material and motivation for research into non-invasive methods of monitoring ICP has been explained; including a brief introduction to the anatomy of the ear within the context of this research. Also covered was an introduction to the TCCS techniques, with specific focus on the active and passive TMD techniques (the latter of which is the focus of this research).

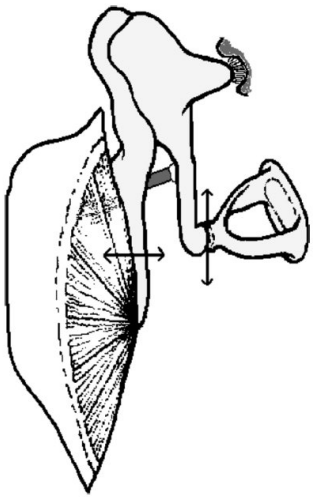

Figure 1.10: This schematic illustrates movement of the ossicles during static (or slow) pressure changes. Reproduced from [40].

Lastly, possible sources of nonlinear behaviour in the passive TMD measurements were identified; specifically the nonlinear flow characteristics of the CA, the possible existence of a valve-mechanism at the interface between the CA and the inner ear, and finally the possibility of nonlinear transmission properties of the ossicles (although the last is not investigated in detail in this work).

The next chapter begins the modelling process by examining the different sources of the TMD waveform and deriving appropriate models for each.

Chapter 2

Modelling

The physiological system which generates the passive TMD measurements is formed of collection of complex biological components. This chapter will describe models for each of the various components and how they interact with one another. The modelling is divided into four sections each dealing with a group of components or interfaces in the physical system.

The first of these sections is concerned with the CA; the bony channel filled with fluid which the primary link between ICP and the inner ear. Discussion of the properties of various anatomical features and the variety of properties they posses leads to a model involving fluid dynamics and linear elasticity.

The second section considers the inner ear. The CC is the part of the of the inner ear focused upon in the modelling because the CA exits into one end of it - near the round window membrane (RWM) - and the oval window membrane (OWM) which is where the ossicles interface with the CC and pressure transfer between the inner ear and the external ear canal occurs.

The third section focuses on the interface between the CA and the inner ear, and the effects of the structures around this interface. It has yet to be proven, but as outlined in Section 1.6 of Chapter 1 there is evidence that the RWM, which

is located next to the exit of the CA into the CC (within the inner ear), may cause nonlinear changes to the fluid communication properties between ICP and the inner ear pressure (IEP). This section combines research from our own group, data from human CA slices (provided by [35], see Fig.2.6) and detailed studies on the guinea pig to form anatomically based models that accurately represent the behaviour of the anatomical system. It is thought that this component of the model, incorporating these nonlinear mechanisms, is most likely to reproduce the nonlinear effects that have been observed in some TMD measurements.

The fourth section in the modelling considers additional aspects within the physical system that may contribute or influence TMD measurements. These physiological processes, in addition to IEP and ICP, that may affect the TMD signal are believed to have limited effect on TMD measurements relative to the effect of IEP. However, they are included in the model in order to determine the approximate proportion of their contribution to TMD measurements. These processes receive less detailed mathematical modelling as they are believed to interact with TMD measurements through less complex mechanisms.

The fifth and final section of this chapter considers the system as a whole and links the models developed from each section together to form a model for the entire physical system considered in this work, this is referred to as the complete model.

2.1 The Cochlear Aqueduct

It is understood that the cochlear aqueduct (CA) is the most likely route of fluid communication between ICP and the inner ear; understanding its propagation properties is crucial to understanding the relationship between ICP waves and passive TMD measurements. Here modelling of the CA is broken down into two parts: One for the connective tissue which lines the CA, and a second for the fluid which transmits changes in ICP through the CA into the inner ear. Before a de-

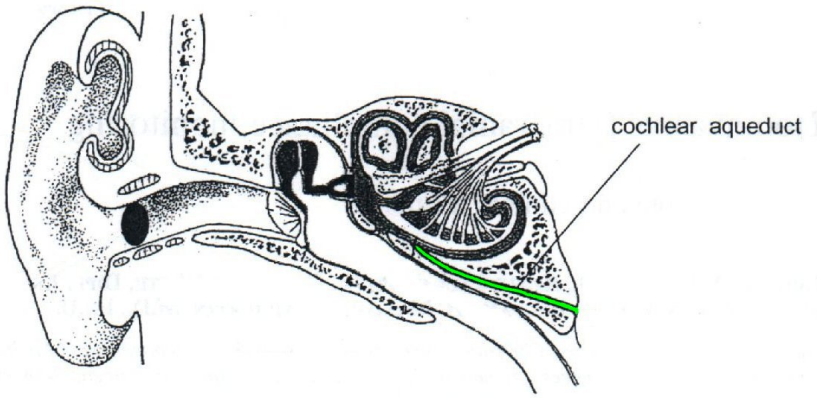

Figure 2.1: Anatomy of the ear, showing the cochlear aqueduct CA in green. Reproduced and modified from [30].

tailed model is formed an outline of the physical properties of the anatomy are outlined, followed by some basic analysis to determine what method of mathematical modelling is appropriate for the CA component of the system.

2.1.1 Anatomical properties

Despite large inter-subject variations it is reasonable to model the geometry of the CA as a cylindrical tube filled with fluid and connective tissue. The path the CA takes through the temporal bone is usually a gentle "S" shape, but for modelling purposes the CA is assumed to take a straight course through the temporal bone. The typical length of the CA, L, is 12 mm and at the narrowest point radii values range between 34 - 122 μm; a typical radius is 35 - 90 μm[4, 24]. For this model the typical radius, $\bar{R}$, will be taken to be 45 μm, thus the Aqueduct can be modelled as a long thin tube with aspect ratio, $\varepsilon = \bar{R}/L$, of order 0.005.

The connective tissue within the CA also has a high level of inter-subject variation, in terms of both amount of tissue media and types of structures formed by the tissue. Small amounts of tissue may form layers along the walls of the CA and,

although they may affect fluid flow, they do not occlude (block) the CA. Large amounts of tissue can form a matrix structure across the diameter of the CA; in some cases this can occlude the CA if the density of the matrix reaches critical levels along its length. This study focuses on the first of these cases, where the CA is patents (open), thus it is appropriate that the tissue is modelled as a thin layer of elastic medium lining the walls of the CA.

The fluid within the CA is a mix of CSF and perilymphatic fluid, these two fluids have very similar properties and, as such, will be considered as one fluid in this work (only CSF will be referred to from here on). In the past there have been some concerns within the scientific community that CSF might possesses non-Newtonian properties due to suspended particles or increased levels of glucose. However, studies have shown that CSF is described well as a Newtonian fluid [8], thus it is appropriate for CSF to be modelled as a Newtonian fluid in this work. The dynamic viscosity (μ) of CSF is typically 1 $\times 10^{-3}$ Pa s, and its density (ρ) is 1000 kg m^{-3}; therefore the kinematic viscosity ($\nu = \mu/\rho$) is 1 $\times 10^{-6}$ m^{2}s^{-1}[52, 8].

2.1.2 Preliminary analysis

When deriving the IEP model it is best to first consider some of the basic characteristics of the CA model. Due to the nature of the geometry of the CA it is best described using cylindrical polar coordinates, (r, θ, z) - with corresponding velocities (u, v, w) - oriented with the z-axis running directly along the centre of the CA from the intracranial space to the inner ear. The system presented here is assumed to be symmetric in the θ direction, about the z-axis, thus an arbitrary reference point for the θ coordinate can be chosen. Starting from the full Navier-Stokes (NS)s and continuity of mass equations in cylindrical polar coordinates the system can be simplified by exploiting the properties of the geometry and making some assumptions based on the properties of the fluid. The density and viscosity of CSF are assumed to be constant. The small aspect ratio implies that fluid

velocities, u, in the radial direction are significantly smaller than those along the z-axis, w, and therefore terms of order u^2 are negligible. The flow is assumed to be rotationally symmetric around the z-axis, thus $\partial/\partial\theta = 0$, and it is taken that there is no flow in the θ direction. Exploitation of these properties allows the NSs equations to reduce to the following equations.

$$\frac{1}{r}\frac{\partial}{\partial r}(ru) + \frac{\partial w}{\partial z} = 0 \tag{2.1}$$

$$\frac{\partial u}{\partial t} = -\frac{1}{\rho}\frac{\partial P}{\partial r} \tag{2.2}$$

$$\frac{\partial w}{\partial t} + u\frac{\partial w}{\partial r} + w\frac{\partial w}{\partial z} = -\frac{1}{\rho}\frac{\partial P}{\partial z} + \frac{\mu}{\rho}\left(\frac{1}{r}\frac{\partial w}{\partial r} + \frac{\partial^2 w}{\partial r^2}\right). \tag{2.3}$$

To further simplify the governing equations, the importance of viscous and inertial forces within the flow needs to be determined. In order to determine which dominates the flow the equations must be nondimensionalised so that the relevant coefficients can be examined.

The nondimensionalising of equations (2.1) to (2.3) is done using the following scaling factors,

$$\begin{aligned} z &= L\tilde{z} & r &= \bar{R}\tilde{r} \\ w &= U\tilde{w} & u &= \varepsilon U\tilde{u} \\ t &= \frac{1}{\omega}\tilde{t} & P &= \frac{\mu U}{\varepsilon^2 L}\tilde{P} \end{aligned} \tag{2.4}$$

where $\varepsilon = \dfrac{\bar{R}}{L}$, U is the typical velocity along the CA and a $\tilde{}$ above a variable indicates it is the dimensionless form of the variable. This results in the following dimensionless equations,

$$\left(\frac{1}{\tilde{r}}\frac{\partial}{\partial\tilde{r}}(\tilde{r}\tilde{u}) + \frac{\partial\tilde{w}}{\partial\tilde{z}}\right) = 0 \tag{2.5}$$

$$\varepsilon^2\alpha^2\frac{\partial\tilde{u}}{\partial\tilde{t}} = -\frac{\partial\tilde{P}}{\partial\tilde{r}} \tag{2.6}$$

$$\alpha^2\frac{\partial\tilde{w}}{\partial\tilde{t}} + Re^*\left(u\frac{\partial\tilde{w}}{\partial\tilde{r}} + \tilde{w}\frac{\partial\tilde{w}}{\partial\tilde{z}}\right) = -\frac{\partial\tilde{P}}{\partial\tilde{z}} + \left(\frac{1}{\tilde{r}}\frac{\partial\tilde{w}}{\partial\tilde{r}} + \frac{\partial^2\tilde{w}}{\partial\tilde{r}^2}\right). \tag{2.7}$$

Where $\alpha = \bar{R}\sqrt{\omega/\nu}$ is the Womersleys parameter and $Re^* = \dfrac{U\bar{R}^2}{L\nu}$ is the reduced Reynoldss number. The magnitude of the Womersleys parameter and reduced

Reynoldss number dictate which parts of the fluid flow are dominated by viscous or inertial forces. An analysis of the Womersleys parameter and reduced Reynoldss number follow below.

The Womersleys number, $\alpha = \bar{R}\sqrt{\omega/\nu}$, is a nondimensional parameter which determines the balance of inertial and viscous forces in oscillatory fluid flow; where ω is the angular frequency of the oscillation in pressure gradient, $\bar{R}$ is the typical radius of the CA, and ν is the kinematic viscosity (as introduced earlier) [62]. It dictates the balance of the transient inertia terms with the viscous terms of the governing equations; from equation (2.7) these are $\frac{\partial \tilde{w}}{\partial \tilde{t}}$ and $\left(\frac{1}{\tilde{r}}\frac{\partial \tilde{w}}{\partial \tilde{r}} + \frac{\partial^2 \tilde{w}}{\partial \tilde{r}^2}\right)$ respectively.

In equation (2.6) the transient inertia term, $\frac{\partial \tilde{u}}{\partial \tilde{t}}$, need not be evaluated at this time, due to it being multiplied by ε (which is very small). This term need only be evaluated if the magnitude of the Womersleys parameter (α) is of the order $1/\varepsilon$; which is not expected to be the case for this model.

Returning to the analysis of the Womersleys parameter, if $\alpha \ll 1$ then transient inertia terms are negligible and viscous forces dominate the oscillating component of the fluid flow; and if $\alpha \gg 1$ then transient inertia terms dominate the flow. The frequency of ICP is approximately 1 Hz, which corresponds to an angular frequency of 2π, when combined with the typical values for radius and kinematic viscosity outlined above this gives a Womersleys number for this system of 0.1. This is sufficiently small for it to be appropriate for the transient inertia terms to be neglected and quasi-steady governing equations to be used to model the system.

The Reynoldss number is a nondimensional parameter which characterises the relationship between viscous and inertial forces in the fluid flow [1]. It dictates the balance of viscous forces with inertial forces in equation (2.7), $\left(\frac{1}{\tilde{r}}\frac{\partial \tilde{w}}{\partial \tilde{r}} + \frac{\partial^2 \tilde{w}}{\partial \tilde{r}^2}\right)$ and $\tilde{u}\frac{\partial \tilde{w}}{\partial \tilde{r}} + \tilde{w}\frac{\partial \tilde{w}}{\partial \tilde{z}}$ respectively. Typically, when nondimensionalising the NSs equations, this balance would produce the Reynoldss number of the form $Re^* = \frac{UL^2}{L\nu}$. How-

ever, due to the long, thin geometry of the system considered here, the balance of viscous and inertia terms instead produces the Reynoldss number in a reduced form, $Re^* = \dfrac{U\bar{R}^2}{L\nu} = Re\ \varepsilon^2$. The reduced Reynoldss number behaves in the same way as the Reynoldss number and can be interpreted in a similar manner; they will be referred to interchangeably from hereon. If $Re^* \ll 1$ then viscous terms dominate the flow and for $Re^* \gg 1$ inertia based terms dominate the flow.

To evaluate the Reynoldss number a value for the typical fluid velocity, U, along the CA is required. Measurement of fluid velocities along the CA in living humans would be a highly invasive, and require clinically unnecessary procedures. Thus, an alternative method of analysis using approximations for the typical velocity is used here, instead of experimental data.

In this method the reduced Reynoldss number is assumed to be either $Re^* \gg 1$ (case A) or $Re^* \ll 1$ (case B) so that the NSs equations can be balanced and an equation for U obtained (one equation for each assumption). The equation for U is then used to calculate Re^*, and if the calculated value for Re^* is of the same or similar order to that which was assumed to produce it, then the case is considered self-consistent. In order to ensure the correct order for Re^* is assumed, these two cases are evaluated with different values for the pressure difference across the CA (the only independent variable remaining in the equation for U). If neither case A or B appears self-consistent, or both appear self-consistent, then this implies that the correct order for Re^* is likely to be $O(1)$, and further analysis would be required to determine how the flow might be approximated.

When $Re^* \gg 1$ (case A) inertia and pressure terms are balanced to give $U \approx \sqrt{\Delta P/\rho}$. When $Re^* \ll 1$ (case B) viscous and pressure terms are balanced to give $U \approx \frac{\Delta P \bar{R}^2}{\mu L}$. In both cases ΔP is the typical pressure drop across the CA and this must be established before further analysis can continue.

To approximate the typical pressure drop across the CA, information about ICP is required, as this is what drives the pressure drop. Mean and dynamic ICP varies

greatly between patients, but the clinical study conducted as part of this project has produced a modest amount of data and so that is what is used here. The ICP wave had peaks as high as 37 mm Hg and troughs as low as 15 mm Hg, but there was a trend for the mean pressure to remain around 25 mm Hg with a typical trough to peak amplitude of 8 mm Hg (1 mm Hg $\approx$ 130 Pa). This information about ICP will be used in the analysis of the Reynoldss number below.

Now the relevant information required to conduct the analysis of the Reynoldss number is available, the preliminary analysis continues below.

First analysis of the Reynoldss number is done assuming that the typical pressure drop across the CA is the 'worst case scenario' maximum possible 8 mm Hg. This level of pressure drop is extremely unlikely, but is the highest possible according to the data collected and so is the starting point for analysis. Assuming a high Reynoldss number flow the approximate typical velocity generated by this pressure drop would be $U = 1.03$ m/s and the Reynoldss number would be $Re^* = 0.17$. Assuming low Reynoldss number flow the typical velocity would be $U = 0.18$ m/s and the Reynoldss number would be $Re^* = 0.03$. Even with this maximum high pressure drop and hence unlikely high fluid velocity the high Reynoldss number flow is not self-consistent, where as the low Reynoldss number flow is self-consistent despite the high fluid velocities.

The choice of a 8 mm Hg as the typical pressure drop across the CA is the "worst case" pressure drop when assuming viscous forces dominate. The ICP in our experimental work was measured in the ventricle, which is located in the centre of the brain, and thus the choice of $\Delta P = 8$ mm Hg does not account for any pressure drop between the point of experimental measurement and the intracranial end of the CA. Also a pressure drop of 8 mm Hg assumes that ICP and pressure in the inner ear are in opposite phase, when in fact it is believed that pressure in the inner ear follows ICP with only a slight lag. Thus the pressure in the inner ear is likely to be much closer to ICP than 8 mm Hg.

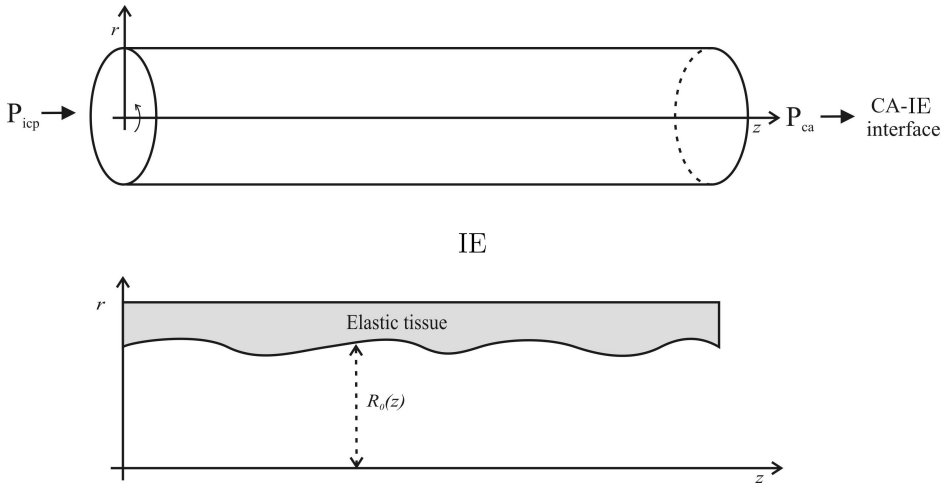

Figure 2.2: Schematic of CA components:
Above: Orientation of the cylindrical polar coordinates within the CA;
Below: schematic of cross-section of CA; illustrating the fluid filled area (clear) and elastic tissue lining (grey).
(Radius $R_0(z)$ is approximately 45 μm and length of CA is 12 mm.)

Using a more realistic ΔP of 1mm Hg and evaluating in the same way as above then the following results are produced: Case A (high Reynoldss number) produces $U =$ 0.13 m/s and $Re^* = 0.0225$; Case B (low Reynoldss number) produces $U = 0.0225$ m/s and $Re^* = 0.0038$. These results further reinforce the conclusion that the low Reynoldss number flow is self-consistent for this system and the high Reynoldss number flow is not. Thus it is appropriate to model fluid flow along the CA as dominated by viscous forces, not inertial forces.

Thus it is acceptable to assume that both the Womersleys parameter and Reynoldss number are sufficiently small for inertia terms to be neglected in the NSs equations.

2.1.3 Derivation of the CA model component

Based on the discussion of Reynoldss number and Womersleys number it is reasonable to take the fluid to be governed by the quasi-steady, low-Reynoldss number limit of the NSs equations with conservation of mass. The equations of this limit are typically referred to as the "lubrication equations" and are as follows [2]

$$\begin{aligned} \frac{1}{r}(ru)_r + w_z &= 0 \\ P_r &= 0 \\ P_z &= \mu\left(\frac{1}{r}w_r + w_{rr}\right) \end{aligned} \tag{2.8}$$

Using "no slip" Dirichlet conditions on the fluid-tissue interface, $r = R(z)$; finite velocity on the central axis, $r = 0$; and the kinematic condition $u = \frac{\partial R}{\partial t}$ on $r = R(z)$; the governing equations are further reduce to

$$\frac{1}{R}\frac{\partial}{\partial z}\left(R^4\frac{\partial P}{\partial z}\right) = 16\mu\frac{\partial R}{\partial t}. \tag{2.9}$$

At this point the governing equations for the fluid flow have been established and so attention must return to the tissue lining the CA and the formulation of a model for its behaviour. Because of the desire to focus the modelling process on the patents CA it was decided that it was appropriate to model the tissue lining the CA as a layer of elastic medium lining the tube; this layer deforms under pressure giving the aqueduct a small amount of compliances. The formulation of governing equations for the tissue are outlined below.

Assume that if the CA is held at P_{base} - the mean pressure around which ICP oscillates - the radius of the CA within the tissue, $\bar{R}_0$, would be constant along the length of the CA. At this point the volume of the tube is $V_{ca0} = \pi R_0^2 L$, where L is the length of the CA. Assume that when the CA is held at an arbitrary pressure $\bar{P}$ the radius is R along its length, thus the volume at this pressure is $V_{ca} = \pi R^2 L$. Compliance is defined to be the increase in volume for a given increase in pressure. Thus if $\Delta P = \bar{P} - P_{base}$ and $\Delta V_{ca} = V_{ca} - V_{ca0} = \pi L(R^2 - R_0^2)$, then when κ_{ca} is

compliances of the CA the following equation apply.

$$\frac{\Delta V_{ca}}{\Delta P} = \kappa_{ca} \tag{2.10}$$

$$\pi L \frac{R^2 - R_0^2}{\bar{P} - P_{base}} = \kappa_{ca} \tag{2.11}$$

$$R = \sqrt{R_0^2 + \frac{\kappa_{ca}}{\pi L}(\bar{P} - P_{base})} \tag{2.12}$$

For small ΔR $(= R - R_0)$ this can be approximated as

$$R = R_0 + \frac{\kappa_{ca}}{2R_0 L\pi}(\bar{P} - P_{base}). \tag{2.13}$$

Since the pressure $\bar{P}$ is arbitrary, this equation for the radius within the CA tissue can be applied at any point along the CA with $\bar{P} = P(z)$ to determine the radius $R(z)$ at that point. Thus the final equation for the fluid-tissue interface is

$$R(z) = R_0 + \frac{\kappa_{ca}}{2R_0 L\pi}(P(z) - P_{base}). \tag{2.14}$$

Compliance need not be constant and can depend on the pressure, however, for the conditions within this model it is believed that patients will be in a well defined part of the pressure-volume curve for the inner ear, where the gradient is approximately linear, and therefore the compliances is assumed to be constant in this work.

Substitution of equation (2.14) into equation (2.9) gives the following governing equation for the fluid within the CA,

$$\frac{\dfrac{\partial}{\partial z}\left(\left(R_0 + \dfrac{\kappa_{ca}}{2R_0 L\pi}(P - P_{base})\right)^4 \dfrac{\partial P}{\partial z}\right)}{\left(R_0 + \dfrac{\kappa_{ca}}{2R_0 L\pi}(P - P_{base})\right)} = \frac{8\mu\kappa_{ca}}{R_0 L\pi}\frac{\partial P}{\partial t}. \tag{2.15}$$

The intracranial space contains a far larger volume of fluid than the inner ear; thus fluid exchange between the inner ear and the intracranial space will have little effect on ICP, but can cause dramatic changes in IEP. Because of this the ICP acting on the CA can be modelled as a given source of pressure which is dictated by the ICP and is unaffected by pressure of the fluid within the CA. Thus

the boundary condition at the ICP end of the CA ($z = 0$) is $P(0, t) = P_{ICP}(t)$. At the inner ear end of the CA ($z = L$) there will be an interface between the CA and the inner ear, this is defined in a separate model outlined in Section 2.3. However, mass must be conserved and the flux out of the CA must balance with the flux into the inner ear.

Integrating the velocity w over the cross-sectional area of the CA at $z = L$ gives the volume flux out of the CA (past the RWM-valve and into the inner ear). Multiplying this by the density of the fluid then gives the following equation for mass flux out of the CA,

$$Q_{ca} = -\frac{\pi\rho}{8\mu}\left(R_0 + \frac{\kappa_{ca}}{2R_0L\pi}(P|_{(z=L)} - P_{base})\right)^4 \frac{\partial P}{\partial z}|_{(z=L)}. \tag{2.16}$$

2.2 The Inner Ear

The cochlea chamber (CC) is only one part of the inner ear, but it is the compartment which contains many of the components believed to affect TMD measurements. The exit of the CA, the round window membrane (RWM) and the oval window (the interface through which pressure changes are communicated between the inner ear and the external ear canal, via the ossicles) are all located within the CC. For the purposes of modelling the inner ear is considered fully represented by the CC aspect of the model when considering TMD measurements; as such the CC and inner ear will be referred to interchangeably in the modelling aspect of this work.

A reasonable model for the inner ear is a compliant, fluid-filled chamber of uniform pressure, which is in communication with the CA. This is because the volume of fluid in the inner ear is dramatically higher than that of the CA, and the larger geometry is such that viscous stresses are significantly lower. It is reasonable to expect pressure gradients through the inner ear to be negligible compared with those in the CA and the interface between the two. The bony nature of the inner

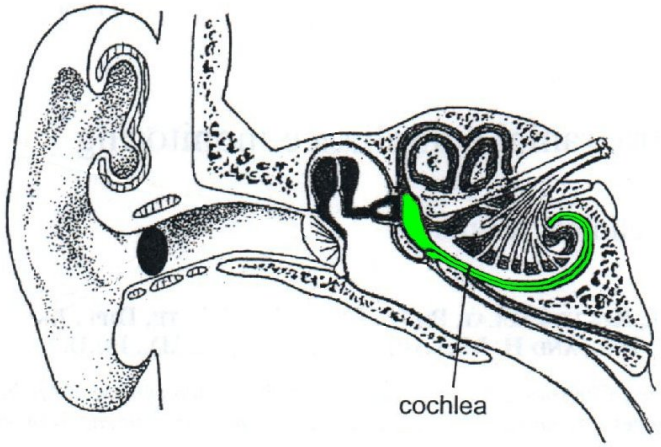

Figure 2.3: Anatomy of the ear, showing the cochlea in green (not the cochlear aqueduct CA). Reproduced and modified from [30].

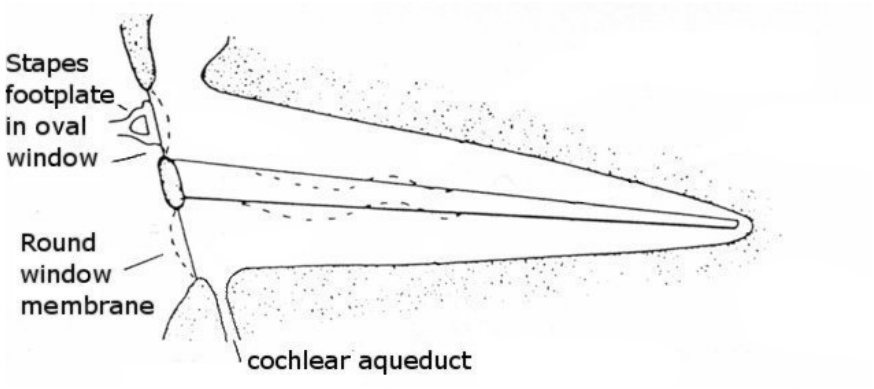

Figure 2.4: A schematic of the cochlea (CC) uncoiled. The dashed lines indicate the membranes that deform within the inner-ear when sound waves are communicated to from the external ear canal (via the stapes). These membranes also allow pressure waves to be communicated in the opposite direction, from the CA to the stapes footplate. Reproduced and modified from [51].

ear is such that there is little compliances in its general structure, the significant contributions to compliances in the inner ear come from the oval and round windows which are covered in membranes that can deform and displace under stress. The discussion of compliances in section 1.4 states that it is widely accepted in the medical community that compliances in the brain varies along the volume-pressure curve. This is also true of the inner ear, however, compliances in the inner ear comes from a different mechanisms and we now consider how this compliances might be modelled.

The round window membrane can be modelled as having a tension proportional to its extension, this opposes the pressure increase; and the oval window membrane has the same properties except that the stapes foot plate attached to the middle ear side of the membrane increases the tension at higher extensions. Due to the pressure in the inner ear being uniform throughout, it is suitable to model the compliances of the inner ear, κ_{ie}, as a function only of the pressure in the inner ear, and not include any direct influence from other pressure sources, as shown in

$$\frac{dV_{ie}}{dP_{ie}} = \kappa_{ie}(P_{ie}). \tag{2.17}$$

Because the compliances depends on the extension/contraction of the RWM and the oval window membrane under stress, the characteristics of the pressure-volume curve of the inner ear is likely to be different to that of the intracranial space (where compliances comes from the compression/expansion of tissue). It is believed that for the pressure ranges being modelled the pressure-volume curve is approximately linear, implying that compliances is constant for this range. Thus in this model it is assumed that compliances is constant, leading to the following equation relating pressure to volume within the inner ear.

$$V_{ie} = \kappa_{ie} P_{ie} + const. \tag{2.18}$$

We now consider conservation of fluid within the inner ear and use the above to give

$$\text{Fluid volume flux} = \frac{\partial V_{ie}}{\partial t} = \kappa_{ie} \frac{\partial P_{ie}}{\partial t}. \tag{2.19}$$

Volume flux into the inner ear then gives mass flux into the inner ear, which is used with conservation mass to link each component of the model, which is

$$\text{Total Mass Flux} = Q_{ie} = \rho\kappa_{ie}\frac{\partial P_{ie}}{\partial t}. \tag{2.20}$$

2.3 The 'CA - inner ear' interface

There is some debate as to the exact nature of the interface between the CA and inner ear. It has been indicated that in early literature a membrane over the entrance to the CA was described, but these findings were not repeated in subsequent studies[5, 24]. Recent research has revealed that, in the guinea pig, the round window membrane has a pouch-like extension which is tethered in the opening where the CA enters the inner ear [33]. It has also been observed that the flow resistance in the guinea pig's CA depends on the position of the round window membrane [19]. It is still unclear whether the human round window also has this pouch-like structure extending into the entrance of the CA. If the anatomy in the human shares similar properties to that of the guinea pig then this dependence on RWM position will be a crucial mechanism affecting the propagation of ICP waves through the CA and into the inner ear. For the modelling here it is assumed that the guinea pig anatomy is valid and scaled up in humans.

The anatomy of CA's exit into the inner ear is unclear, however, a set of pictures of human temporal bone slices were obtained through collaboration with Dr Linthicum of the House Ear Institute [35]. Through analysis of these slices the course of the CA could be traced and followed from the cerebrospinal space through to its opening within the inner ear [38]. At the point where the CA enters the inner ear a structure which might cause of valve-like behaviour was identified (See Figure 2.6). Combining this with more detailed imaging of the anatomy in the guinea pig a speculative model for a valve has been created.

This model assumes that there is a "pouch" within the RWM, the base of which

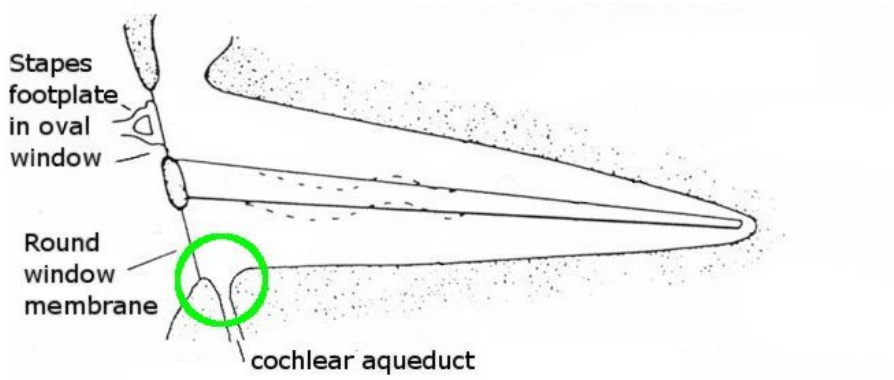

Figure 2.5: A schematic of the cochlea uncoiled, with the interface between the CA and inner ear circled in green. Reproduced and modified from [51].

is anchored in the opening where the CA enters the inner ear. This anchor is in the form of an arm with a bulge on it, and by varying the position of this arm the flow resistance of the CA can be varied also.

To model the flow of fluid from the CA into the inner ear this valve-like mechanism must be understood. The first process is to model the valve and do a force balance to determine the geometry of the point of maximum resistance. The second is to consider the flow near the point of maximum resistance and determine the flow rate as a function of the local valve geometry.

A simple model of the pouch is to consider a 2D valve comprised of a finite, rigid arm; one end of which is freely hinged to the CA exit, the end of which is tethered to an infinite membrane (the RWM), figure 2.8 is a schematic of this model. The side of the CA exit not fixed to the arm becomes the wall of the inner ear and acts as a rigid barrier. The RWM is the barrier between the inner ear and the middle ear and because of this the tension and angle at which the membrane (RWM) acts on the arm can be dictated by the pressure difference between the inner ear and the middle ear. In this model it is assumed that because the "pouch" is small, compared to the RWM, variations in the position of the arm have no effect on the tension of the membrane and its angle of deflection. The arm obstructs the fluid

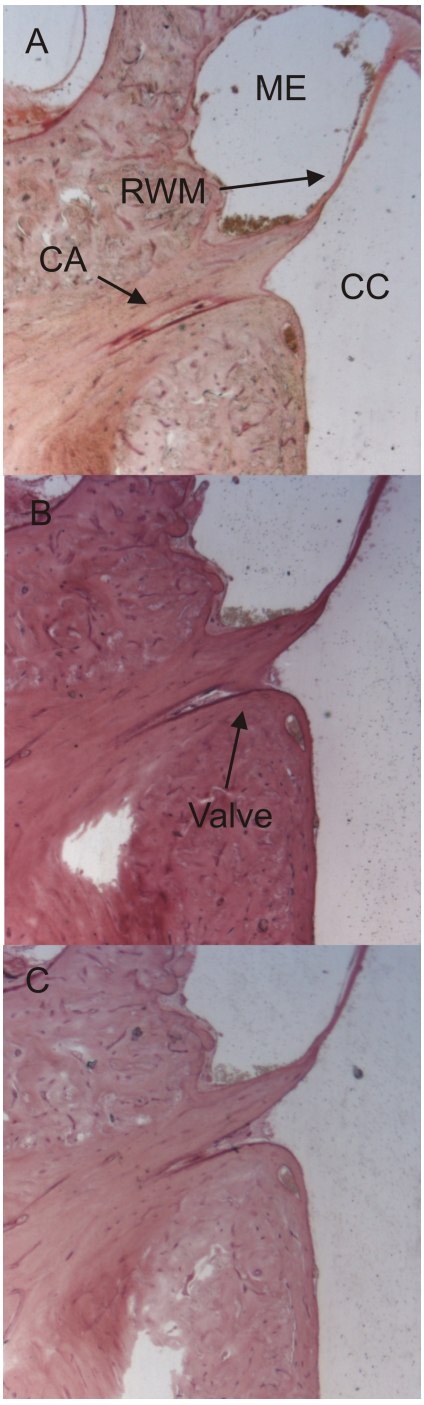

Figure 2.6: Three consecutive slices of human temporal bone tissue [35]. The proximity of the CA to the RWM can be seen clearly all three figures. Figures A and B show a structure that may act as a valve mechanism and forms part of the basis of these models.

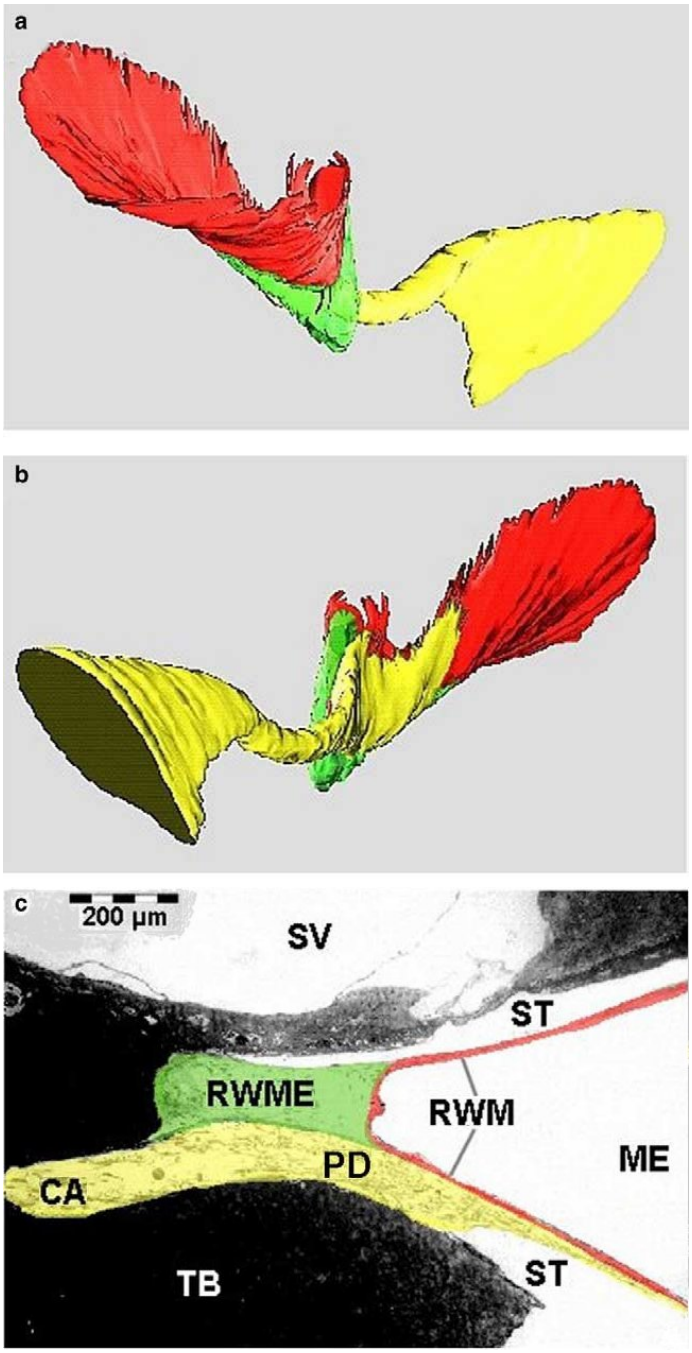

Figure 2.7: 3D imaging of the RWM and CA in a guinea pig [27]. (Image c has been rotated into the same orientation as the slides in Figure 2.6 and schematics of Figure 2.8 and 2.9.)

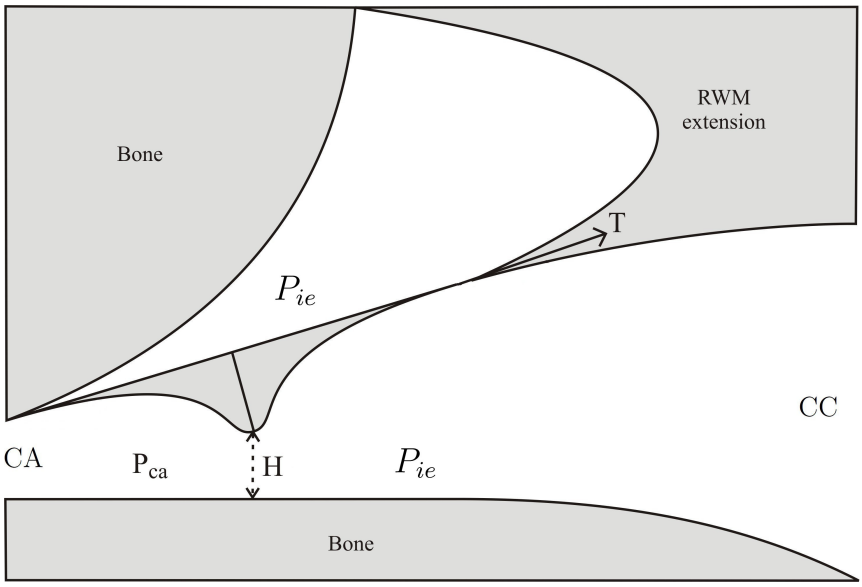

Figure 2.8: Schematic for the valve arm anatomy.

flow out of the CA due to a bulge on the CA side of the arm and thus the flux past the valve is dependent on the distance between the bulge and the fixed wall at this narrowest point. H is the distance at this narrowest point.

The distance at the narrowest point between the bulge and the immobile wall of the CA (H) is obtained by resolving the balance of moments on the arm about the hinged end. For this purpose we assume that the pressure on the CA side of H is uniform and equal to P_{ca} (the output pressure of the CA); and the pressure on the inner ear side of H (and above the arm) is uniform and equal to P_{ie}. The RWM is attached to the end of the valve arm, which is length $2l$ from the hinged end, and is held at constant tension, T, at angle ϕ_1 from the horizontal. This model assumes that both T and ϕ_1 are unaffected by displacements of the arm. A possible alternative model would have both T and ϕ_1 dependent on the pressure difference between the inner ear and the middle ear, but at this point information is limited so they are held constant in this model. The angle of displacement, ϕ_2, is the angle at which there is no moment on the arm, i.e. the force moment from the pressure difference is balanced by that of the tension from the RWM; it is this

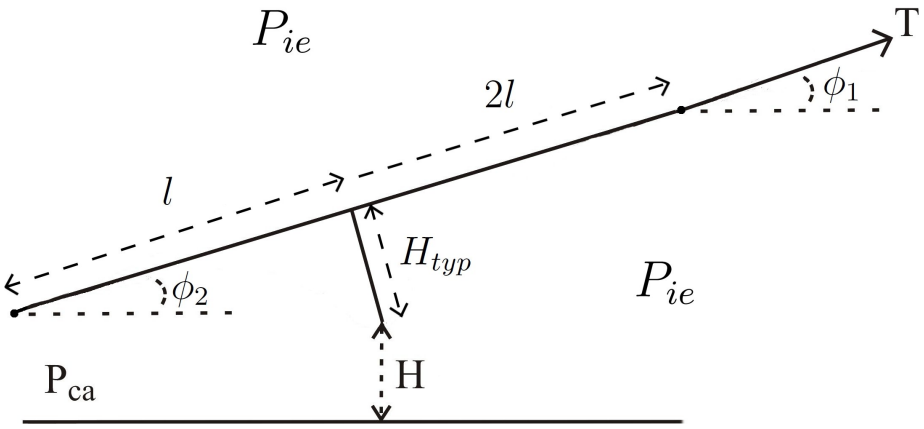

Figure 2.9: Schematic for the valve arm model.

angle of displacement of the arm, ϕ_2, which determines the magnitude of the valve opening, H.

Since the precise geometry of the arm is unknown a straight line approximation will be used as a simple model for the balance of moments. The top side of the arm is a straight line of length $2l$, it is assumed that the bottom side is the same except for a perpendicular extension of length H_{typ} dropping down from its centre point. (These simple lines are shown in figure 2.9.) It is the gap created by this extension, H, which provides the point of resistance for the flow from the CA to the inner ear. If more information on the anatomy were to be found this model could be extended or adapted to incorporate more complex and realistic geometries.

To obtain an equation for H the balance of forces on the valve arm must be considered. For the purpose of considering the balance of moments it is appropriate to use a Cartesian coordinate reference system rotated relative to that used in the rest of this work. For the balance of moments the hinge of the valve arm is considered the origin, the x coordinate extends along the length of the arm and the y coordinate extends perpendicular to the arm and parallel to the extension below the arm. In this reference the force balance required for there to be zero

moment about the hinge is

$$\begin{aligned}\mathbf{M} = &\int_{(0,0,0)}^{(l,0,0)} \mathbf{r} \times (0, k(P_{ca} - P_{ie}), 0)\, dr \\ &+ \int_{(l,-H_{typ},0)}^{(l,0,0)} \mathbf{r} \times (k(P_{ca} - P_{ie}), 0, 0)\, dr \\ &+ (2l, 0, 0) \times (T\cos(\phi_1 - \phi_2), T\sin(\phi_1 - \phi_2), 0)\end{aligned} \tag{2.21}$$

where k is the width of the surface under pressure.

Then, returning to the original reference system shown in figure 2.9, equation (2.21) leads to the following equation for ϕ_2,

$$\phi_2 = \phi_1 + \sin^{-1}\left\{\frac{k}{4lT}(l^2 + H_{typ}^2)(P_{ca} - P_{ie})\right\}. \tag{2.22}$$

The following equation for H is deduced from the geometry and physical properties of the system shown in figure 2.9,

$$\begin{gathered}H = \max\left\{0, H_{typ} - \sqrt{l^2 + H_{typ}^2}\sin(\phi_2 - \phi_3)\right\} \\ \text{where } \phi_3 = \tan^{-1}\left(\frac{H_{typ}}{l}\right).\end{gathered} \tag{2.23}$$

Thus using equation (2.22), and trigonometric identities, the equation for H can be expressed in the following form

$$\begin{aligned}H = \max\Bigg\{&0, H_{typ} + (H_{typ}\sin\phi_1 + l\cos\phi_1)\frac{k(l^2 + H_{typ}^2)}{4lT}(P_{ca} - P_{ie}) \\ &+ (l\sin\phi_1 - H_{typ}\cos\phi_1)\sqrt{1 - \left(\frac{k(l^2 + H_{typ}^2)}{4lT}\right)^2 (P_{ca} - P_{ie})^2}\Bigg\}.\end{aligned} \tag{2.24}$$

Due to the geometry of the CA and the RWM valve the function H will be scaled with $R_o = H_{typ}$ as part of the nondimensionalisation that occurs in chapter 3, for this reason it is appropriate to choose a value of ϕ_1 such that $H = 2H_{typ}$ when $P_{ca} = P_{ie}$ and the opening of the RWM-valve is of the same order as the diameter of the CA. When such a value for ϕ_1 is chosen the equation governing the size of

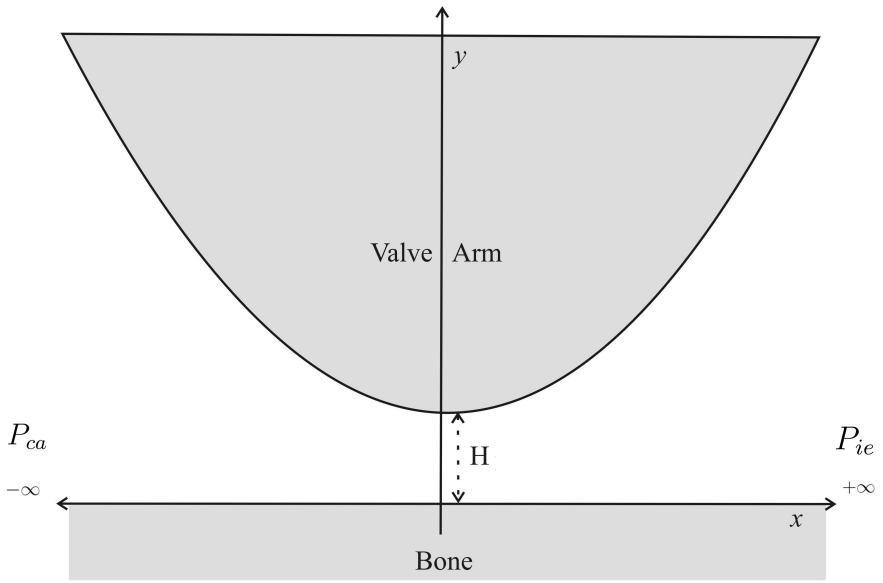

Figure 2.10: Schematic for the limit of the flow through point of maximum resistance.

the opening, H, reduces to the following,

$$H = \max\Bigg\{0, H_{typ} + l\frac{k(l^2 + H_{typ}^2)}{4lT}(P_{ca} - P_{ie}) + H_{typ}\sqrt{1 - \left(\frac{k(l^2 + H_{typ}^2)}{4lT}\right)^2 (P_{ca} - P_{ie})^2}\Bigg\}. \tag{2.25}$$

The second part of the modelling of the CA-inner ear interface involves determining the flux of fluid through the valve as a function of the pressure difference across the valve and the height of the narrowest point. For this an approximation of the geometry at the bulge is made and then the fluid flow around this simplified geometry is evaluated. (Fig.2.10 shows a schematic for the geometry and flow.)

The fluid and geometry of this system have similar properties to that of the CA modelled earlier and thus this flow is also governed by a simplified form of the

lubrication equations,

$$\begin{aligned} u_x + v_y &= 0 \\ P_x &= \mu \frac{\partial^2 u}{\partial y^2} \\ P_y &= 0. \end{aligned} \tag{2.26}$$

No slip Dirichlet conditions are used on the upper and lower bounds, $y = 0$ and $(y = Ax^2 + H)$, and it is assumed that $P(x) \to P_{ie}$ as $x \to +\infty$, and $P(x) \to P_{ca}$ as $x \to -\infty$.

As with the other components of the complete model, this section will be coupled to the other components through mass balance. Thus the mass flux though the line $x = 0$ is evaluated and used to give the following equation which will be used to couple the CA to the inner ear.

$$\text{Total Mass Flux past RWM-valve} = Q_{rwm} = \frac{2\rho k A^{1/2}}{9\pi\mu} H^{5/2}(P_{ca} - P_{ie}). \tag{2.27}$$

2.4 Additional Aspects

When modelling TMD measurements it is important to keep in mind that although the waveform is predominantly of intracranial origin other sources affect the TMD waveform as well. It is believed that these influences are small, relative to the contribution of ICP via IEP, which is why the model presented so far does not account for them, however, they should not be ignored and they need to be considered. Possible sources are thought to be vasculature (particularly within the inner ear, middle ear and external ear canal), pressure variations transmitted to the middle ear via the Eustachian tube, and small pressure artefacts produced by body movement.

It is necessary to assess the importance of these direct signals in the TMD, but without adding unnecessary complexities to the modelling process. Hence these were modelled by taking the pressure within the inner ear, P_{ie}, and then adding a

weighted pressure waveform from each potential source. This leaves the complete model for TMD unchanged regardless of how many additional sources are considered, and limits the number of new parameters introduced with each new source in the TMD waveform. Models for each of the additional sources are presented in this section.

2.4.1 Arterial blood pressure and pathological sources

It is believed that arterial blood pressure (ABP) contributes to the TMD waveform directly. Such a contribution might arise through vasculature in the inner ear, middle ear and or external ear canal communicating the pressure directly into the TMD waveform. Although other mechanisms by which ABP might contribute to TMD may exist it is believed that they would be considerably less significant than direct communication through vasculature. As such, the contribution of ABP is modelled by including a component directly proportional to the ABP waveform, P_{art}, in the complete model of TMD and is referred to as the ABP component of the model.

As stated throughout this work there is a general consensus that the CA is the primary route of communication between ICP and IEP, and hence between ICP and TMD. However, for completeness the possibility of ICP acting through an alternative, perhaps pathological, route of communication between ICP and TMD is included in this work. This contribution of ICP is modelled by including a component directly proportional to the ICP waveform in the complete model. To prevent confusion with the likely route of communication of ICP, via the CA, this pathological route is indicated in the model as P_{path} and referred to as the PathICP component of the model.

2.4.2 Ventilator-driven components

It is believed that respiration might affect the TMD waveform directly and one possible mechanism by which this might occur is through direct communication of airway pressure to TMD, perhaps via the Eustachian tube. In this work direct communication of airway pressure is modelled by including a component directly proportional to the ventilator-driven airway pressure, P_{vent}, in the complete model of TMD and is referred to as the VentP component of the model.

During the first analysis of the experimental TMD data it was hypothesised that there may be a second mechanism by which respiration waves were affecting TMD; through respiration-driven movement of the patient's body. This body movement mechanism might be instead of, or in addition to, airway pressure acting directly on the ear; because of this hypothesis it was decided that airway volume should be included as an additional aspect of the model. It is possible for lung volume data to be measured by the ventilation system during data acquisition, but the set-up used had not allowed for this so instead a mathematical model is used to generate model lung volume data from the experimentally measured airway pressure data. This in turn is used to generate respiration-driven body movement data, M_{vent}, and is referred to as the VentM component of the complete model. The derivation of the mathematical model for body movement now follows.

There is a large body of work concerned with modelling respiration and lung inflation, however, most of it is more complicated than is necessary to model body movement as a function of airway pressure. Because of this a simple mathematical model is used where lung volume and lung pressure (or airway pressure) are related by the following equation[55].

$$P_{lung} = F(V_{lung}) + G(\dot{V}_{lung}) \tag{2.28}$$

Where $F(V_{lung})$ is defined by the static pressure-volume curve of the lungs, and $G(\dot{V}_{lung})$ is dependent on the ability of the lungs to change volume (inflate or

deflate) in response to dynamic changes in pressure. Because the static pressure-volume curve and dynamic properties of lung volume are different for each patient it was decided that a linear approximation would be used for each in this model. Thus the equation used to determine airway volume is

$$P_{lung} = C_v(V_{lung} + \tau_v \dot{V}_{lung}), \tag{2.29}$$

where C_v is a scaling coefficient of static pressure changes and τ_v is the inverse of the time-scale of dynamic volume changes in lung volume (rescaled to remove C_v).

Even though it is believed that the artefact observed in the TMD data is generated by respiration-driven body movement it is reasonable to assume that airway volume is proportional to body movement in this work. This is because chest-wall displacement is proportional to lung volume [29].Thus an equation of the same form is applied for the ventilator-driven movement artefact.

$$P_{vent} = C_m(M_{vent} + \tau_v \dot{M}_{vent}) \tag{2.30}$$

where M_{vent} is body position determined by ventilator-driven airway-pressure, P_{vent}, recorded in the experimental data.

2.5 Complete Model

This section draws together the equations and relationships presented earlier in this chapter to form what will be referred to as the complete model. This occurs first with the coupling of the components of the inner ear model described in sections 2.1 to 2.3 to form a system which can be used to describe the fluid dynamics of the inner ear and its relationship to ICP. Following this all the components outlined in the chapter are then combined to form a model to approximate experimental TMD waveforms and determine the proportion of the TMD waveform provided by each source.

2.5.1 Coupling the inner ear components

To couple the components outlined in sections 2.1 to 2.3 conservation of mass is enforced between each section; first between the CA and the RWM-valve, then between the RWM-valve and the inner ear. This represents the fluid flowing between each space in the inner ear.

In all of these mass flux equations P_{ca} is used interchangeably with $P|_{(z=L)}$ (and vice versa) as the pressure at the end of the CA is the same as the pressure in the inner ear (they are simply different labels applied during the derivation of the model).

Mass flux out of the CA, equation (2.16), must be equal to mass flux through the RWM-valve, equation (2.27), thus $Q_{ca} = Q_{rwm}$ is as follows.

$$\begin{aligned} -\frac{\pi\rho}{8\mu}\left(R_0 + \frac{\kappa_{ca}}{2R_0L\pi}(P|_{(z=L)} - P_{base})\right)^4 \left.\frac{\partial P}{\partial z}\right|_{(z=L)} \\ = \frac{2\rho k A^{1/2}}{9\pi\mu} H^{5/2}(P_{ca} - P_{ie}). \end{aligned} \tag{2.31}$$

Mass flux into the inner ear, equation (2.20), is equal to the mass flux from the RWM-valve, equation (2.27), thus $Q_{ie} = Q_{rwm}$ is as follows,

$$\rho\kappa_{ie}\frac{\partial P_{ie}}{\partial t} = \frac{2\rho k A^{1/2}}{9\pi\mu} H^{5/2}(P_{ca} - P_{ie}). \tag{2.32}$$

This represents mass flux through the system, driven by ICP at one end of the CA into the inner ear at the other end of the system.

Thus the system of equations used to govern the inner ear component of the model is:

$$\frac{\dfrac{\partial}{\partial z}\left(\left(R_0 + \dfrac{\kappa_{ca}}{2R_0L\pi}(P - P_{base})\right)^4 \dfrac{\partial P}{\partial z}\right)}{\left(R_0 + \dfrac{\kappa_{ca}}{2R_0L\pi}(P - P_{base})\right)} = \frac{8\mu\kappa_{ca}}{R_0L\pi}\frac{\partial P}{\partial t} \tag{2.33}$$

with the following conditions:

$$P(z,t) = P_{icp}(t) \quad \text{at} \quad z = 0, \tag{2.34}$$

$$-\left(R_0+\frac{\kappa_{ca}}{2R_0L\pi}(P|_{(z=L)}-P_{base})\right)^4\left.\frac{\partial P}{\partial z}\right|_{(z=L)} = \frac{16kA^{1/2}}{9\pi^2}H^{5/2}(P|_{(z=L)}-P_{ie}), \tag{2.35}$$

$$\frac{\partial P_{ie}}{\partial t}=\frac{2kA^{1/2}}{9\pi\mu\kappa_{ie}}H^{5/2}(P|_{(z=L)}-P_{ie}), \tag{2.36}$$

where H is defined as

$$H=\max\left\{0, H_{typ}+l\frac{k(l^2+H_{typ}^2)}{4lT}(P_{ca}-P_{ie}) + H_{typ}\sqrt{1-\left(\frac{k(l^2+H_{typ}^2)}{4lT}\right)^2(P_{ca}-P_{ie})^2}\right\}. \tag{2.37}$$

Once the above system of equations is solved and the solution for function P_{ie} has been found this can be substituted into global model equation as the IEP. This is referred to as the IEP component of the complete TMD model.

2.5.2 Formulation of the model TMD waveform

The research presented in this work is primarily concerned with the relative contribution of each source in the model TMD waveform. It is for this reason that the output of each model component is normalised before being inserted into the complete TMD model equation and used to produce the model TMD waveform. The normalising process is such that after being normalised all values of a component waveform are between plus and minus one; this is done by dividing each data stream by its maximum absolute value, so that the maximum absolute value of the normalised data stream is equal to exactly one.

The complete TMD model brings together a weighted combination of all the normalised components of the model; ABP (P_{art}), ventilator-driven airway pressure (P_{vent}), ventilator-driven body movement (M_{vent}), ICP acting via IEP (P_{ie}), and pathological sources of ICP (P_{path}).

As indicated in section 2.4 the contributions ABP, ventilator-driven airway pressure, and pathological sources of ICP are taken from the experimental data mea-

sured. They are inserted into the complete model with no mathematical manipulation, other than the simple data preparation (outlined in section 4.4). The respiration-driven body movement data is generated as per the equations set out in section 2.4.2, normalised, and then inserted into the complete model as M_{vent}. The contribution of ICP acting via IEP is introduced through the IEP component of the model which once solved for provides the P_{ie} term in the complete model, the contribution from the IEP component is also normalised.

Thus the complete TMD model, and the function used to generate the model TMD signal, is

$$TMD_{model} = a_0\frac{P_{path}}{|P_{path}|} + a_1\frac{P_{art}}{|P_{art}|} + a_2\frac{P_{vent}}{|P_{vent}|} + a_3\frac{M_{vent}}{|M_{vent}|} + a_4\frac{P_{ie}}{|P_{ie}|} + \delta, \quad (2.38)$$

where a_0, a_1, a_2, a_3 and a_4 are parameters which determine the contribution from components PathICP, ABP, VentP, VentM and IEP respectively; δ is an offsetting parameter used in the optimisation process; and $|P_{path}|, |P_{art}|, |P_{vent}|, |M_{vent}|$ and $|P_{ie}|$ are the normalising factors for each respective model component. The coefficients a_0 through a_4 allow for the contribution of each component of the complete model to be varied, or even suppressed to produce a variety of different cases of the complete TMD model to be considered. In each case considered a selection of the coefficients are varied, along with other parameters within the components of the complete model, in an attempt to achieve the best fit to the experimental TMD data. Details of the optimisation process are outlined in chapter 5.

2.6 Chapter Summary

Within this chapter each component of the physiological system which produces TMD has been analysed and a model formed to represent the key features or effects of each component.

The IEP component was formed of three parts: pressure transfer along the CA (driven by ICP), through the CA-inner ear interface (with valve-like characteris-

tics) and then into the inner ear (a compliant fluid filled chamber). These three parts were coupled through mass flux balance to form the IEP component of the model.

The additional aspects of the model were discussed; arterial blood pressure, ABP, acting directly on the TMD; two ventilator-driven components, one based on direct action from airway pressure on TMD, VentP, the second being an indirect artefact driven by body movement during respiration, VentM; and, lastly, pathological routes of ICP transmission, PathICP (i.e. not communicated via the CA and IEP as is anticipated a typical individual).

Finally all components of the model were normalised and combined to form the complete TMD model, equation (2.38). Thus the model and all components are in a suitable format for further analysis.

In the next chapter the model components will be nondimensionalised, specific model components will be examined for special cases to determine particular characteristics, and finally numerical approximations to the solutions will be obtained for all components so that the complete TMD model can be driven by an experimental data sample.

Chapter 3

Solution Methods

This chapter analyses and attempts to solve or approximate the solutions of the governing equations from the complete model as outlined in chapter 2; the work is presented across three sections.

The first section deals with the nondimensionalisation of the equations in the IEP component of the complete model. The second section applies analytical techniques to systems of ODEs and PDEs generated by taking limits of particular variables in the IEP component of the complete model. These limit-cases are considered in an attempt to provide insight and highlight some typical behaviours possessed by the physical IEP system.

The third section of the chapter applies numerical approximation techniques to the systems of ordinary differential equations (ODEs) and partial differential equations (PDEs) which form the VentM and IEP components of the complete model. These numerical predictions are driven by the ICP, ABP and ventilator-driven airway pressure (VAP) data measured in the clinical study. The output of these numerical approximations are used in the complete TMD equation, along with experimental ABP and airway pressure, to produce a predicted TMD waveform. It is these predicted TMD waveforms which are optimised to the experimental TMD data and from which the majority of the results presented in this work are obtained.

(Details of the optimisation process are presented in chapter 5 of this thesis.)

3.1 Nondimensionalisation of the model

Starting with the dimensional systems of equations (2.33) - (2.37), set out in section 2.5, the system of equations is nondimensionalised. The scaling factors used in the nondimensionalising process are obtained from the geometry of the physical problem. Most scaling factors are taken to be values defined during the formulation of the model in chapter 2 and a brief explanation of each scaling is given here for clarity.

The radius of the CA is scaled with the equilibrium radius of the CA, R_0; the length of the CA is scaled with its length, L. The scaling factor for the width of the RWM valve should be of the same order as the scaling factor for the radius of the CA; for this reason the scale $H_{typ} = R_0$ is used to scale the width of the opening of the RWM valve.

All the pressure changes in the inner ear system are driven by the ICP; for this reason all pressure function are redefined with base pressure removed and the remaining pressure variations are scaled to typical variations in ICP P_0. Because the system is driven by ICP the time scale of the system is also dependent on ICP. The time scale of the system is scaled using the dominating frequency of the ICP waveform; thus scaling factor for time is $\frac{2\pi}{\omega}$, where ω is the dominating frequency of ICP. Below are the scaling factors where a $\tilde{}$ above a letter indicates that it is a dimensionless variable.

$$\begin{array}{cc} z = L\tilde{z} & r = R_0\tilde{r} \\ H = H_{typ}\tilde{H} \qquad \text{where} & H_{typ} = R_0 \\ t = \frac{2\pi}{\omega}\tilde{t} & P = P_{base} + P_0\tilde{P} \\ P_{icp} = P_{base} + P_0\tilde{P}_{icp} & P_{ie} = P_{base} + P_0\tilde{P}_{ie} \end{array} \tag{3.1}$$

Thus the non-dimensional equations are:

$$\left(1+\beta\tilde{P}\right)^{-1}\frac{\partial}{\partial\tilde{z}}\left(\left(1+\beta\tilde{P}\right)^{4}\frac{\partial\tilde{P}}{\partial\tilde{z}}\right)=\alpha\frac{\partial\tilde{P}}{\partial\tilde{t}} \tag{3.2}$$

with

$$\tilde{P}=\tilde{P}_{icp}(\tilde{t}) \quad \text{at} \quad \tilde{z}=0, \tag{3.3}$$

$$\left(1+\beta\tilde{P}|_{(\tilde{z}=1)}\right)^{4}\left.\frac{\partial\tilde{P}}{\partial\tilde{z}}\right|_{(\tilde{z}=1)}=\gamma_1\tilde{H}^{5/2}(\tilde{P}|_{(\tilde{z}=1)}-\tilde{P}_{ie}), \tag{3.4}$$

$$\text{and} \quad \frac{\partial\tilde{P}_{ie}}{\partial\tilde{t}}=\gamma_2\tilde{H}^{5/2}(\tilde{P}|_{(\tilde{z}=1)}-\tilde{P}_{ie}). \tag{3.5}$$

Where

$$\tilde{H}=\max\left\{0\ ,\ 1+\eta_1(\tilde{P}|_{(\tilde{z}=1)}-\tilde{P}_{ie})+\sqrt{1-\eta_2(\tilde{P}|_{(\tilde{z}=1)}-\tilde{P}_{ie})^2}\right\},$$

$$\alpha=\frac{16\omega\mu\kappa_{ca}L}{{R_0}^4}, \quad \beta=\frac{\kappa_{ca}P_0}{2(R_0)^2L\pi}, \quad \gamma_1=\frac{16kA^{1/2}L}{9\pi^2{R_0}^{3/2}}, \tag{3.6}$$

$$\gamma_2=\frac{kA^{1/2}{R_0}^{5/2}}{9\pi^2\omega\mu\kappa_{ie}}, \quad \eta_1=\frac{k(l^2+{R_0}^2)P_0}{4TR_0} \quad \text{and} \quad \eta_2=\frac{k^2(l^2+{R_0}^2)^2{P_0}^2}{16l^2T^2}.$$

The IEP component of the model has 6 parameters that govern its behaviour, they are each identified as lower case Greek letter and act in the following ways. The parameters α and β affect the damping and phase shift of the ICP wave as it propagates along the CA. Here α characterises the ratio of CA wall "stiffness" to fluid viscosity and β characterises the ratio of pressure applied to CA over resistance to deformation. The parameters γ_1 and γ_2 characterise the conductivity of the RWM valve-interface between the CA and the inner ear. They depend on the geometry of the valve and the compliances of the inner ear, and affect the damping and phase shift of the pressure waveform as it propagates from the CA into the inner ear. The parameters η_1 and η_2 dictate the behaviour of the valve arm itself. The parameter η_1 is characterised by the relative length of the valve arm to valve height; dictating the change in flow resistance achieved for a given

change in the angle of displacement. And parameter η_2 is characterised by the typical force applied to the valve arm by the tension in the attached membrane; dictating the valve arm's resistance to displacement caused by pressure difference across the valve.

3.2 Analytical Methods

The system of equations (3.2) - (3.5) is nonlinear and cannot be solved analytically. However, some limiting cases can be solved for analytically and provide insight into the behaviour of the system. One such limiting cases is now considered.

In the limiting case, the compliances of the CA is sufficiently small that displacements of the CA wall are negligible without removing all compliances from the CA, and where tension in the RWM dominates the valve arm position. The small CA wall displacements are represented by the limit $\beta \to 0$. When tension in the RWM dominates the valve arm position, such that the arm position is fixed, $\eta_1 \to 0$ and $\eta_2 \to 0$ i.e. $\tilde{H} = 2$. The remaining equations follow:

$$\frac{\partial^2 \tilde{P}}{\partial \tilde{z}^2} = \alpha \frac{\partial \tilde{P}}{\partial \tilde{t}} \tag{3.7}$$

with

$$\text{at } \tilde{z} = 0 \qquad \tilde{P} = \tilde{P}_{icp}(\tilde{t}) \tag{3.8}$$

$$\text{at } \tilde{z} = 1 \quad -\tfrac{\partial \tilde{P}}{\partial \tilde{z}} = \gamma_1(\tilde{P} - \tilde{P}_{ie}) \quad \text{and} \quad \tfrac{\partial \tilde{P}_{ie}}{\partial \tilde{t}} = \gamma_2(\tilde{P} - \tilde{P}_{ie}) \tag{3.9}$$

This simplified system, equations (3.7) - (3.9), can be solved analytically for P_{icp} of the form $\sin \omega \tilde{t}$.

The solution to the problem where $P_{icp} = \sin \omega \tilde{t}$ produces an output pressure wave (P_{ie}) which is a damped and phase shifted version of the input pressure wave: i.e. $\tilde{P}_{ie}(\tilde{t}) = A(\omega)\tilde{P}_{icp}(\tilde{t} - c(\omega))$. The amplitude damping coefficient, $A(\omega)$, is inversely dependent on the frequency ω, and the phase shift coefficient, $c(\omega)$, is also inversely

dependent on the frequency ω. This means the system acts as a low pass filter on the ICP waveform driving the system, but does not emulate any of the other observed characteristics of the IEP system.

This limiting case could be extended with P_{icp} being formed of linear combinations of sine and cosine functions of a variety of frequencies and this might enable the P_{icp} function to more closely resembled the experimental ICP data. However, the nature of the system is such that no effects, other than damping and phase shift, would be applied and thus no nonlinear effects would be seen. For this reason this limiting case provides little additional insight into the behaviour of the IEP component of the model and is not explored further.

The lack of nonlinear effects within this limiting-case of the IEP component mean it is unlikely to replicate the expected characteristics of the transform from ICP to TMD waveform predicted from experimental results. This indicates that such limit-models where the nonlinear components are removed are unable to produce the desired transmission properties expected of the system.

The expected nonlinear characteristics of the transmission route between ICP and TMD can only be modelled by systems of equations which include appropriate nonlinear components. Such nonlinear equations cannot be easily solved using analytical techniques and so numerical approximations to solutions must be sought instead.

3.3 Numerical Methods

The limiting cases outlined in the previous sections provide useful insight into the general characteristics of the model, however, a main objective of this study is to produce a model which is directly comparable to the experimental data gathered. In this work numerical methods are used to create approximate solutions which are directly comparable with the experimental data. All code was written in cochlea

(CC)s as it was compatible with the data acquisition software and capable of the required optimisation processes (as outlined in chapter 5).

Various finite difference (FD) methods for numerical approximation were considered, but the implicit method of Crank-Nicolson is used because of its characteristic to be convergent, consistent, accurate and stable for most problems.

FD methods involve approximating differential equations with discretized difference equations. The Crank-Nicolson method uses central difference in space and the trapezoidal rule in time. It is an implicit method which means that to obtain the value of the function at the "next time step" a system of simultaneous equations must be solved. The region over which the equations are to be solved is discretized in space and time.

The relative size of the time steps and the space steps in this discretization process is important for some systems of equations; this is because, in general, if the ratio of time step to the square of the space step is large (40 or more) then decaying finite oscillations can be introduced to the solution. In this work the problem of finite oscillations can be overcome because the difference equations are used to approximate a quasi-steady system of differential equations. The system is run for a sufficient number of time steps for the system to exhibit quasi-steady characteristics; by this point any errors associated with the finite oscillations will have decayed to negligible levels. To be certain that finite oscillations do not occur, the ratio of time step relative to space steps is maintained at less than the effective diffusivity of the system, $\frac{\alpha}{(1+\beta P)^3}$, for all numerical approximations carried out in this work. (The effective diffusivity is obtained by balancing the order of terms in equation (3.10), below.) The full outline of the Crank-Nicolson FD method can be found in [54]; the work presented here uses the methods outlined in this text, unless otherwise specifically stated.

FD methods require initial conditions from which the system can start. For this work the initial condition used is that the pressure starts at a baseline pressure of

zero throughout the system; this is represented by $\mathbf{p}_i^{n=0} = P_{base}, \forall i$. To accurately represent the quasi-steady solution, and reduce any anomalies related to the initial conditions, the system is run across two identical cycles of the experimental data sample placed 'back to back'. (The data sample is chosen such that the start and end values are suitable for this process.) The second half of the resulting numerical output is stable and appears to accurately represent the quasi-steady solution for the system. The first half of the output is then disregarded and the remaining data used as the output of the IEP component of the model.

The governing equation of the fluid flow in the IEP model, (3.2), can be rearranged to the following form

$$4\beta\left(1+\beta\tilde{P}\right)^2\left(\frac{\partial\tilde{P}}{\partial\tilde{z}}\right)^2+\left(1+\beta\tilde{P}\right)^3\frac{\partial^2\tilde{P}}{\partial\tilde{z}^2}-\alpha\frac{\partial\tilde{P}}{\partial\tilde{t}}=0$$

and thus the FD approximation to the governing equation using Crank-Nicolson is as follows

$$\begin{aligned}
&\frac{\beta\epsilon}{2}\left(1+\beta\mathbf{p}_i^{n+1}\right)^2\left(\mathbf{p}_{i+1}^{n+1}-\mathbf{p}_{i-1}^{n+1}\right)^2\\
&+\frac{\epsilon}{2}\left(1+\beta\mathbf{p}_i^{n+1}\right)^3\left(\mathbf{p}_{i+1}^{n+1}-2\mathbf{p}_i^{n+1}+\mathbf{p}_{i-1}^{n+1}\right)\\
&+\frac{\beta\epsilon}{2}\left(1+\beta\mathbf{p}_i^{n}\right)^2\left(\mathbf{p}_{i+1}^{n}-\mathbf{p}_{i-1}^{n}\right)^2\\
&+\frac{\epsilon}{2}\left(1+\beta\mathbf{p}_i^{n}\right)^3\left(\mathbf{p}_{i+1}^{n}-2\mathbf{p}_i^{n}+\mathbf{p}_{i-1}^{n}\right)\\
&-\alpha\left(\mathbf{p}_i^{n+1}-\mathbf{p}_i^{n}\right)=0\ ,
\end{aligned}\tag{3.10}$$

where ϵ denotes $\dfrac{\delta t}{(\delta z)^2}$, $\mathbf{p}$ denotes the numerical approximation to $\tilde{P}$, ^{n} denotes the time index, and $_i$ denotes the position index which runs from $i = 1$ (ICP interface, $z = 0$) to $i = N$ (the section of CA interfacing with the RWM, $z = 1$). The discrete step in time, δt, and the discrete step in space, δz, are used to form the difference equations which approximate derivatives in time and space respectively.

Note that the entire equation has been written at each time step and then averaged in time; an alternative to this would be to inserting time-averaged values into the difference equation. In a linear equation there would be no difference in the solution

of these two methods, however, since these equations are nonlinear there might be small differences between the solutions when they are solved. However, these differences are negligible and not discussed further here.

When the Crank-Nicolson FD scheme is applied to the remaining equations in the system (3.2) - (3.6) the following FD equations result.

Equation (3.3) at $\tilde{z} = 0$ is represented as

$$\mathbf{p}_0^{n+1} - \tilde{P}_{icp}((n+1)\delta t) = 0 \tag{3.11}$$

and at $\tilde{z} = 1$ the two boundary conditions use derivatives and thus a fictitious point $N+1$ is introduced. To represent the inner ear in the numerical scheme an additional entry, IE, is also included. Thus the following are finite difference approximations for equations (3.4) to (3.5)

$$\frac{1}{2\delta z}\left(1+\beta\mathbf{p}_N^{n+1}\right)^4\left(\mathbf{p}_{N+1}^{n+1}-\mathbf{p}_{N-1}^{n+1}\right) = \gamma_1\tilde{H}^{5/2}\left(\mathbf{p}_N^{n+1}-\mathbf{p}_{IE}^{n+1}\right) \tag{3.12}$$

and

$$\frac{1}{\delta t}\{\mathbf{p}_{IE}^{n+1}-\mathbf{p}_{IE}^{n}\}-\frac{\gamma_2}{2}\left(\tilde{H}^{n+1}\right)^{5/2}(\mathbf{p}_N^{n+1}-\mathbf{p}_{IE}^{n+1})-\frac{\gamma_2}{2}\left(\tilde{H}^{n}\right)^{5/2}(\mathbf{p}_N^{n}-\mathbf{p}_{IE}^{n}) = 0 \tag{3.13}$$

where

$$\tilde{H}^{n+1} = \max\left\{0\ ,\ 1+\eta_1(\mathbf{p}_N^{n+1}-\mathbf{p}_{IE}^{n+1})+\sqrt{1-\eta_2(\mathbf{p}_N^{n+1}-\mathbf{p}_{IE}^{n+1})^2}\right\} \tag{3.14}$$

and equivalent for H^n.

All these equations are nonlinear in $\mathbf{p}^{n+1}$ terms (as was noted with the finite difference approximation to the governing equation) and so the system cannot be solved for $\mathbf{p}^{n+1}$. Because of this a further iterative process must be used to approximate the nonlinear system of difference equations with a linear system. Relaxation methods were considered, but not used as a fixed point iteration procedure is sufficient in this case. Newton and quasi-Newton methods could also have been used, but it

was established that the extra computational cost these procedures would enforce is unnecessary.

The FD equations, with iterative approximation terms being denoted by $\mathbf{p}^*$, are

$$\begin{aligned}
&\frac{\beta\epsilon}{2}\left(1+\beta\mathbf{p}_i^*\right)^2\left(\mathbf{p}_{i+1}^*-\mathbf{p}_{i-1}^*\right)\left(\mathbf{p}_{i+1}^{n+1}-\mathbf{p}_{i-1}^{n+1}\right)\\
&+\frac{\epsilon}{2}\left(1+\beta\mathbf{p}_i^*\right)^3\left(\mathbf{p}_{i+1}^{n+1}-2\mathbf{p}_i^{n+1}+\mathbf{p}_{i-1}^{n+1}\right)\\
&+\frac{\beta\epsilon}{2}\left(1+\beta\mathbf{p}_i^n\right)^2\left(\mathbf{p}_{i+1}^n-\mathbf{p}_{i-1}^n\right)^2\\
&+\frac{\epsilon}{2}\left(1+\beta\mathbf{p}_i^n\right)^3\left(\mathbf{p}_{i+1}^n-2\mathbf{p}_i^n+\mathbf{p}_{i-1}^n\right)\\
&-\alpha\left(\mathbf{p}_i^{n+1}-\mathbf{p}_i^n\right)=0
\end{aligned} \tag{3.15}$$

$$\mathbf{p}_0^{n+1}-\tilde{P}_{icp}(\tilde{t}=(n)\delta t)=0 \tag{3.16}$$

$$\begin{aligned}
&\frac{1}{4\delta x}\left(1+\beta\mathbf{p}_N^*\right)^4\left(\mathbf{p}_{N+1}^{n+1}-\mathbf{p}_{N-1}^{n+1}\right)+\frac{1}{4\delta x}\left(1+\beta\mathbf{p}_N^n\right)^4\left(\mathbf{p}_{N+1}^n-\mathbf{p}_{N-1}^n\right)\\
&+\frac{\gamma_1}{2}\left(\tilde{H}^*\right)^{5/2}\left(\mathbf{p}_N^{n+1}-\mathbf{p}_{IE}^{n+1}\right)+\frac{\gamma_1}{2}\left(\tilde{H}^n\right)^{5/2}\left(\mathbf{p}_N^n-\mathbf{p}_{IE}^n\right)=0
\end{aligned} \tag{3.17}$$

and

$$\frac{1}{\delta t}\{\mathbf{p}_{IE}^{n+1}-\mathbf{p}_{IE}^n\}-\frac{\gamma_2}{2}\left(\tilde{H}^*\right)^{5/2}\left(\mathbf{p}_N^{n+1}-\mathbf{p}_{IE}^{n+1}\right)-\frac{\gamma_2}{2}\left(\tilde{H}^n\right)^{5/2}\left(\mathbf{p}_N^n-\mathbf{p}_{IE}^n\right)=0 \tag{3.18}$$

with

$$\tilde{H}^*=\max\left\{0\ ,\ 1+\eta_1(\mathbf{p}_N^*-\mathbf{p}_{IE}^*)+\sqrt{1-\eta_2(\mathbf{p}_N^*-\mathbf{p}_{IE}^*)^2}\right\} \tag{3.19}$$

At each time step of the FD process the fixed point iteration process is run. The first run is with $\mathbf{p}^*=\mathbf{p}^n$; subsequent iterations use the solution of the previous iteration in the substitution $\mathbf{p}^*=\mathbf{p}^{n+1}$. This process is repeated until a required accuracy is obtained or until a limit on the number of iteration is reached; at which point the numerical approximation procedure terminates. For the work presented in this thesis the limit on the number of fixed point iterations per time step is 100. The required accuracy is a 0.001% difference defined with the following error function

$$\frac{Abs(\mathbf{p}^*-\mathbf{p}^{n+1})}{Abs(\mathbf{p}^{n+1})+10^{-20}} \tag{3.20}$$

where $+10^{-20}$ is included in the denominator to prevent "divide by zero" errors in the numerical code. Once the desired accuracy is achieved in the fixed point iteration process the numerical approximation procedure returns to the main iterative Crank-Nicolson process.

Convergence and stability cannot be proven for many nonlinear FD systems; because this system is not a standard system a proof is not attempted here. However, examination of the numerical code showed that the system appears to be stable and convergent.

The ventilator-driven movement component of the complete model must also be approximated numerically. The numerical approximation for the VentM equation, (2.30), is also performed with a forward difference FD method; because it is a linear ODE and its time scale is less than that of the IEP model this is sufficient. $\mathbf{P}_{vent}^{n+1} = \mathbf{M}_{vent}^{n+1} + \tau_v \frac{1}{\delta t}(\mathbf{M}_{vent}^{n+1} - \mathbf{M}_{vent}^{n})$, where $\mathbf{P}_{vent}^{n}$ and $\mathbf{V}_{vent}^{n}$ are vectors where each term is the value of P_{vent} and V_{vent} at that time step n. The initial condition used in the VentM model is that the ventilator-driven movement artefact is initially at the same level as the ventilator-driven airway pressure, i.e. $\mathbf{M}_{vent}^{n} = \mathbf{P}_{vent}^{n}$ for $n = 0$.

The results of the numerical approximations of the IEP and VentM models are substituted into the complete TMD model. This is the model used in the remainder of this work and is optimised to the experimental TMD data.

3.4 Chapter Summary

In this chapter the governing equations for the components of the complete TMD model have been nondimensionalised. Special cases of the IEP component were then examined to highlight particular behaviours exhibited by the physical system. Insight gained from this was limited to observing damping and phase-shifting of the waveform, however, as a result an additional case was found that might be

considered for future work.

Following this numerical approximations were established for all components of the model using the implicit finite difference method of Crank-Nicholson, including a fixed point iteration process to approximate the nonlinear terms of the system.

The result of this is a system of numerical approximations to the ODEs and PDEs of the IEP and VentM model components of the complete TMD model. These numerical approximations will be driven by experimental data streams (ICP and ventilator-driven airway pressure (VAP)) and combined with the direct ABP and VAP data, to produce the complete TMD model waveform output. It is this complete TMD model waveform that will be compared to the simultaneously recorded TMD data sample, and then in turn optimised to the recorded TMD data sample. Details of the optimisation process are presented in chapter 5 of this thesis, following the chapter 4 which explains the data acquisition and preparation processes.

Chapter 4

Data Acquisition

This chapter outlines the actions taken to set up the clinical research study and data acquisition process which produced the experimental data required for the TMD modelling process. The material presented in sections 4.1 and 4.2 is a summary of work jointly conducted by Dr A.A. Birch, Dr R.J. Marchbanks and myself; the material presented in section 4.3 is a summary of works conducted by Dr A.A Birch and R.J. Marchbanks; and section 4.4 is a summary of my own data preparation process.

The first section, 4.1, summarises the patient recruitment process and briefly explains the motivations for each of the study's selection criteria. Sections 4.2 and 4.3 outline the equipment used in the data acquisition process and the measures taken to ensure all data stream are simultaneous. The final section, 4.4, explains the post-acquisition data handling that is carried out so that the experimental data can be used in the numerical modelling process, the results of which this work focuses on.

The purpose of the clinical study is to collect simultaneous invasive ICP and non-invasive TMD measurements (both passive and active). The data collected in the study is used to increase the level of understanding of the relationship between ICP and TMD and take a further step towards reliable assessment of ICP non-

invasively via the ear. In the work presented here this is achieved through the mathematical modelling of TMD data.

Simultaneous ICP and TMD measurements had not been collected before this research project. A few similar measurements had been recorded, but these measurements could not be used in the mathematical modelling in this work for the following reasons: The data streams were not synchronised to sufficiently accuracy in time, and only the TMD and ICP data had been collected; other useful data, such as respiration data or arterial blood pressure (ABP) data, had not been recorded. For this reason the data collected in the clinical trials form an integral part of the research presented in this thesis.

4.1 Research Outline and Set-up

The material in the following sections is included as it was carried out as part of the work for this thesis and is included for completeness. It relates to project setup and administration, and indicates that best practice for clinical trials was adhered to.

All the procedures and protocol for this research were agreed, and set up in collaboration, with the clinicians treating the patients.

The research project has been approved as valuable and scientifically valid by an independent peer review panel within the hospital; the Clinical Services Directorate peer review panel.

It has also been approved as ethical by the Southampton and South West Hampshire local regional ethics committee (Southampton & South West Hampshire Research Ethics Committee B).

The research project was originally drawn up to be a pilot study, but due to the longer than anticipated time it took to obtain confirmed approval from the

appropriate ethics committee, it was decided that the study should be extended and used as the main source of data for the work presented in this thesis.

In addition to collecting direct ICP and TMD measurements the research study also collects additional simultaneous measurements which are valuable in the study of TMD techniques. These additional measurements are a middle ear analysis, arterial blood pressure (ABP) data and respiration data. A middle ear analysis is done to check the integrity of TMD measurements which can be distorted by abnormalities in the middle ear anatomy. ABP is measured because it is a potential source of the TMD waveform and this research aims to determine if ABP acts on TMD through a direct mechanism or indirectly through ICP. Respiration data is collected because respiratory waves are a source of ICP and distortion of TMD must be ruled out. At the commencement of the project only airway pressure is recorded, but in future the respiration measurements recorded may be altered to include airway volume or other respiration related measurements in addition to or in place of airway pressure. Carbon dioxide levels in the blood are also measured, but this data is not analysed as part of the research in this thesis.

When choosing which patient groups to recruit, gathering data from minors was considered. There are various difficulties when including minors in a research study such as this - where the target patient group for the study are in a serious condition - but because of the known negative correlation between the patency of the CA and the age of a patient the study obtained ethical approval to include minors in addition to adults.

In order to be able to collect the data required for this research study in an ethical manner all potential patients must meet certain criteria to considered in this trial. These criteria range from patient ages to particular strategies of clinical management; a summary of the criteria used in this research study follows.

Patients can be recruited if they are aged between 4 and 18, being treated in the Paediatrics Intensive Care Unit (PICU) or between 16 and 70, being treated in the

Neuroscience Intensive Care Unit (NICU) (there is some overlap between wards). Patients outside this age range are excluded either because the equipment used in this study is not suitable to be used on them or because of the increased risk of CA blockage.

Measurement of direct ICP and ABP are invasive procedures, to obtain these important data sets ethically only patients who are having these measurements taken as part of their routine clinical management can be included in this study. To monitor breathing the patient must be on a ventilator and unconscious; thus only patients for whom this is part of their routine clinical management can be included in the study. Patients who have suffered trauma that may have compromised the structure of their ear (inner, middle or outer) are excluded from the study as such injuries may affect the integrity of the TMD measurements.

A full, comprehensive list of inclusion and exclusion criteria is contained in the full research project protocol which is included in the appendices of this thesis.

Normally for a patient to take part in a research project their informed consent must be obtained. However, since the nature of this research project requires patients who are unconscious to gather data consent can rarely obtained; and if it were there might be questions as to whether the patient was capable of giving informed consent. Instead this project was granted permission to approach the next of kin of each patient and obtain informed consent from them and also informed assent that the next of kin believed that if the patient were conscious they would agree to take part in the research project. A copy of the information sheet provided to relatives is included in the appendix of this thesis.

Once a patient has been identified by the clinicians an appropriate opportunity to approached the relatives about the research project is arranged. If informed consent and assent is obtained then an appropriate time for data acquisition is arranged.

4.2 Acquisition Process

This study is conducted on patients whom all invasive measurements are performed as a part of their clinical therapy. Because of this some data is collected by hospital patient monitoring systems and then sent to our data acquisition computer. ICP was monitored with an extracranial strain gauge transducer with short fluid filled catheter coupling (TruFlow, Edwards Lifesciences, Washington DC). ABP was measured from the radial artery with a standard fluid filled catheter linked strain gauge transducer (TruFlow, Edwards Lifesciences, Washington DC). Both ICP and ABP systems are monitored using a Marquette patient monitoring system and it is from this that the data is acquired. TMD was measured with the MMS-11 Cerebral and Cochlear Fluid pressure Analyser (Marchbanks Measurement Systems Ltd, Lymington, UK). All three analogue signals were sampled with 12 bit resolution at a rate of 125 points per second. Airway pressure was recorded from the 125Hz digital output of the ventilator (Evita 2, Drager Medical, Lubeck, Germany) and used to time the analogue channel recording.

During the data acquisition and analysis process it was discovered that the Marquette patient monitoring system applies a filter to the data before outputting it to the acquisition computer.

The filter is a form of low-pass filter; as well as altering the waveform of each data stream, the application of this filter introduces a delay to the data stream before it is output to the data acquisition computer. The delay introduced by the Marquette patient monitoring system is dramatically reduced when cut-off frequency of the filter is raised from 12Hz to 40Hz. However, this is not precise enough to conduct the planned mathematical analysis, as it is required that data points be sampled simultaneously, and further analysis of the data acquisition system is required to ensure the integrity of the data acquired.

In order to re-adjust the data, and remove the time delay introduced by the Mar-

quette's filter process, the frequency response of the Marquette monitoring system needed to be known. Unfortunately this study required technical specifications the level of which was not available from the manufacturer, and thus our research group had to examine the transducers and Marquette patient monitoring systems itself.

Such analysis for the MMS-11 Cerebral and Cochlear Fluid pressure Analyser (MMS-11 analyser), and the Evita 2 Ventilator are not required. For the TMD data this is because the MMS-11 analyser outputs the raw TMD data without any post acquisition processing. For the Ventilator data this is because the Evita 2 system is driving the airway pressure, not simply monitoring it, thus there is no delay in the signal. Neither of these two pieces of equipment are connected to the Marquette monitoring system, and so its filter is not applied to them.

4.3 Frequency Response Analysis

This section is the summary of works carried out by Dr A. Birch and Dr R. Marchbanks. All data and figures were provided and analysed by them. The information presented here was exchanged in private communications and is reproduced with their permission.

In this study ICP was measured with either an extracranial "TruWave" strain gauge pressure transducer from Edwards Lifesciences or an intraventricular Camino MicroVentricular Bolt Pressure Monitoring Kit from Integra Neurosciences. Arterial Blood Pressure is measured from the radial artery with a "TruWave" strain gauge pressure transducer from Edwards Lifesciences.

The natural frequency of the TruWave pressure transducer is specified as > 200Hz. When used at the end of a prescribed narrow bore rigid catheter of length 1.2m the systems natural frequency is 40Hz. When used for Intracranial pressure measurements a much shorter narrow bore rigid catheter is used and therefore a natural

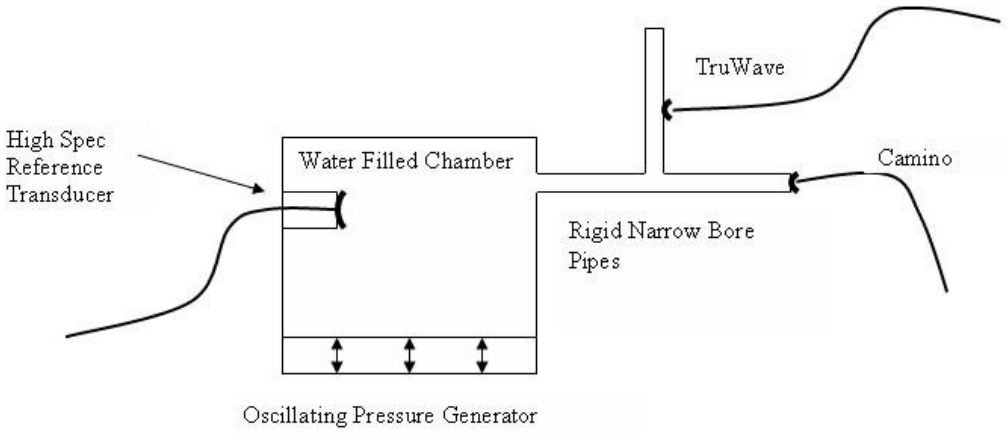

Figure 4.1: System set-up.[7]

frequency well in excess of 40Hz is expected. Arterial blood pressure measurements are made with the prescribed catheter and are therefore expected to have a natural frequency of 40Hz. The Camino catheter tipped transducer is specified as having frequency cut off at approximately 100Hz (-3db point).

Both measurements are recorded using a Marquette patient monitoring system that filters the signals with a low pass filter, this is set to 12Hz during routine patient monitoring but increased to 40Hz for collection of the most recent and all future study data. Both transducers were connected to a frequency generator as illustrated in figure 4.1.

Outputs from all three transducers were recorded simultaneously while the pressure generator was driven sinusoidally with a range of frequencies from 0.5Hz to 60Hz. The reference transducer output was connected directly to the data acquisition system, the two medical transducers were connected after filtering by the Marquette monitoring system. The sampling interval was 125Hz. The amplitude and phase at the driven frequency were determined for all three transducers using the FFT function in MatLabs. The gain was determined for the two clinical

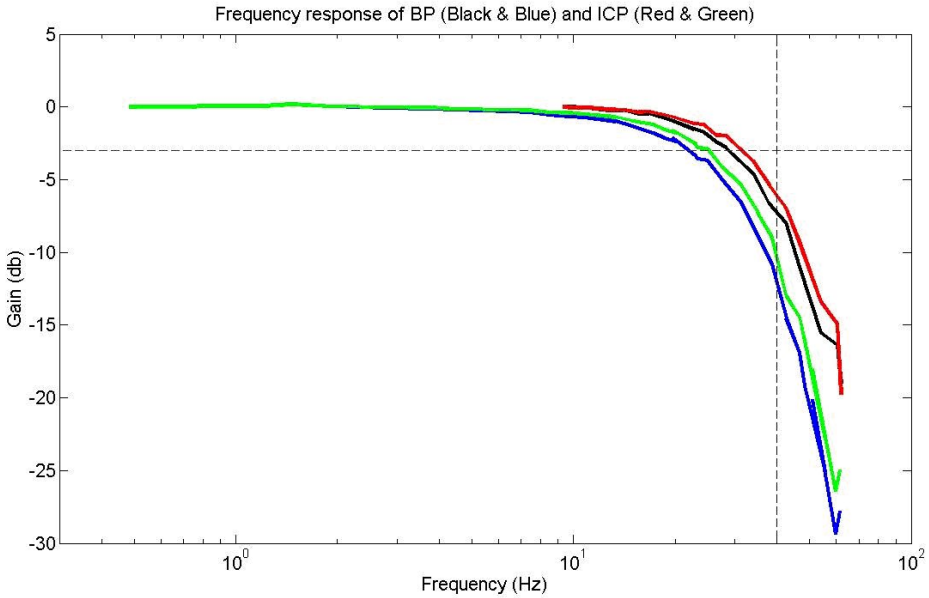

Figure 4.2: Gain Response. Horizontal and vertical dashed lines show -3 db and 40 Hz respectively. Blue and Green are the results of the first run; the Red and Black are the results of the second run with altered mean pressure [7].

transducers using equation 4.1.

$$\text{Gain} = 20\log_{10}\left\{\left(\frac{A_{clin}}{A_{ref}}\right) \times \left(\frac{A^{cal}_{ref}}{A^{cal}_{clin}}\right)\right\} \tag{4.1}$$

$$A_{clin} = \text{Amplitude of clinical transducer,}$$
$$A_{ref} = \text{Amplitude of reference transducer}$$
$$\text{and}$$
$$A^{cal} = \text{Amplitude at the calibration frequency (lowest frequency measured.)} \tag{4.2}$$

The phase response was determined by subtracting the phase of the clinical transducer from the phase of the reference transducer. The frequency response of gain and phase are shown in figures 4.2 and 4.3 respectively. The amplitude response is as expected for a low pass filtered system with a smooth roll off and no evidence of resonance or ringing. The two transducers have very similar responses.

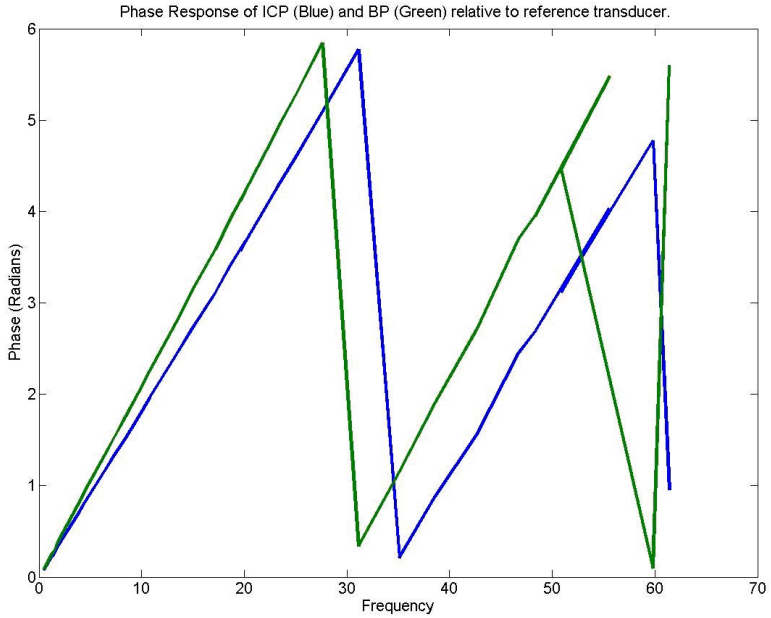

Figure 4.3: Phase Response. Blue indicates the ICP and the green indicates ABP.[7]

This suggests that the monitoring system's "40Hz" filter dominates the amplitude response. The results indicate that 40Hz corresponds to the 10db point rather than the more commonly quoted 3db point. The 3db point appears to be in the order of 30Hz.

The measurements were repeated after flushing through the system and setting a different value for the mean pressure. These results are the black and red plots shown in figure 4.2. The second set of results are very similar in shape but shifted slightly along the frequency scale. The reasons for the shift are not clear although the lower limit of frequency tested was higher and therefore the calibration gain of 1 was determined near to 10Hz as oppose to 0.5 Hz in the first run. This will have contributed to the shift on the frequency scale but no attempted has been made to estimate if this is the full explanation.

The phase response is not as expected. There is a large linear increase in phase as frequency increases. This is characteristic of a delay. The gradient of the slope

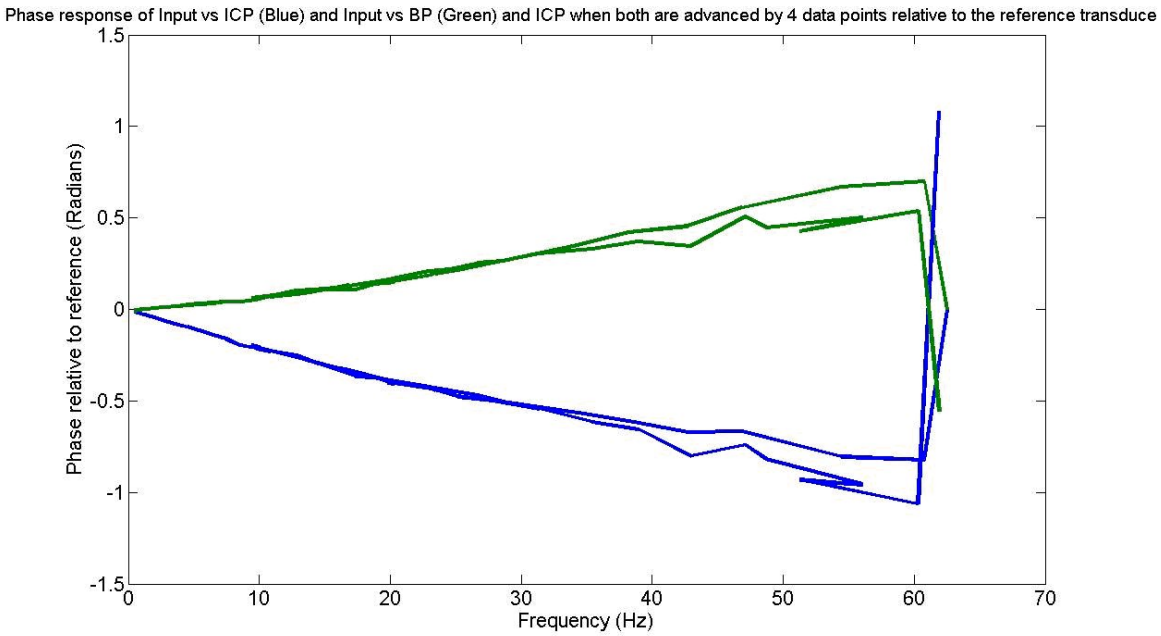

Figure 4.4: Phase Response with partial delay correction. Blue indicates the ICP and the green indicates ABP.[7]

suggests a delay of approximately 30-40ms corresponding to 4 - 5 data points. The phase response was recalculated with the medical transducers shifted forwards in time by 4 data points relative to the reference. The result, shown in figure 4.4, indicates that the ICP is now ahead of the reference while the BP lags slightly behind. The error in both cases is within 1 data point. Disregarding the slope due to this minor synchronization error there does not appear to be any significant phase distortion up to 50Hz. These results suggest that in addition to applying a 40Hz low pass filter the Marquette monitoring system adds a short delay in the order of 30-40 ms. The delay is slightly different for the different data channels; which channel is ICP and which is used for BP may alter from one patient to the next. Advancing the ICP & BP by 4 data points relative to the other channels would seem to be the best compromise.

4.4 Post-acquisition Data Preparation

Once the initial data acquisition process is complete all the data from that acquisition session is stored in one or several large files; at this stage the data is not in a condition suitable for use in the mathematical modelling process. This section outlines the processes used to prepare the data for use in the mathematical modelling process.

The first task in preparing the data for use in the mathematical modelling process is to select a suitable section of data from the main data acquisition file. A section of data is deemed suitable if it is at least 10 seconds in length and all signals are stable and uninterrupted over the entire interval. The longest suitable section is prepared first. Because TMD is approximately periodic the sample section is chosen to match this period; thus the sample can also be assumed periodic.

The next step in the preparation process is to align all data streams so that they are simultaneous. As outlined in section 4.3 the direct ICP and ABP signals suffer

a small delay; this delay is compensated for by adjusting the direct ICP and ABP data steams forward in time by four data points.

TMD measurements sometimes suffer from drift during data acquisition; it is unclear what causes this drift since it varies from measurement to measurement. To minimise the drift on the TMD data stream, TMD measurements are limited to 20 seconds in length. Over a period of 20 seconds or less the drift appears to be linear, although there have been indications on some longer data samples that it may be quadratic or exponential. The drift on the data sample analysed as part of the work presented in this thesis is sufficiently stable for linear drift to be assumed.

To counter any problems introduced by drift the TMD data samples are "detrended". The detrending process is simply the removal of the first and second moments from the data stream (i.e. removal of the mean value and the linear line of best fit so that the wave form oscillates about the origin throughout the sample). To conserve consistency and remove any longer term effects recorded in the data all of the data streams are detrended.

The final stage of the data preparation process is to normalise each data stream, such that all values are between plus and minus one. This is done because the research presented here is concerned with the relative proportion that each source contributes to the TMD signal. The normalising process consists of dividing all elements of the data stream by the maximum absolute value of the elements of that data stream, such that the maximum absolute value within each normalised data stream is exactly one.

Once the preparation process is complete the data is fit for use in the mathematical modelling process.

Analysis of the original TMD data used in this study showed there was significant noise on the data; this was due to earthing problems between the MMS-11 Analyser and the data acquisition computer. TMD data with reduced levels of noise is required for the optimisation process to be reliable.

The problem of noise on the TMD signal can be partially overcome by applying an averaging filter to the TMD waveform to remove the noise. However, because the averaging filter also removes a large proportion of the variations of the TMD waveform, particularly at the peaks and troughs, this has been deemed unacceptable as such variations are an important characteristic of the TMD waveform [38].

Instead less noisy data was acquired directly from the MMS-11 Analyser's storage system. The data stored on the MMS-11 Analyser is sampled at 500Hz, opposed to the 125Hz sample rate of the data acquisition computer, and is not synchronised with the other data signals during the acquisition process. For the data to be used in the mathematical modelling process it must be first synchronised with the other data streams and then interpolated to a 125Hz sample frequency. Synchronisation is carried out post acquisition in two stages: each data sample is time stamped in the MMS-11 Analyser and this is used to indicate which section of the raw acquisition data it is related to, the synchronisation is then complete by overlaying the MMS-11 Analyser data with the raw data from the data acquisition and matching key features of the waveform. Because the sample frequency is being reduced linear interpolation is sufficient, and is used to change the sample frequency from 500Hz to 125Hz. The data is then detrended and normalised in the same manner as the other data streams outlined above.

4.5 Data Limitations

Data samples were collected from a total of seven patients over the course of this project. However, as described throughout this chapter, there were significant obstacles which caused significant delays during the study and rendered many datasets unusable. The first four patients data samples were unusable, due to the effects of the automatic data processing of the Marquette patient monitoring system. The next set of data from a patient was unusable due to unintentional

interference from a member of staff in the NICU.

The data acquired from the sixth patient was acceptable and is the data used throughout this thesis. The data from the seventh patient was not acquired in time for a full analysis to be conducted and as such was not able to be include in this thesis.

It is as a direct result of the challenges and delays experienced during experimental data acquisition process that the data analysed in this thesis is from a single patient only. This is a significant shortcoming of this research, however, cannot be avoided at this time.

4.6 Chapter Summary

This chapter outlined the set up of the clinical research study, and data acquisition process, through which the experimental data required for the TMD modelling process were produced. This includes the measures taken to ensure data integrity, along with the data preparation process required to ensure the experimental data is suitable for use in the numerical TMD model. The limitations of available data were also highlighted; in particular the fact that data from only one patient has been analysed due to the difficulties of obtaining suitable data samples.

The next chapter, Parameter Estimation, discusses the process applied to the numerical model, driven by the experimental data, to optimise the numerical TMD model components to the experimental TMD data sample. This is conducted in order to estimate the values for parameters in the model which cannot be measured at this time.

Chapter 5

Parameter Estimation

Within the complete model there are several parameters and their values are, in general, unknown for any specific patient. These are condensed into 13 parameters within various components of the complete TMD model as outlined in Chapters 2 and 3; a_0, a_1, a_2, a_3, a_4, δ, τ_v, α, β, γ_1, γ_2, η_1, and η_2. It is a goal of this research to investigate what parameter values provide a reasonable prediction of experimental TMD data; using a model driven by experimental ICP, ABP and or ventilator (airway pressure or volume) data. Investigation of possible parameter values is conducted by optimising various cases of the complete TMD model to experimentally measured TMD data. The purpose of this chapter is to outline a selection of optimisation processes which can be used to estimate parameter values, by fitting such cases of the complete TMD model to experimental TMD data.

The parameter estimation problem in this work has been considered in the context of seeking to find the optimal parameter values that fit the TMD model to the available data sample. To this end, the parameter estimation process is presented as an optimisation problem from hereon.

Optimisation is a well established area within mathematics. The structure of a general optimisation problem (GOP) and general background information on optimisation is outlined below in section 5.1 of this chapter. Each aspect of the

parameter estimation problem considered in this work is discussed according to the structure of the GOP. Possible methods of optimisation are discussed, followed by an outline of how these methods are implemented for parameter estimation in this research. Many of the methods outlined in this chapter are covered in the textbook "Practical Methods of Optimization" by R. Fletcher (1987); further detail on each subject gain be obtained in the original textbook [21]. Material not covered in this text is referenced separately.

For parameter estimation to be possible, through optimisation of the numerical TMD model to the experimental TMD data, the output from the numerical TMD model must be directly comparable to the experimentally measured TMD data. In order that the model output is comparable to experimental data, they must both be stored in same format. The experimental data is stored as a vector, **ED**, with components $ED_i, \quad i = 0...M$ being the measurements taken at a sample rate of 125Hz . For this reason the model output is stored in the same vector format as the experimental data; **MO** with corresponding entries for each time step $MO_i, \quad i = 0...M$.

5.1 Background information

Optimisation problems are normally presented in a general framework, in this chapter that framework is defined as the general optimisation problem (GOP). This section outlines the GOP and explain each aspect such that the parameter estimation problem considered in this work can be presented and discussed using the framework of the GOP.

Optimisation techniques are used to find a set of design parameters that minimizes an objective function representing the difference between some desirable data and the data produced by the model being optimised; in this work the desirable data are the experimentally measured TMD data. The optimisation process can include

additional limits on the parameter values; these can take the form of upper bounds, lower bounds, equality conditions and or inequality conditions that the parameter values must satisfy.

The GOP is defined to be of the following form

$$\min_{x} \; f(x) \tag{5.1}$$

subject to

$$\begin{aligned} G_i(x) &= 0, && i = 1, \ldots, m_e \\ G_i(x) &> 0, && i = m_{e+1}, \ldots, m \\ (x_l)_i &< x_i < (x_u)_i && i = 1, \ldots, n, \end{aligned} \tag{5.2}$$

where $x = \{x_1, x_2, \ldots, x_n\}$ is the set of parameters being optimised; $x_l = \{(x_l)_1, (x_l)_2, \ldots, (x_l)_n\}$ is the set of lower bounds on the parameters; $x_u = \{(x_u)_1, (x_u)_2, \ldots, (x_u)_n\}$ is the set of upper bounds on the parameters; $f(x)$ is the objective function which returns a scalar value indicating the measure of fit; $G_i(x) = 0$ $(i = 1, \ldots, m_e)$ are equality constraints and $G_i(x) > 0$ $(i = m_{e+1}, \ldots, m)$ are inequality constraints such that when $G(x)$ is evaluated it returns a vector of length m containing the values of the equality and inequality constraints evaluated at x.

An efficient and accurate solution of the GOP depends partly on the size of the problem, in terms of the number of constraints and design parameters, and the starting parameters of the optimisation. However, the characteristics of the objective function and constraints applied to the optimisation have considerable effect as they restrict which optimisation methods can be used. When an objective function is linear and the constraints are linear, or an objective function is quadratic and the constraints are linear there are reliable solution procedures readily available, these problems are referred to as linear programming (LP) or quadratic programming (QP) problems respectively. When an objective function and or constraints are nonlinear functions of the design parameters the problem is referred to as a

nonlinear programming (NP) problem and is more difficult to solve. The solution of the NP problem generally requires an iterative procedure to establish a direction of search at each major iteration of the optimisation process. This is usually achieved by the solution of a LP, a QP or an unconstrained subproblem.

5.2 Objective Functions

For an optimisation problem to be complete and fit within the framework of the GOP it requires an objective function representing the difference between the model data and the ideal data. This section discusses the objective functions considered as part of the optimisation of parameter estimation carried out in this research.

For optimisation of the TMD model to the experimental TMD data in parameter estimation to be effective, an appropriate objective function must be used. Such an objective function should quantify the differences between the experimental data and the model output in a way that ensures the main properties of the TMD are captured and to make the process of minimisation as simple and efficient as possible. This section examines several objective functions that could be used in the parameter estimation process.

Objective functions can be formed to perform one task or many; thus an objective function can be formed of only a single measure of error or a weighted sum of different error measures. A weighted sum of error functions can be used to form objective functions which can manipulate multiple characteristics of the model during a single optimisation process rather than each component being optimised independently in turn. The weighting allows appropriate levels of influence to be placed on each measure of error within the objective function, so that functions which monitor minor fit characteristics do not have to be removed to prevent a disproportionate influence on the parameter estimation process.

The following functions are considered for use in the optimisation of the parameter estimation process and can be used as objective functions in their own right or as part of a weighted sum for a more complex objective function. All the objective functions considered in this research are nonlinear functions of the design parameters and as such all optimisations problems in this work are NP problems.

A standard measure of error is the L2 norm or root mean square error (RMSE). In this work the first measure of difference between **ED** and **MO** considered is the RMSE of the difference at each point of the time series and is referred to as StdRMSE.

$$\text{StdRMSE} = \frac{125}{M}\sqrt{\sum_{i=1}^{i=M}(MO_i - ED_i)^2}. \tag{5.3}$$

StdRMSE is a reasonable measure of how close the fit is in terms of the average difference at each point in the time series, but it only gives an indication of the fit on a point by point measure. This means that it cannot distinguish between an out of phase copy of the objective waveform and an ill fitting waveform which is in phase with the objective waveform. Thus StdRMSE only gives information about the average level of fit across all data points, and no additional information can be gained from this measure. (Note that because the experimental TMD data and model data have been normalised the units of StdRMSE are seconds^{-1}.)

The following error functions have more specific focuses and can be used to deduce more specific information about the differences between the model output and the experimental data. If used as the sole objective functions these error functions will not preserve the general fit of model output, but when combined with the standard RMSE they provide additional information which may enable an improved fit to be obtained.

AbsFFT is the root mean square (RMS) of the difference between the absolute value of the intensity of MO and ED at each Fourier mode of each sample. It provides information on the difference between Fourier modes of the TMD model output and the experimental TMD data. AbsFFT is the RMSE of the difference

between the absolute values (Abs) of the discrete Fourier transform of **MO** and **ED**. In each case the discrete Fourier transform is calculated using MatLabs's Fast Fourier Transform and thus is referred to as FFT in the notation.

$$\text{AbsFFT} = \frac{125}{M}\sqrt{\sum_{j=1}^{j=M}\left(\text{Abs}\{\text{FFT}(\mathbf{MO})_j\} - \text{Abs}\{\text{FFT}(\mathbf{ED})_j\}\right)^2} \tag{5.4}$$

When applied to a periodic data set this error function is completely insensitive to phase, and does not distinguish between positive and negative amplitudes. As such AbsFFT would not distinguish between one waveform and an identical waveform which has been inverted and or shifted in time. AbsFFT must be applied to a data set which can be repeated periodically such as the sample in this work. (Note that because the experimental TMD data and model data have been normalised the units of AbsFFT are Hertz^{-1}.)

An alternative to AbsFFT would be the RMSE of the difference between the power spectrum of **MO** and the power spectrum of **ED**, referred to as PowFFT.

$$\text{PowFFT} = \frac{1}{M}\sqrt{\sum_{j=1}^{j=M}\left(\{\text{FFT}(\mathbf{MO})_j\}^2 - \{\text{FFT}(\mathbf{ED})_j\}^2\right)^2} \tag{5.5}$$

PowFFT has similar properties to AbsFFT and is very widely used in signal processing. However, PowFFT is not used in this research because if it is included as part of a weighted combination objective function it might vary at a rate significantly higher than other component functions in the weighted function. This might lead to its component dominating when the power spectrum of the model TMD output differs only slightly from the power spectrum of the experimental TMD or becoming negligible before an appropriate optimum is found. AbsFFT is more suitable because although it may suffer from similar problems to PowFFT each term is not squared and so its rate of change is inherently less and so it would be less likely to dominate a component objective function. (Note that because the experimental TMD data and model data have been normalised the units of PowFFT are the same as AbsFFT, Hertz^{-1}.)

The RMSE of the difference between the arguments (Arg) of the discrete Fourier transform of **MO** and **ED** will be referred to as ArgFFT. Again the discrete Fourier transform was calculated using MatLabs's Fast Fourier Transform and thus is referred to as FFT in the notation.

$$\text{ArgFFT} = \frac{1}{M}\sqrt{\sum_{j=1}^{j=M}\left(\text{Arg}\{\text{FFT}(\mathbf{MO})_j\} - \text{Arg}\{\text{FFT}(\mathbf{ED})_j\}\right)^2} \tag{5.6}$$

This function uses the argument of the FFT to break both the model output and experimental data into components for each of the M frequencies and compares the phase difference between the two waveforms at each frequency. This measure of error is sensitive to frequency distribution and phase, but as with AbsFFT it does not distinguish between positive and negative amplitudes. As such it will help determine the phase shift, but only if the frequency distribution is of the model data is similar to that of experimental data - as can be determined by AbsFFT. (Note that because the experimental TMD data and model data have been normalised the units of ArgFFT are Radians Hertz^{-1}.)

One objective function used in this work, ObjFun1, is formed of a weighted sum of the StdRMSE, AbsFFT and ArgFFT functions. The units of each weighting coefficient are the inverse of its respective function to ensure that the objective function is dimensionless; WgtStd has units seconds, WgtAbs has units Hertz and WgtArg has units Hertz radians^{-1}. The inclusion of AbsFFT and ArgFFT is intended to improve the efficiency of the parameter estimation process through their combined effects during the optimisation estimated parameter values. Initially AbsFFT will contribute heavily to the objective function while the frequency distribution of the model TMD data and the experimental TMD data do not match, this will force the parameter estimation process to match the frequency distributions. Once the frequency distributions become more similar the contribution from AbsFFT will become negligible and the contribution from ArgFFT will become more noticeable. This will force the optimisation procedure to try and reduce the difference in phase between the two data sets. Once this is achieved the contributions to the objective

function from both AbsFFT and ArgFFT will be negligible and StdRMSE will dominate. During the final part of the parameter estimation process StdRMSE will dominate and this should fine tune the model fit.

$$\text{ObjFun1} = \text{WgtStd} \times \text{StdRMSE} + \text{WgtAbs} \times \text{AbsFFT} + \text{WgtArg} \times \text{ArgFFT} \quad (5.7)$$

The weighting is based on typical differences in the magnitude of each error function, and the relative importance of each fitting component. For the work presented here the magnitude of the weighting coefficients were WgtStd = 0.8 seconds, WgtAbs = 0.1 Hertz and WgtArg = 0.1 Hertz radians^{-}1.

During the optimisation of the parameter estimation processes it became a concern that the optima being achieved were not sufficient to prevent AbsFFT and ArgFFT from dominating the objective function. This would mean that, close to the optimum of the parameter estimation process, the inclusion of AbsFFT and ArgFFT in the objective function adversely affects the optimisation of the estimated parameter values. For this reason an alternative objective function which does not include AbsFFT and ArgFFT is formed. This alternative objective function is formed only of StdRMSE and is referred to as ObjRMSE.

5.3 Methods Considered

This section discusses a variety of different optimisation methods that could be applied to the parameter estimation problem considered in this work. Because the code of the numerical model is written in MatLabs the optimisations for parameter estimation are performed in MatLabs also. MatLabs has many optimisation methods built into its optimisation toolbox and the discussion of methods in this section makes reference to these procedures to indicate which methods they apply.

In all the problems considered in this research the objective functions are nonlinear

functions of the design parameters; and as such, all optimisations problems in this work are NP problems.

The optimisation methods considered for parameter estimation can be separated firstly according to how much freedom is given to the parameters during the optimisation process; whether they are suitable for unconstrained or constrained optimisation. Within this category they are then separated according to the different levels of derivative information required for the method and how the derivative information is obtained.

The principal algorithms for unconstrained minimization are the Nelder-Mead simplex search method, gradient methods and the BFGS quasi-Newton method.

Search methods use only function evaluations (e.g. the simplex search of Nelder-Mead [42]) and are only suitable for problems that are very nonlinear or have a number of discontinuities. The method can be applied as part of a constrained or unconstrained optimisation process. The problems in this research a nonlinear, but do not have any discontinuities; this makes the use of a Nelder-Mead simplex search method inefficient for the parameter estimation problem considered in this work.

Gradient methods use information about the slope of the function to dictate a direction of search where the minimum is thought to lie. The simplest of these methods is the method of steepest descent, in which a search is performed in a direction, $-\bigtriangledown f(x)$, where $\bigtriangledown f(x)$ is the gradient of the objective function. Gradient methods are generally more efficient than line search methods when the function to be minimized is continuous in its first derivative, but is very inefficient when the function to be minimized has long narrow valleys. The objective functions considered in this work are continuous in their first derivative, however, during preliminary objective function surface plots it appeared that a property of the objective functions considered in this work is that they have long narrow valleys which means optimising the TMD model with a gradient method is likely to be

extremely inefficient.

Many higher order methods, such as Newton's method, are only really suitable when first order derivative information is readily available or easily calculated. This is because calculation of such information, using numerical differentiation, can be computationally expensive and is likely to reduce the overall efficiency of the optimisation procedure. Derivative information is not readily available for the objective functions used in this work and so the use of such methods is not appropriate.

Quasi-Newton methods use numerical approximation of derivative information, but these methods are computationally viable because they do not calculate the information at every iteration. Instead they use the observed behaviour of $f(x)$ and $\bigtriangledown f(x)$ to build up curvature information and approximate the derivative information using an appropriate updating technique. There are a large number of updating techniques which have been developed, however, the Broyden [9], Fletcher [20], Goldfarb [23], and Shanno [53] (BFGS) is thought to be the most effective for use in a General Purpose method. Many quasi-Newton methods are only suitable for unconstrained optimisation.

For constrained optimisation, variations of sequential quadratic programming (SQP) are used. The SQP method is very similar to Quasi-Newton methods, but can be applied to constrained optimisation problems, such as the parameter estimation problem presented in this work.

The SQP method is based on the work of Biggs [6], Han [25], and Powell [44, 45], and closely mimics Newton's method for constrained optimisation just as is done for unconstrained optimisation. The SQP method is implemented in three main stages at each main iteration: updating the Hessian matrix of the objective function; solving the quadratic programming (QP) subproblem; and, lastly, line search and merit function evaluation.

The approximation of the Hessian (the matrix of all the second derivatives) of the

objective function is made using the BFGS formula [16, 17]. This is then used to generate a QP subproblem which is solved using an active set strategy similar to that described in [9]. The solution of the QP subproblem is used to form a search direction for a line search procedure which uses a merit function similar to that proposed in [13], [14], and [15]. A more detailed overview of SQP is found in Fletcher [21], Gill et al. [22], Powell [46], and Schittkowski [26].

The three MatLabs optimisation procedures considered for use in this research are `fminsearch`, `fminunc` and `fmincon`. Both the `fminsearch` and the `fminunc` procedures minimise the specified objective function using unconstrained optimisation methods. The difference between the two is that the `fminsearch` procedure applies search methods where as the `fminunc` procedure applies methods which use first derivative information (such as gradient methods) as well search methods. The `fmincon` procedure minimises the objective function using constrained optimisation methods. These constraints can be in the any of the forms outlined in the GOP; upper bounds, lower bounds, linear inequalities, linear equalities and or nonlinear inequalities. Before applying the standard methods outlined above, the MatLabs procedures `fminunc` and `fmincon` both attempt to apply what the MatLabs literature refers to as large-scale methods. These large-scale algorithms required user generated gradient information which cannot be explicitly calculated for the objective functions applied to the TMD model in this work. Although approximating gradient information is a possibility it would increase the computation load at each iteration of the optimisation process and thus is likely to decrease the over all efficiency of the optimisation procedure. For this reason large-scale methods are not used in the optimisation of the parameter estimation problems considered in this work.

5.4 Estimated Parameter Constraints

Attempts to optimise the model with unconstrained Quasi-Newton optimisation methods produced poor results. Although when sufficiently optimal starting parameters were chosen the method produced some improvement in fit, when less optimal values were chosen the parameter estimation process attempted to evaluate the model with inappropriate parameter values. A parameter value is deemed inappropriate if it is either impossible for the physical system to produce or it causes difficulties in running the numerical model.

These inappropriate parameter values mean the model presented here cannot be optimised with unconstrained optimisation methods and constrained optimisation methods such as SQP methods must be used for the parameter estimation problem presented in this work.

A discussion of the constraints applied in the parameter estimation processes considered in this work now follows. These constraints follow the same structure as constraints in the GOP; upper bounds, lower bounds, equality and or inequality conditions.

All parameters discussed in this section are dimensionless parameters and thus no units of measure are discussed. Most parameters of the TMD model do not require constraints to be applied for the parameter estimation processes to be effective, however, there are two reason why constraints might be applied to parameters in the optimisation process. The first is to limit parameters to values which are physically realistic, and the second is to ensure the solvability of the numerical model.

Although it might be possible to optimise the model TMD data to the experimental TMD data as an unconstrained problem there are significant risks. Even when the parameter estimation process is started from a parameter set that is considered relatively optimal, there is a high risk that the estimation procedure may

attempt to evaluate the objective function for parameter values that cause the numerical model to encounter solvability issues. Because of this the main bulk of the optimisation problems presented in this work include some parameter constraints.

The ranges of parameter values due to physical constraints is not currently known and the measurement of many physical parameters with living patients is highly unethical and so cannot be carried out. It is the purpose of the parameter estimations in this work to ascertain what reasonable physical parameter values are, however, some parameter value ranges can be roughly estimated. For those parameters which an approximate range has been estimated the use of constraints to enforce this range is likely to increase the efficiency of the optimisation process. Constraints relating to physically unrealistic parameter values do not have any mathematical complications, in this work they are restricted to simple upper or lower bounds on the parameter value.

Where parameter values might affect the solvability of the TMD model the reason is due to the numerical approximation of the TMD model. The system of equations used to numerically approximate the PDE equations of the TMD models are stored in matrix form. If one of these matrices becomes nearly singular then the system encounters difficulties with solvability which cannot be overcome using the methods applied in this work. Constraints on parameter values reduce the chances of the model encountering such difficulties during the parameter estimation process.

Equality and inequality constraints might be effective at preventing parameter values that cause the solvability difficulties from being chosen, but the formulation of all but the simplest inequality constraints encounter difficulties due to increased computational load. The main difficulty is related to dependence of matrix elements on local dependent variables in the modelling process. Such elements are updated at each iteration throughout the modelling process and thus a different equality or inequality constraint might be needed to ensure the matrix remains non-singular for each updated valued of the matrix. This in turn would cause an

Parameter		Lower Bound	Upper Bound
a_0	(PathICP)	none	none
a_1	(IEP)	none	none
a_2	(ABP)	none	none
a_3	(VentP)	none	none
a_4	(VentM)	none	none
δ	(Offset)	none	none
τ_v	(VentTS)	0	10^3
α	(Visc)	0	10
β	(CA Comp)	0	10^{-2}
γ_1	(CC Comp)	0	1
γ_2	(Cond)	0	10^{13}
η_1	(Non-lin Cond)	0	10^8
η_2	(Non-lin Cond)	0	10^8

Table 5.1: Parameter Estimation: Parameter Boundary Values - all parameters are dimensionless.

unacceptable increase in the computational load of the process. Due to the complexity of determining equality constraints that are appropriate to the parameter estimation process, simple upper and lower parameters bounds are applied instead. These bounds are determined by using observations of the model behaviour to deduce what parameters values are likely to cause difficulties during the modelling and optimisation of parameter estimation process.

In the remainder of this section each parameter is considered separately and a the necessity of upper and lower bounds is discussed. Table 5.1 shows the final upper and lower boundary values which are applied to the parameters throughout the parameter estimation procedures.

Parameters a_0, a_1, a_2, a_3, a_4 and δ require no bounds on them to keep the system

non-singular. There are bounds to what the physical parameter values could be, however, there is no data to establish this with. It is unlikely to cause problems if any outlying values are chosen for these parameters as they will quickly be removed during the optimisation process. Thus these 6 parameters are left unbounded so that each source can contribute to the TMD waveform in its standard form, an inverted form, or not at all. An alternative bounding for these parameters would be an upper bound of 1 and a lower bound of -1; these values would enforce each parameters to be of the same order as the TMD waveform. This alternative set of bounds is not needed for the parameter estimation process to be effective and efficient.

The ventilator-driven movement artefact time constant, τ_v, must be positive. A negative value is physically impossible and implies that changes in the ventilator-driven movement artefact are preceding the ventilator-driven airway pressure change. The optimisation procedure in parameter estimation removes any unrealistic values for this parameter assuming values are less than $\pm 10^3$. More precise upper and lower bounds could be found through further analysis of the VentM model component, however, this is not necessary to obtain a reasonable fit to the experimental data. Thus the upper and lower bounds of τ_v are set as 10^3 and 0 respectively.

The parameter, α, relates to damping due to viscous forces in the CA and must be positive as a negative value is physically impossible and implies that pressure waves would increase in amplitude as they propagated along the CA. However, if the order of α is 1 or greater then the damping applied to the pressure wave as it propagates down the CA removes an undesirable proportion of the high frequency component of the ICP waveform. Thus the upper bound is set as 10, and the lower bound is set to 0 to allow a reasonable level of ICP damping to remain in the IEP model.

The parameter β is compliances of the tissue lining the CA, thus a negative value for parameter β is physically impossible. However, if the tissue lining the CA is too

compliant then the ICP pressure wave travelling along the CA will be suppressed. This implies that parameter β must be smaller than order 1. The upper and lower bounds of β are imposed as 1 and 0 respectively.

Physically γ_1 must not be negative, but other than that there are no physical restrictions on γ_1. However, if the compliances of the CC is not low then there will be high levels of damping on the pressure waveform, so γ_1 must be order 1 or smaller. Therefore the upper and lower bounds are set as 1 and 0 respectively.

The parameter governing the behaviour of the linear conductance at RWM valve, γ_2, cannot be negative. However, very little else can be determined about the order of this term and so the lower boundary value for γ_2 is 0. There should be no physical upper bound, but large values cause singularity issues with the numerical model and so the upper bound is set at the highest value for which no singularity issues have occurred, 10^{13}.

Very little is known about the physical limits of parameters η_1 and η_2 because they depend on the tension of the RWM and the "natural" position of the RWM valve structure. It is clear that they must be non-negative and have lower bounds of 0. The upper bounds of 10^8 are established to prevent singularity issues related to the numerical model during optimisation stage of parameter estimation.

5.5 Implementation of the Parameter Estimation Process

In this section the implementation of the parameter estimation process, in the form of a constrained optimisation method, is explained.

The process of finding the optimal estimated parameter values that make the predictions of the model fit the measured data is broken down into stages; the optimisation of estimated parameter values at each stage is called a "case" and

is given a reference called its ID. These cases are separated into five groups each providing insight into the behaviour of the model, or a component of the model, and enabling the best fit to be obtained by the model.

During the first case of an optimisation, only a limited set of parameters in the model are free to vary in the estimation process; these parameters are referred to as free parameters. As the parameter estimation process progresses from one case to the next case an additional parameter in the model is allowed to vary, thus becoming a free parameter in the parameter estimation process.

The progression from one case to the next in the parameter estimation process occurs when the optimisation of the current case finds an optimum. The next case is then optimised using the optimal parameter estimations from the previous case as the starting parameter estimations. To minimize the chance of the optimisation achieving only a local minima at least four optimisation procedures are run on the case and given a sub-case ID. In each of the sub-cases the new free parameter is given a different starting value. For particular cases interactions between the free parameters mean that if only the new parameter is given an altered starting value there may be an increased risk of achieving only a local minima. For such cases more than four sub-cases are optimised and the starting values of other free parameters are varied in addition to the newly added free parameter. The best fitting optimum of the sub-cases is then used as the input for the next parameter estimation case.

This process is repeated until all parameters to be considered in the group of cases are free parameters in the parameter estimation process. The results of these cases are then examined and the conclusions used in the choices of free parameters for other cases.

The cases considered in this work are displayed in groups, and each group is displayed in its own table. The groups are the TMDinit cases, the TMDwVentP cases, the IEP only cases, the Component Testing cases (with various ID's), and

the Composite cases (NoPathICP and Global); they are displayed in tables 5.2 to 5.6 respectively.

Each table lists all the parameters of the complete model along the top and each case ID on the left hand side. Within each section the status of the parameters for each case is shown - which is either "free", the value it is fixed at for the case, or n/a if its not required for the case.

The cases in the tables are organised according to the order in which they were optimised, so that the progression of the parameter estimation process in each group can be seen clearly.

5.6 Chapter Summary

Within this chapter the parameter estimation process of optimising the complete TMD model to experimental data was discussed; including establishing that the unknown properties of the physical system are encompassed by 13 parameters in the complete TMD model. Suitable constraints that should be applied to the parameters during the parameter estimation process were established (see Table 5.1), along with appropriate objective functions. The suitable methods that can be applied to the complete TMD model were discussed, along with how the parameter estimation process should be implemented.

Combining this information with the data as sampled and prepared in Chapter 4 and the numerical TMD model as presented in Chapter 3 the complete TMD model can be optimised to the experimental TMD data sample in order to estimate the 13 unknown parameter values. The results of the parameter estimation process are outlined in the following Chapter, Results.

Case ID	a_0 (PathICP)	a_1 (IEP)	a_2 (ABP)	a_3 (VentP)	a_4 (VentM)	τ_v	δ	α	β	γ_1	γ_2	η_1	η_2
TMDinit1	0	free	0	0	0	n/a	free	0	0	0	10^{13}	0	0
TMDinit2	0	free	0	0	0	n/a	free	free	0	0	10^{13}	0	0
TMDinit3	0	free	0	0	0	n/a	free	free	free	0	10^{13}	0	0
TMDinit4	0	free	0	0	0	n/a	free	free	free	free	10^{13}	0	0
TMDinit5	0	free	0	0	0	n/a	free	free	free	free	free	0	0
TMDinit6	0	free	0	0	0	n/a	free	free	0	free	free	free	0
TMDinit7	0	free	0	0	0	n/a	free	free	0	free	free	free	free
TMDinit8	0	free	free	0	0	n/a	free	free	0	free	free	free	free

Table 5.2: Parameter Estimation for the TMDinit cases: "free" denotes a parameter being allowed to vary in the parameter estimation process and "n/a" denotes that that aspect of the complete model is not required due to the choice of parameters a_0 to a_4.

Case ID	a_0 (PathICP)	a_1 (IEP)	a_2 (ABP)	a_3 (VentP)	a_4 (VentM)	τ_v	δ	α	β	γ_1	γ_2	η_1	η_2
TMDwVentP1	0	free	0	free	0	n/a	free	0	0	0	10^{13}	0	0
TMDwVentP2	0	free	0	free	0	n/a	free	free	0	0	10^{13}	0	0
TMDwVentP3	0	free	0	free	0	n/a	free	free	0	free	10^{13}	0	0
TMDwVentP4	0	free	0	free	0	n/a	free	free	0	free	free	0	0
TMDwVentP5	0	free	0	free	0	n/a	free	free	0	free	free	free	0
TMDwVentP6	0	free	0	free	0	n/a	free	free	0	free	free	free	free

Table 5.3: Parameter Estimation for the TMDwVentP Cases: "free" denotes a parameter being allowed to vary in the parameter estimation process and "n/a" denotes that that aspect of the complete model is not required due to the choice of parameters a_0 to a_4.

Case ID	a_0 (PathICP)	a_1 (IEP)	a_2 (ABP)	a_3 (VentP)	a_4 (VentM)	τ_v	δ	α	β	γ_1	γ_2	η_1	η_2
IEP1	0	free	0	0	0	n/a	free	0	0	0	10^{13}	0	0
IEP2	0	free	0	0	0	n/a	free	free	0	0	10^{13}	0	0
IEP3	0	free	0	0	0	n/a	free	free	free	0	10^{13}	0	0
IEP4	0	free	0	0	0	n/a	free	free	free	free	10^{13}	0	0
IEP5	0	free	0	0	0	n/a	free	free	free	free	free	0	0
IEP6	0	free	0	0	0	n/a	free	free	free	free	free	free	0
IEP7	0	free	0	0	0	n/a	free	free	free	free	free	free	free

Table 5.4: Parameter Estimation for the IEP only cases: "free" denotes a parameter being allowed to vary in the parameter estimation process and "n/a" denotes that that aspect of the model was not required due to the choice of parameters a_0 to a_4.

Case ID	a_0 (PathICP)	a_1 (IEP)	a_2 (ABP)	a_3 (VentP)	a_4 (VentM)	τ_v	δ	α	β	γ_1	γ_2	η_1	η_2
ABP1	0	0	free	0	0	n/a	free	n/a	n/a	n/a	n/a	n/a	n/a
ABP2	free	0	free	0	0	n/a	free	n/a	n/a	n/a	n/a	n/a	n/a
VentP1	0	0	0	free	0	n/a	free	n/a	n/a	n/a	n/a	n/a	n/a
VentP2	free	0	0	free	0	n/a	free	n/a	n/a	n/a	n/a	n/a	n/a
VentM1	0	0	0	0	free	free	free	n/a	n/a	n/a	n/a	n/a	n/a
VentM2	free	0	0	0	free	free	free	n/a	n/a	n/a	n/a	n/a	n/a
VentBoth	0	0	0	free	free	free	free	n/a	n/a	n/a	n/a	n/a	n/a
NoPathICP_NoIEP	0	0	free	free	free	free	free	n/a	n/a	n/a	n/a	n/a	n/a
NoIEP	free	0	free	free	free	free	free	n/a	n/a	n/a	n/a	n/a	n/a

Table 5.5: Parameter Estimation for the Component Testing cases: "free" denotes a parameter being allowed to vary in the parameter estimation process and "n/a" denotes that that aspect of the model was not required due to the choice of parameters a_0 to a_4.

Case ID	a_0 (PathICP)	a_1 (IEP)	a_2 (ABP)	a_3 (VentP)	a_4 (VentM)	τ_v	δ	α	β	γ_1	γ_2	η_1	η_2
NoPathICP1	0	free	free	free	free	free	free	0	0	0	10^{13}	0	0
NoPathICP2	0	free	free	free	free	free	free	free	0	0	10^{13}	0	0
NoPathICP3	0	free	free	free	free	free	free	free	free	0	10^{13}	0	0
NoPathICP4	0	free	free	free	free	free	free	free	free	free	10^{13}	0	0
NoPathICP5	0	free	free	free	free	free	free	free	free	free	free	0	0
NoPathICP6	0	free	free	free	free	free	free	free	free	free	free	free	0
NoPathICP7	0	free	free	free	free	free	free	free	free	free	free	free	free
Global	free	free	free	free	free	free	free	free	free	free	free	free	free

Table 5.6: Parameter Estimation for the Composite cases: "free" denotes a parameter being allowed to vary in the parameter estimation process and "n/a" denotes that that aspect of the model was not required due to the choice of parameters a_0 to a_4.

Chapter 6

Results

To aid the understanding of the results presented in this chapter a short explanation of the waveforms used and produced in the modelling process, along with an informal "by eye" evaluation of their importance and relevance, is performed in section 6.1. All the results presented here are from one simultaneous experimental data set obtained on one ear of a single patient. The sample TMD data from this patient is analysed, but the data has a significant amount of noise on it which reduces the relevance of many of the results. However, limited insight is gained from this analysis and so some of the results are discussed here. Subsequently a different source of the same data was found, but with much lower noise levels, and this data is used for the bulk of the analysis presented in this chapter.

In many of the figures presented here the main waveform from the optimised model is plotted, along with the TMD waveform which was used in the parameter estimation process. The TMD waveform is plotted in light grey and the main waveform from the model output for the case is plotted in dark blue. This is done to clarify which TMD waveform was used optimisation in the parameter estimation process, significantly noisy or less noisy, and thus better demonstrates the level of fit achieved by the model case during the parameter estimation process.

6.1 The basic waveforms

This research is concerned with the relative proportion each of the waveforms measured contributes to the measured TMD waveform and because of this all waveforms are discussed and compared in their normalised form. (A detailed explanation of how each waveform is normalized in preparation for use in the model is in section 4.4 of chapter 4.) Figure 6.4 shows the noisy TMD waveform and figure 6.5 shows the same TMD waveform from the less noisy source. (The acquisition of the less noisy signal is outlined in section 4.4 of chapter 4.) Figures 6.1 to 6.3 show the Direct ICP, ABP and ventilator-driven airway pressure which were all measured simultaneously with the TMD.

Figure 6.1 shows the airway pressure imposed on the patient by the ventilation system they are attached to. This is not the same waveform as would be produced by a typical unventilated patient as the pressure is driven in a manner prescribed by the mechanical ventilator system rather than the muscles of the patient's chest. The key characteristics of this waveform are the steep increase in pressure, the square top of the pressure being maintained whilst the lungs are partially inflated and the gentle decline as the patients lungs deflate under their own mechanical properties. A secondary characteristic is the high frequency oscillations that occur at the peaks and troughs of the airway pressure. These oscillations are imposed to improve airflow during inflation and deflation of the lungs, but are of no relevance to the research presented here.

The ABP signal is shown in figure 6.2. The main characteristic of this are the double peaks at the top of each main wave. The "double peaks" are the pressure variations induced by the heart pumping to move the blood into the lungs and then around the body. Note that in the ABP waveform the first of the double peaks is much larger than the second. The ABP is affected by lung pressure and a second characteristic of the ABP waveform is a small sinusoidal increase and decrease in the baseline pressure of the same periodicity as respiration. This increase and

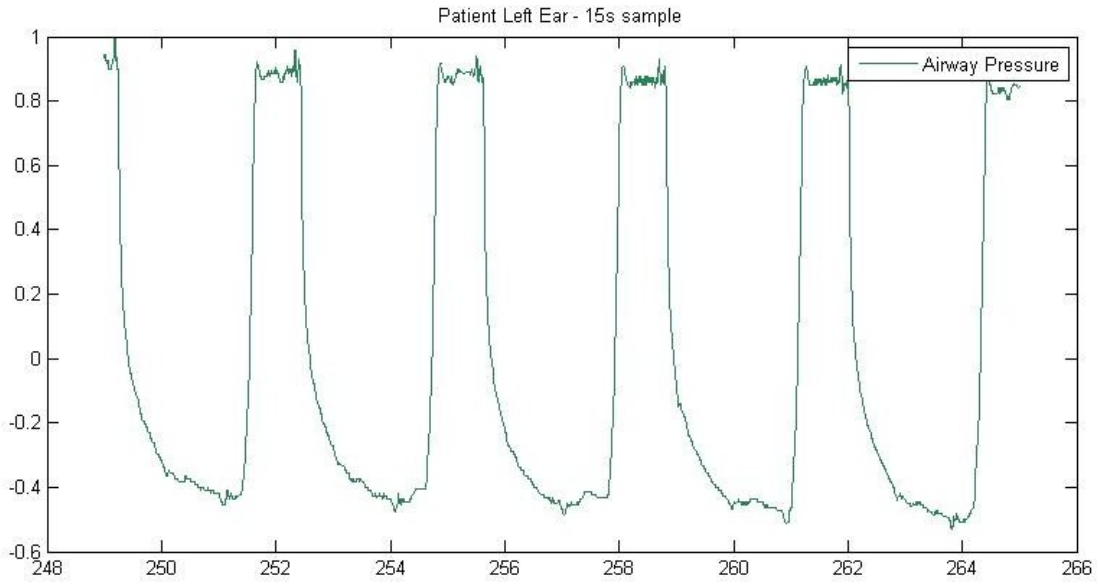

Figure 6.1: Normalised airway pressure data sample. The horizontal scale shows time in seconds (this is within the master sample file).

decrease in the pressure can be seen on figure 6.2 in the periodic increase and decrease in the pressure of the peaks and troughs of the waveform.

Figure 6.3 shows the ICP waveform. ICP is driven by ABP and thus one of its main characteristics is the "double peak" associated with ABP. In ICP the difference between the first and second peak is not as large as in ABP. ICP is more affected by the baseline pressure change cause by respiration, this is evident in the ICP waveform, as the peak and trough pressure values of ICP vary proportionally more than those in ABP.

The basic form of the TMD signal can be clearly seen in both the noisy data (figure 6.4) and the less noisy data (figure 6.5). The TMD waveform has a variety of components acting at different frequencies. One of the distinctive characteristics of the TMD waveform are the "double peaks" which occur approximately 1 second apart. These "double peaks" are originally of cardiovascular origin, but it is not clear whether this contribution to TMD is from direct action of the cardiovascular

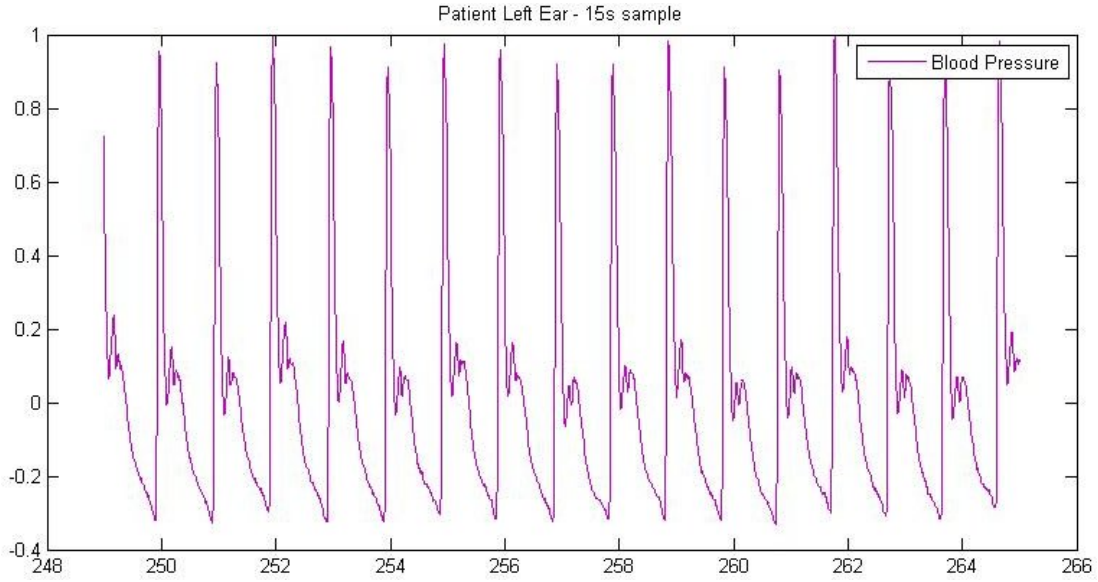

Figure 6.2: Normalised blood pressure data sample. The horizontal scale shows time in seconds (this is within the master sample file).

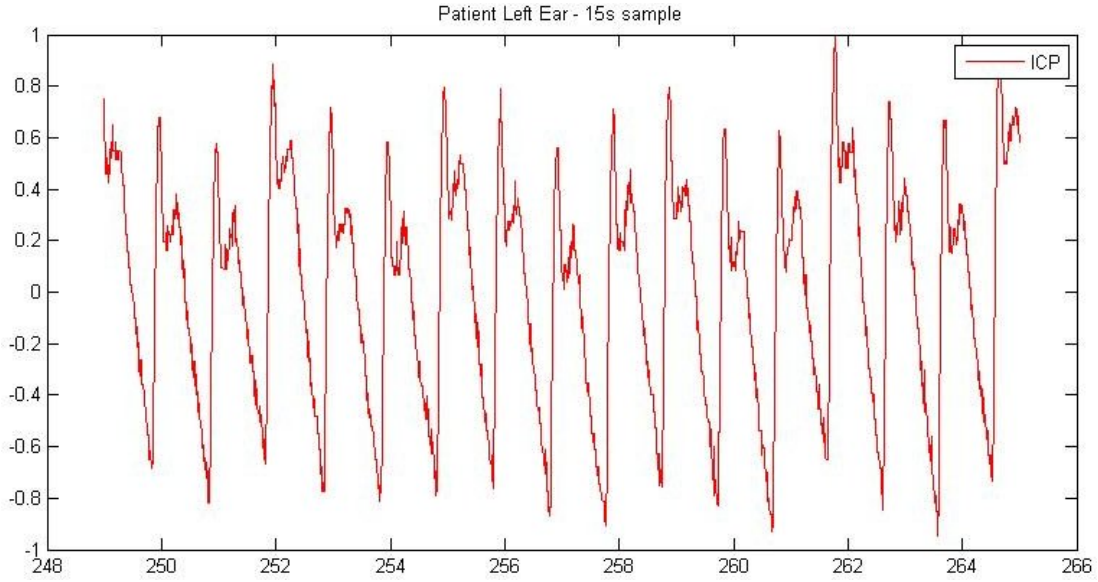

Figure 6.3: Normalised ICP data sample. The horizontal scale shows time in seconds (this is within the master sample file).

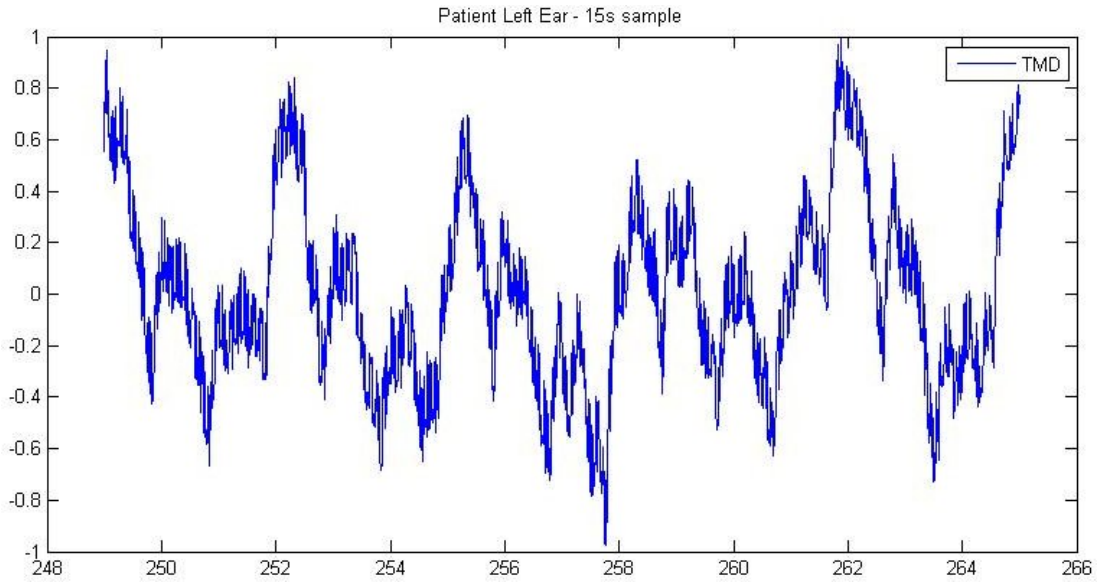

Figure 6.4: Normalised TMD data sample suffering from significant noise on the signal. The horizontal scale shows time in seconds (this is within the master sample file).

system, the cardiovascular system acting through ICP, or a combination of the two. These "double peaks" are not clear in the TMD signal affected by noise, but are clearer in the less noisy TMD data. The amplitude of the "double peaks" increase and decrease periodically over a period of approximately 3 seconds, this is a low frequency component likely to be related to respiratory waves. It believed that respiration can only affect TMD indirectly through ABP and ICP (as both of these waveforms are affected directly by respiration). The respiration component is evident in both the noisy and less noisy TMD data sets.

6.2 Initial Cases - TMDinit

On commencement of this research it was believed that the two main sources acting on TMD were ABP pressure variations transmitted directly to TMD through blood vessels in the inner ear and external ear canal, and IEP driven by ICP via the CA.

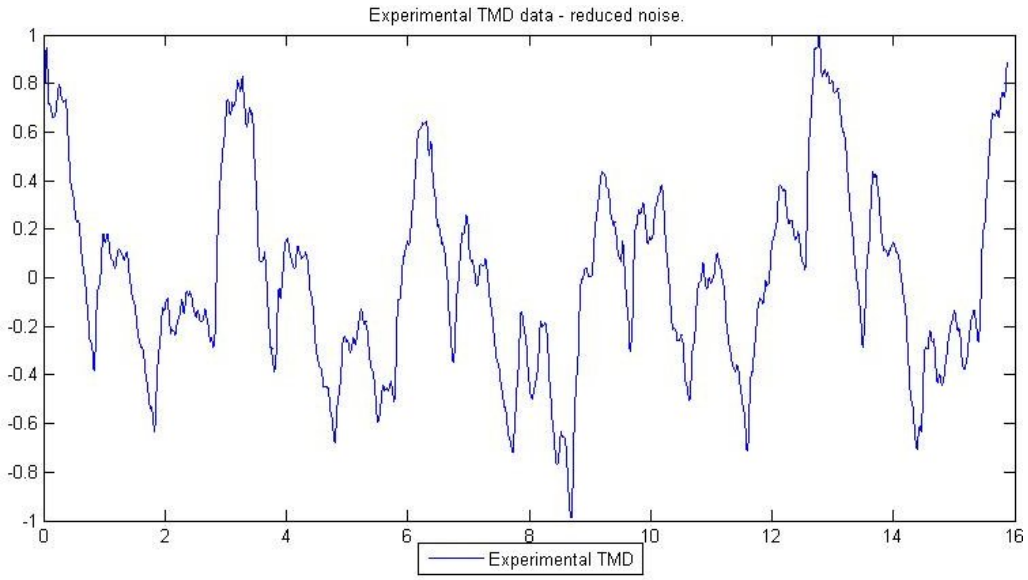

Figure 6.5: Normalised TMD data sample from less noisy source. The horizontal scale shows time in seconds (note the scale has been reset over the smaller sample period).

Thus it was expected that a model with the IEP component - driven by ICP - and the ABP component would be sufficient to accurately model the experimental TMD waveform. These model cases are called the TMDinit cases and were only optimised to the original noisy TMD data, they were optimised using ObjFun1. The results obtained using the noisy data are less accurate and for this reason only a general discussion of the results is presented here and no specific results are given. (The structure of the cases is presented in table 5.2.)

The fit improved between optimisation of case TMDinit1 and TMDinit2, but as the optimisation process progresses to other cases the level of improvement dropped off quickly and no significant improvement was seen between cases TMDinit4 and TMDinit8. When ABP is introduced as a free parameter in case TMDinit6 of the optimisation process the fit does not improve, and this implies that ABP does not contribute substantially to the TMD waveform. The same is found when the nonlinear parameters β, η_1 and η_2 are introduced to the optimisation process; the

results imply that nonlinear effects in the TMDinit model cases do not improve the fit.

These results are unexpected and it is believed they are caused by the noise on the TMD data. The noise on the TMD data dominates the signal throughout the waveform and prevents ObjFun1 from effectively discerning if there is an improvement in the fit, this is especially crucial at key points, such as at peaks and troughs in the waveform.

Examination of the residual error of the TMDinit8 case output and the experimental TMD data showed there was a low frequency component of the experimental TMD waveform which is not accounted for by the TMDinit cases. The frequency was close to that of typical human respiration, and it was also in phase with the respiration pressure wave being produced by the ventilator to which the patient is connected. From this it can be deduced that respiration may be affecting the TMD waveform directly, but it is unclear what the mechanism for this is. Other than the importance of a low frequency respiration component little else could be deduced from the residue due to the large amount of noise on the TMD waveform.

6.3 Ventilator-driven Airway Pressure Cases - TMDwVentP

The results from the TMDinit cases showed that the potential influence of respiration on TMD is a key factor in the modelling process. The TMDwVentP cases test this theory by introducing the ventilator-driven airway pressure (VentP) component of the model. The ABP component is not included in the TMDwVentP cases and the CA compliances parameter, β, is fixed at zero and not optimised; this is due to their lack of importance in the optimisation of the TMDinit cases.

The TMDwVentP cases are optimised to the same noisy TMD data as the TMDinit

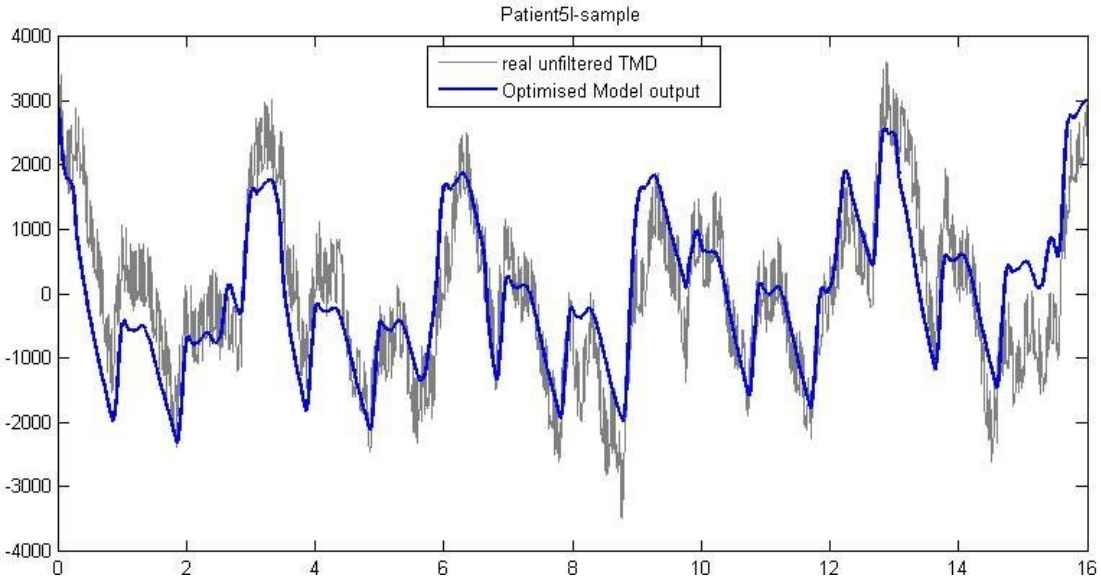

Figure 6.6: TMDwVentP6

cases using ObjFun1, and thus the TMDwVentP suffer similar difficulties during the optimisation process. Again the results of the optimisations to the noisy data are less accurate and for this reason only a general discussion of the results is presented here with no table of results given. (The structure of the cases is presented in table 5.3.)

There was no significant improvement in fit when the nonlinear parameters η_1 and η_2 are included as free parameters in the optimisation process. However, inclusion of the VentP component of the model increases the level of fit greatly over those achieved in the TMDinit cases.

Analysis of the case TMDwVentP6 optimum waveform (figure 6.6) and the residue of the case TMDwVentP8 optimum and experimental TMD data shows that although including ventilator-driven airway pressure improved the fit, it does not account for all of the low frequency component of the TMD waveform. The ventilator-driven airway pressure waveform is too "square", and the inclusion of the rapid increase in ventilator-driven airway pressure does not provide an ideal fit to the experimental TMD data.

During the optimisation process of TMDwVentP several cases starting from different parameter values produced unexpected results. These optimisation attempts terminated in local minima which removed the IEP component from the model. Although it is expected that some optimisation attempts will find local minima rather than the global minimum it is unexpected that some of these local minima would completely remove the IEP component of the model. This unexpected occurrence raises concerns that noise on the TMD waveform increases the chances of the optimisation process obtaining only local minima. This in turn raises concerns over earlier results, such as the removal of the ABP component during the optimisation of the TMDinit cases. Such a result may be due to local minima in the optimisation process and not produce a true representation of the physical system.

These concerns indicate that it is necessary to reconsider the assumptions used in construction of the model, especially those assumptions based on the results of the optimisations of cases TMDinit and TMDwVentP. It is clear that respiration has a clear effect on the TMD waveform, but it may not be possible to dismiss the relevance of ABP and the nonlinear effects within the IEP component of the model when optimising to TMD data with such high noise levels. To more accurately determine the importance of each different component and the nonlinear effects within the IEP model component, the optimisation process must be conducted using a waveform from a less noisy source.

6.4 The IEPonly Cases

Due to the concerns about noise on the TMD data a new set of cases are optimised to the same data but from a source with much lower noise. In these cases the objective function ObjFun1 is much better able to distinguish between the different levels of fit achieved in each case of the optimisation process. Because of this the results in this section are more accurate and provide greater insight, thus they are

shown in more detail than those results obtained using the noisy TMD signal.

The results of the important optimisation processes produced using the less noisy TMD data are presented in tables and graph figures from hereon. The figures use the same format outlined at the beginning of this chapter and the tables 6.1 to 6.8 use the following format (see for example table 6.1). The table is broken into blocks, each block contains results from one optimisation case. The first row of each block indicates which of the parameters are free to vary or fixed for the case being optimised, if they are fixed then the specific value they are fixed at is shown. The second row of each block contains the optimum parameter values found for that case and the value of the objective function at the optimum (note that the objective function used is indicated at the top of the table). Only the values of free parameters are shown in the second row and the value of the objective function has been multiplied by 10^3 for clarity of presentation when comparing results obtained with ObjFun1 and ObjRMSE. (The alternate objective function, ObjRMSE, is introduced later in this section.) The subsequent blocks show cases, typically with more free parameters, allowing the importance of each parameter to be assessed. Parameters in the complete model which are not used in the optimisation case are not shown in the table.

From the optimisations carried out using noisy TMD data it is unclear whether the nonlinear effects in the IEP component of the model are able to improve the level of fit achieved. Because of this the IEP component of the model is optimised to the less noisy TMD data using ObjFun1 and no other components of the complete model are included. These IEP only cases are IEP1 - IEP7 and table 6.1 shows the results of the optimisation of these cases using ObjFun1 in the optimisation process.

During the optimisation of case IEP2 using ObjFun1 the fit improves by 29.5% when compared to that achieved during the optimisation of case IEP1 using ObjFun1. By comparison the improvement in fit of the remaining IEP cases is poor;

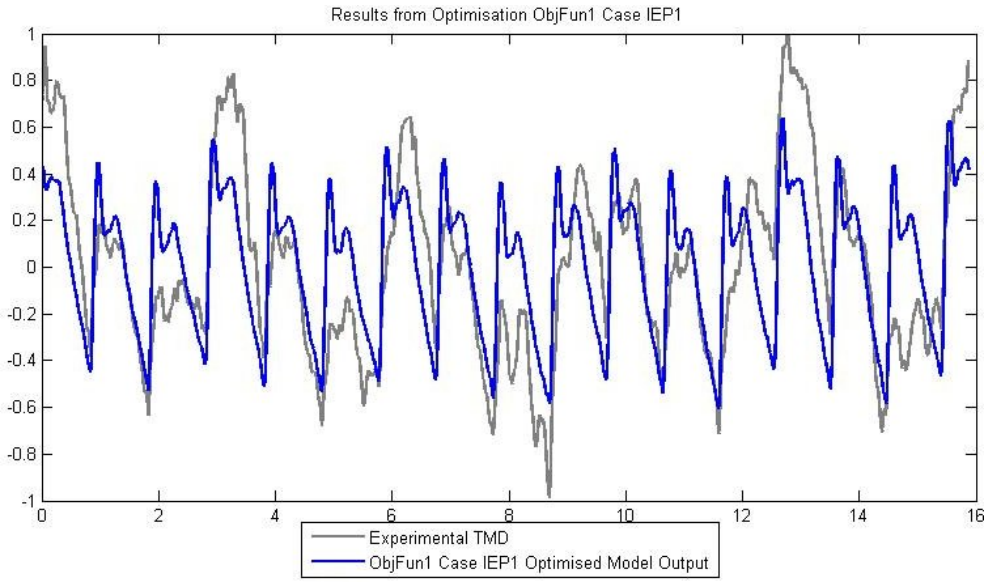

Figure 6.7: Model output from Case IEP1 using ObjFun1.

the total improvement in fit between case IEP2 and case IEP7 is less than 7%.

The waveforms of case IEP1 and IEP2 are shown in figure 6.7 and 6.8 respectively. The waveform from case IEP2 is different to that of case IEP1; it lacks the "double peak" at the top of each wave, which is exhibited in case IEP1, and has a slight phase shift compared to the case IEP1 waveform.

The complete loss of the "double peak" and the clear phase shift between the model data and the experimental data are undesirable results of the optimisation process. Testing of the individual components of the composite objective function, ObjFun1, indicate that this is due to the error function ErrFun2 dominating the objective function. (ErrFun2 provides information about the difference between the frequency distributions of the model output and the experimental TMD data.) ErrFun3 also dominates over ErrFun1, but not to the same extent as ErrFun2. (ErrFun3 provides information about the difference between the phase of the model output and the experimental TMD data.) To solve this problem the alternate objective function is introduced and separate optimisations of each model are carried out using each objective function. This second objective function is the root mean

Case ID	a_1	δ	α	β	γ_1	γ_2	η_1	η_2	ObjFun1 ($\times 10^{-3}$)
IEP1	free	free	0	0	0	10^{10}	0	0	
optimum	0.638	0							37.3
IEP2	free	free	free	0	0	10^{10}	0	0	
optimum	1.0024	0	1.293						28.8
IEP3	free	free	free	free	0	10^{10}	0	0	
optimum	1.0024	0	1.293	0					28.8
IEP4	free	free	free	free	free	10^{10}	0	0	
optimum	1.0024	0	1.293	0	1				28.8
IEP5	free	free	free	free	free	free	0	0	
optimum	1.0019	0	1.293	0	0.9997	10^4			28.8
IEP6	free	free	free	free	free	free	free	0	
optimum	1.0019	0	1.3055	0	0.9997	10^4	10^4		28.6
IEP7	free	free	free	free	free	free	free	free	
optimum	1.0019	0	1.3055	0	0.9997	10^4	10^4	10^{-4}	28.6

Table 6.1: Parameter Estimation - IEP ObjFun1 only Cases: both the parameters allowed to vary in the estimation process and the values at the optimum are shown here.

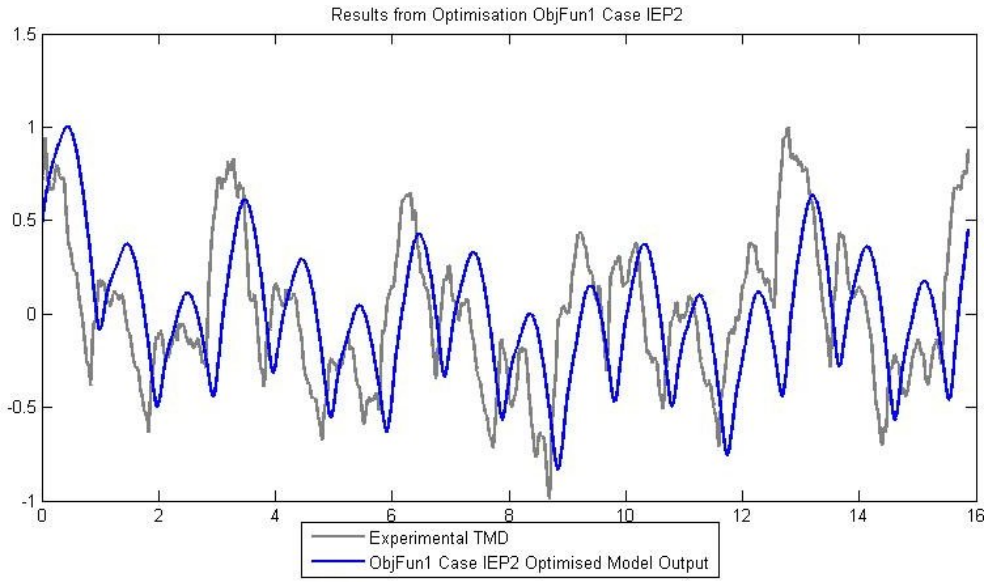

Figure 6.8: Model output from Case IEP2 using ObjFun1.

square of the difference between the model output and the experimental TMD data and is referred to as ObjRMSE.

The optimisation of the IEP only cases for the less noisy TMD data is repeated using ObjRMSE (instead of ObjFun1) to determine if the alternate objective function provides improved fit and or more desirable waveforms. The results of these optimisations are presented in table 6.2.

When optimised using ObjRMSE the improvement in fit from case IEP1 to IEP2 is 8.5%. The improvement from case IEP2 to IEP3 is less than 0.2% and there is no significant improvement in fit from case IEP3 to IEP4. Case IEP5 is a 2.8% improvement over case IEP4, and although the fit does not improve greatly between cases IEP5 and IEP7 there is a slight improvement of approximately 0.2%.

Figures 6.9 and 6.10 show the waveforms from cases IEP2 and IEP5 when optimised using ObjRMSE. Case IEP2 clearly still contains the “double peak” which is desirable for modelling the TMD waveform, but the waveform from case IEP5 does not contain the “double peak”.

Case ID	a_1	δ	α	β	γ_1	γ_2	η_1	η_2	ObjRMSE $\times 10^{-3}$
IEP1	free	free	0	0	0	10^{10}	0	0	
optimum	0.5739	0							6.5295
IEP2	free	free	free	0	0	10^{10}	0	0	
optimum	0.6121	0.0015	0.1762						6.0175
IEP3	free	free	free	free	0	10^{10}	0	0	
optimum	0.6121	0.0014	0.1760	10^{-2}					6.0166
IEP4	free	free	free	free	free	10^{10}	0	0	
optimum	0.6121	0.0014	0.1760	10^{-2}	10^{-2}				6.0166
IEP5	free	free	free	free	free	free	0	0	
optimum	0.6704	-0.009	0	0.0009	0	1.0405			5.8511
IEP6	free	free	free	free	free	free	free	0	
optimum	0.6705	-0.0084	0	9×10^{-4}	0	1.0407	0.0108		5.8413
IEP7	free	free	free	free	free	free	free	free	
optimum	0.6705	-0.0078	0	9×10^{-4}	0	1.0409	0.0117	10^{-4}	5.8403

Table 6.2: Parameter Estimation - IEP ObjRMSE only Cases: both the parameters allowed to vary in the estimation process and the values at the optimum are shown here.

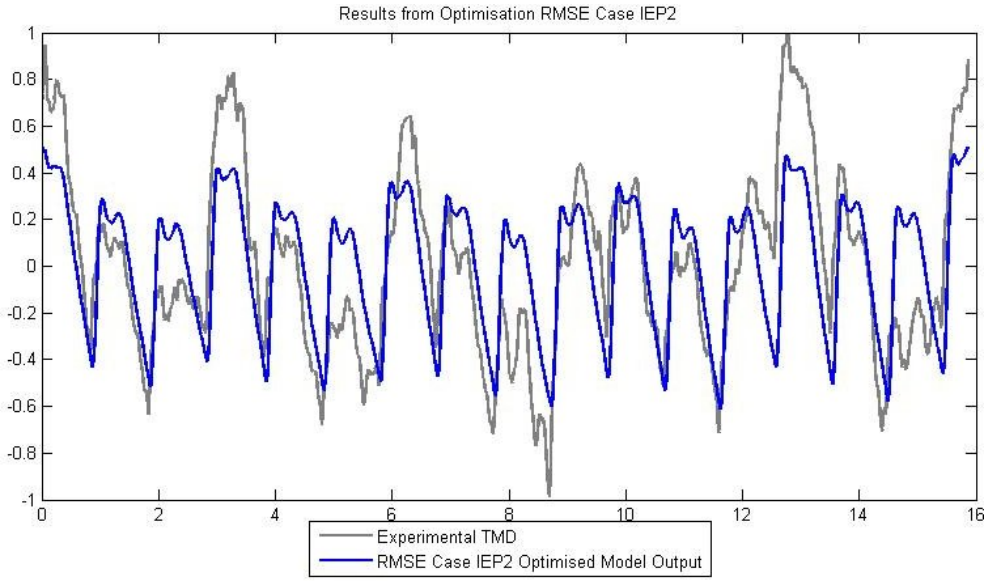

Figure 6.9: Model output from Case IEP2 using ObjRMSE.

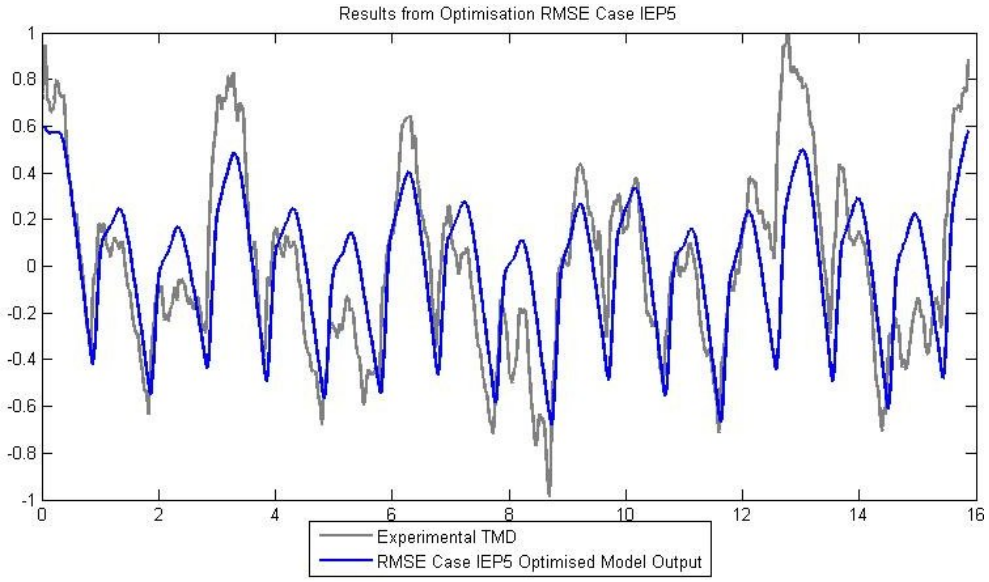

Figure 6.10: Model output from Case IEP5 using ObjRMSE.

Comparison of the tabular results obtained using ObjFun1 and ObjRMSE show that the rate at which fit improves is similar with both objective functions, but ObjFun1 showed slightly higher improvement in fit. However, examination of the waveforms shows that the optimisations using ObjRMSE produce more waveforms with desirable characteristics than those using ObjFun1. The fact that both objective functions sacrifice the "double peak" to obtain an improved average fit during the optimisation process is not desirable and suggests that when only the IEP component of the complete model is used as a model for experimental TMD data the output is unlikely to closely recreate typical TMD characteristics when fitted to the data.

6.5 Component Testing Cases

The component testing cases, as displayed in table 5.5, are designed to quickly obtain medium level fits with low computational load; this enables them to quickly provide intuitive information on each component of the complete model. These cases focus on each component of the complete model in turn, except the IEP component which is excluded to maintain a low computational load. Once each single component case is evaluated extended cases combining the components of the complete model are evaluated. The aim of the component testing cases is to aid the construction of more complex cases and provide a benchmark for data fitting; specifically, the results from these cases are used to try and prevent improper removal of model components due to local minima during the optimisation process of future cases. A breakdown of the free parameters in each component testing case can be found in table 5.5 from chapter 5, but the results of the optimisations of the cases are displayed in tables 6.3 to 6.6 within this chapter.

Due to the clear importance of the respiration related component of the TMD waveform focus on the respiration component of the TMD waveform increases.

The link between ventilation driven body movement and the TMD waveform as outlined in section 2.4 of chapter 2 is hypothesised; it is referred to as VentM and is included in the composite cases.

As shown in tables 6.3 and 6.5 the ABP, VentP and VentM cases each rely on one component of the complete model and have one case each namely ABP1, VentP1 and VentM1. A second case for each of these components is also presented in tables 6.3 through 6.6, each of these cases also include the single parameter relating to PathICP; these are labelled ABP2, VentP2 and VentM2. Although it is not expected that ICP acts in a way that is as direct as that represented by the PathICP component of the complete model, it is included as a simple substitute to IEP component in the "component testing" cases.

Two additional composite cases, VentBoth and NoICPNoIEP, are considered in tables 6.4 and 6.6 to assess the possibility of TMD being formed without ICP as a source (either by the CA or a pathological route).

All cases are optimised to the less noisy TMD data first using ObjFun1 and then using ObjRMSE. The results of the optimisations involving ObjFun1 are presented in tables 6.3 and 6.4; The results of the optimisations using ObjRMSE are presented in tables 6.5 and 6.6.

When optimised with ObjFun1 these cases, without ICP included as a source, produce an improvement of 20.7% over the best fit from the IEP only cases (see NoPathICPNoIEP in table 6.4). However, three of the composite cases which include ICP as a source produce better fits; VentP2 obtains a 34.9% improvement on the IEP model fit, VentM2 obtained a 52.9% improvement on the IEP model fit and NoIEP obtained a 63.4% improvement on the IEP model fit. Hence component testing cases produce a better fit than IEP only cases. Most component testing cases which include the PathICP component produce a better fit than those cases which don't include PathICP, however this is not true of case ABP2 as both case VentBoth and case NoPathICP_NoIEP produce better fits without including the

PathICP component of the complete model.

Optimisation of the composite cases using ObjRMSE, as seen in tables 6.5 and 6.6, produces similar results to those obtained using ObjFun1. When using ObjRMSE two composite cases without ICP included as a source, VentBoth and NoPathICPNoIEP, produce an improved fit compared to the fits of the IEP only cases. VentBoth obtains a 5.2% improvement in fit, and NoPathICPNoIEP obtains a 20.7% improvement in fit compared to the IEP only cases. When optimised using ObjRMSE only two of the composite cases which include ICP as a source produce a better fit than those that do no include ICP as a source, VentM2 and NoIEP. VentM2 obtains a 36.8% improvement on the fits obtained with the IEP only cases, and case NoIEP obtained a 66.4% improvement on the fits obtained with the IEP only cases. VentP2 also obtained an improvement on the fits of the IEP only cases of 15.6%, but this is less than the improvement that cases VentBoth and NoPathICPNoIEP achieve (neither of which include ICP as a source). Note that the only component in all of the three best fitting component testing cases is VentM. Hence it can be concluded that although the best fit is achieved by a component testing case which includes the PathICP component, the inclusion of the VentM component in the model is also critical.

Figures 6.11 to 6.18 show the model TMD waveforms produced by optimisations of cases VentP2, VentM2, NoPathICPNoIEP and NoIEP using both ObjFun1 and ObjRMSE. Although the case NoPathICPNoIEP obtained a closer fit than all IEP only cases, when using both ObjFun1 and ObjRMSE, it does not recreate typical TMD waveform characteristics - such as a “double peak” in the waveform and semi-matched gradients. This can be seen in figures 6.15 and 6.16 where the first “spike” dominates to such an extent that there appears to only be a “single spike” at the top of each peak in the waveform rather than the typical “double spike”, and the gradient of the troughs are considerably different to those of the experimental TMD data. Those cases which include ICP as a source (through PathICP) produce waveforms which show characteristics closer to those of a typical TMD waveform.

Case ID	a_0	a_1	a_2	a_3	a_4	τ_v	δ	ObjFun1 ($\times 10^{-3}$)
ABP1	0	0	free	0	0		free	
optimum			0.6894				0.0016	44.8
ABP2	free	0	free	0	0		free	
optimum	0.9876		-0.655				0.0009	33.4
VentP1	0	0	0	free	0		free	
optimum				0.5419			0	34.9
VentP2	free	0	0	free	0		free	
optimum	0.505			0.4299			0	21.2
VentM1	0	0	0	0	free	free	free	
optimum					0.6155	50	0	30.7

Table 6.3: Parameter Estimation - NoIEP ObjFun1 Cases - Table 1: both the parameters allowed to vary in the estimation process and the values at the optimum are shown here.

Case ID	a_0	a_1	a_2	a_3	a_4	τ_v	δ	ObjFun1 ($\times 10^{-3}$)
VentM2	free	0	0	0	free	free	free	
optimum	0.4904				0.4806	49.9998	0	18.7
VentBoth1	0	0	0	free	free	free	free	
optimum				-0.1461	0.7250	50.0057	0	30.7
NoPathICP_NoIEP	0	0	free	free	free	free	free	
optimum			0.5859	-0.1567	0.6948	50.0061	0	23.7
NoIEP	free	0	free	free	free	free	free	
optimum	0.5717		-0.1372	-0.1029	0.5599	50.0076	0.0012	17.5

Table 6.4: Parameter Estimation - NoIEP ObjFun1 Cases - Table 2: both the parameters allowed to vary in the estimation process and the values at the optimum are shown here.

Case ID	a_0	a_1	a_2	a_3	a_4	τ_v	δ	ObjRMSE ($\times 10^{-3}$)
ABP1	0	0	free	0	0		free	
optimum			0.4849				0	8.12
ABP2	free	0	free	0	0		free	
optimum	0.8665		-0.5531				0	6.24
VentP1	0	0	0	free	0		free	
optimum				0.4313			0	6.87
VentP2	free	0	0	free	0		free	
optimum	0.4674			0.3465			0	5.05
VentM1	0	0	0	0	free	free	free	
optimum					0.5321	99.9998	10^{-4}	6.20

Table 6.5: Parameter Estimation - NoIEP ObjRMSE Cases - Table 1 : both the parameters allowed to vary in the estimation process and the values at the optimum are shown here.

Case ID	a_0	a_1	a_2	a_3	a_4	τ_v	δ	ObjRMSE ($\times 10^{-3}$)
VentM2	free	0	0	0	free	free	free	4.27
optimum	0.4487				0.4443	99.9981	0.0004	
VentBoth1	0	0	0	free	free	free	free	5.55
optimum				0.2489	0.3974	99.9979	0.0002	
NoPathICP_NoIEP	0	0	free	free	free	free	free	4.84
optimum			0.4840	0.2483	0.3968	99.9979	0.0002	
NoIEP	free	0	free	free	free	free	free	3.51
optimum	0.5742		-0.2698	0.1894	0.3280	100.0017	0	

Table 6.6: Parameter Estimation - NoIEP ObjRMSE Cases - Table 2: both the parameters allowed to vary in the estimation process and the values at the optimum are shown here.

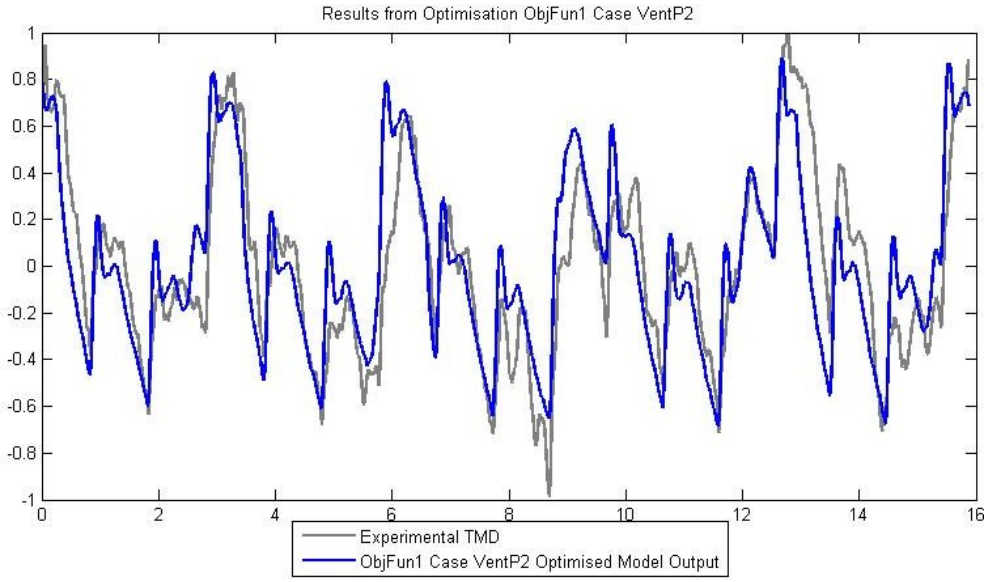

Figure 6.11: Model output from Case VentP2 using ObjFun1.

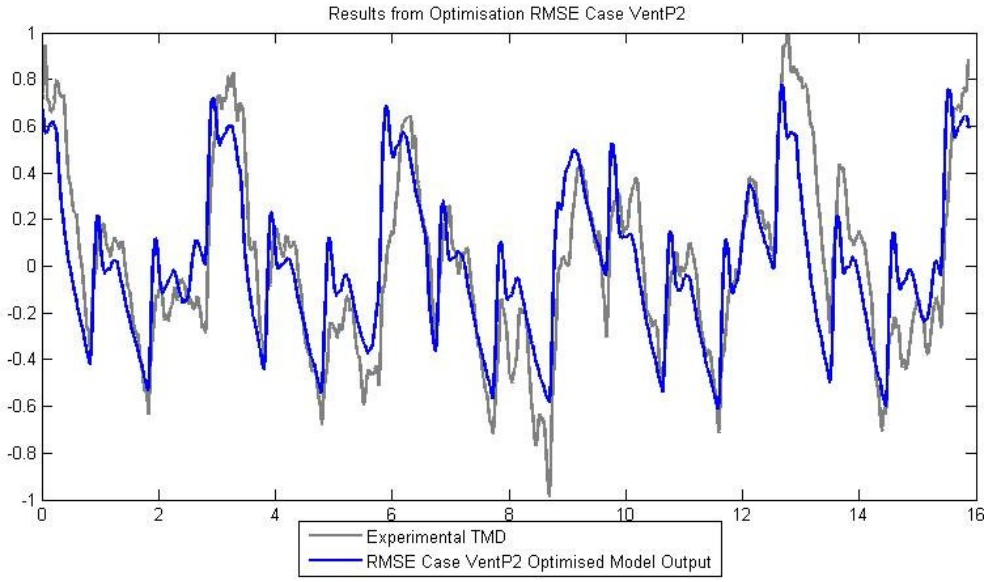

Figure 6.12: Model output from Case VentP2 using ObjRMSE.

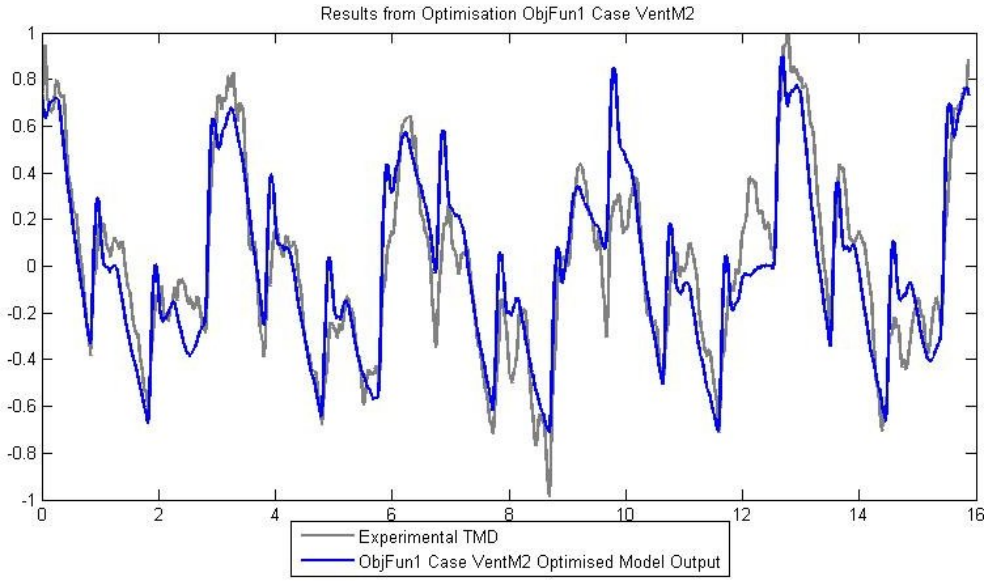

Figure 6.13: Model output from Case VentM2 using ObjFun1.

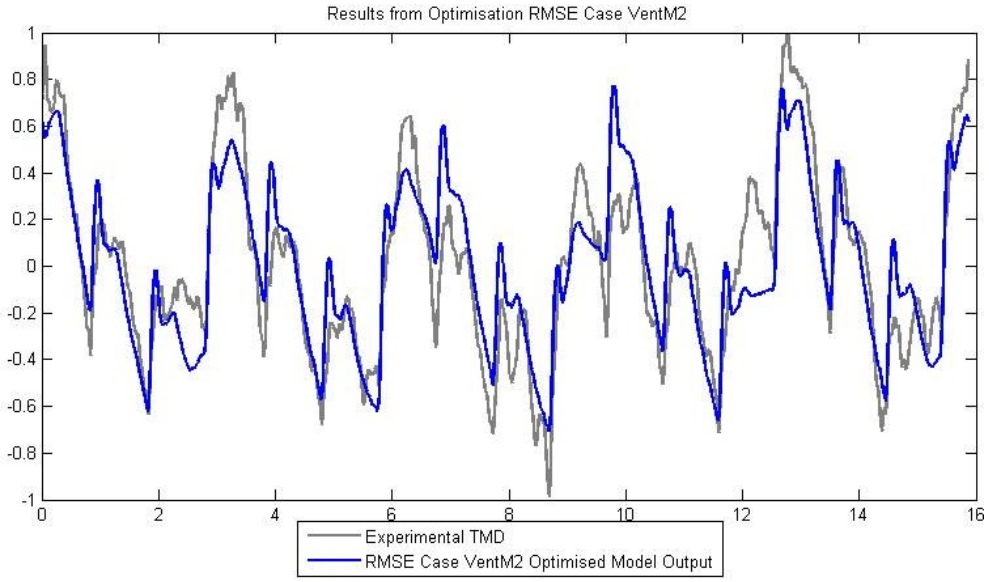

Figure 6.14: Model output from Case VentM2 using ObjRMSE.

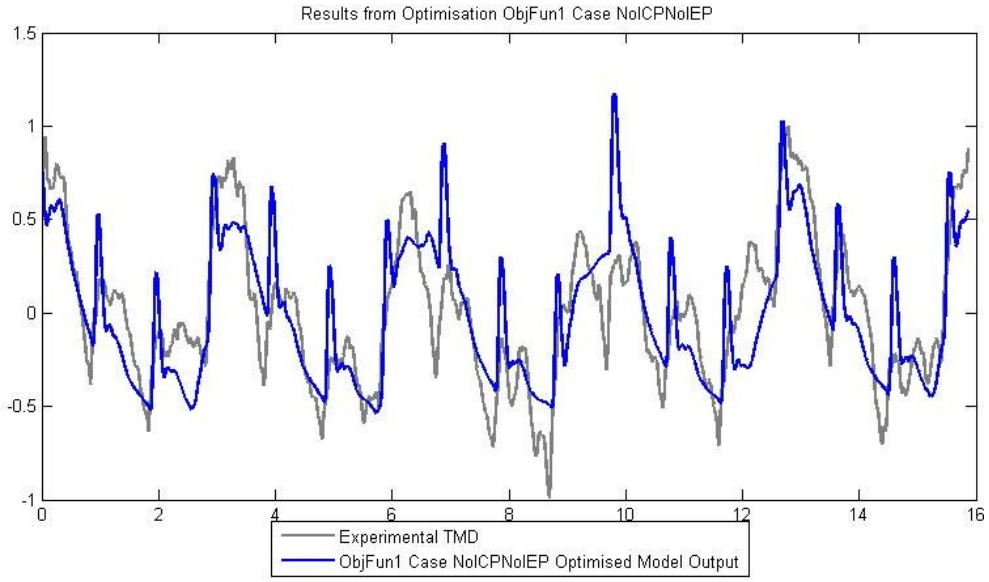

Figure 6.15: Model output from Case NoPathICP_NoIEP using ObjFun1.

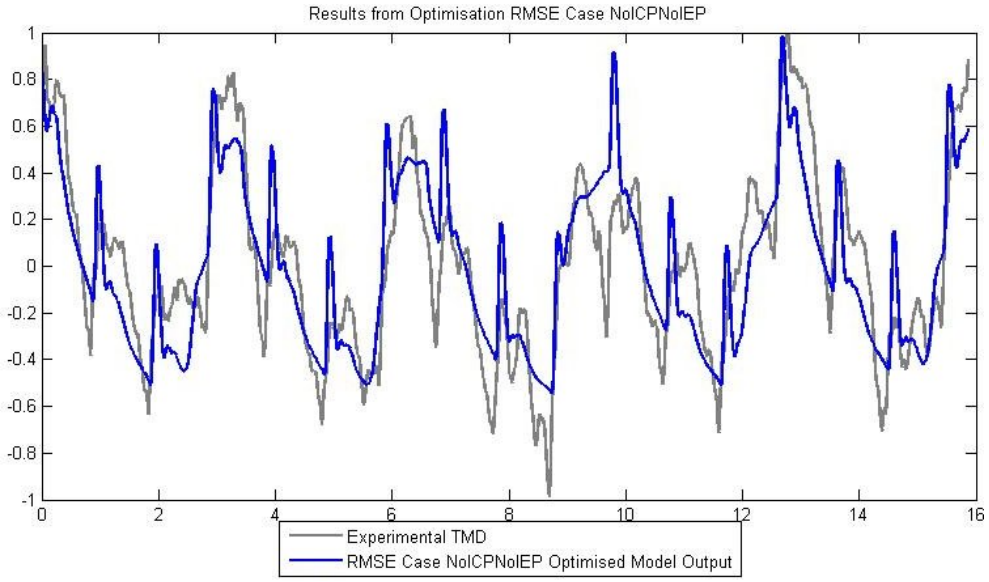

Figure 6.16: Model output from Case NoPathICP_NoIEP using ObjRMSE.

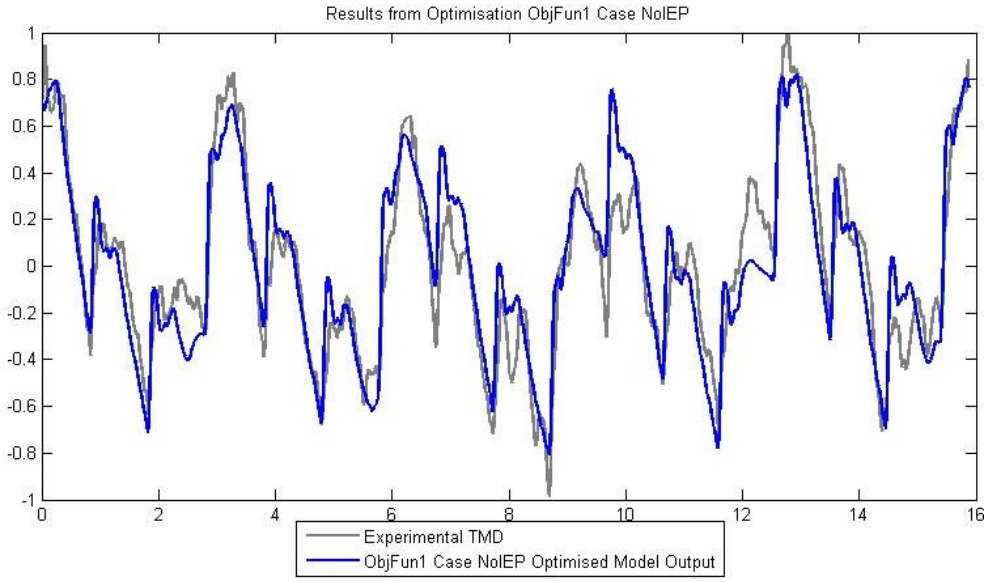

Figure 6.17: Model output from Case NoIEP using ObjFun1.

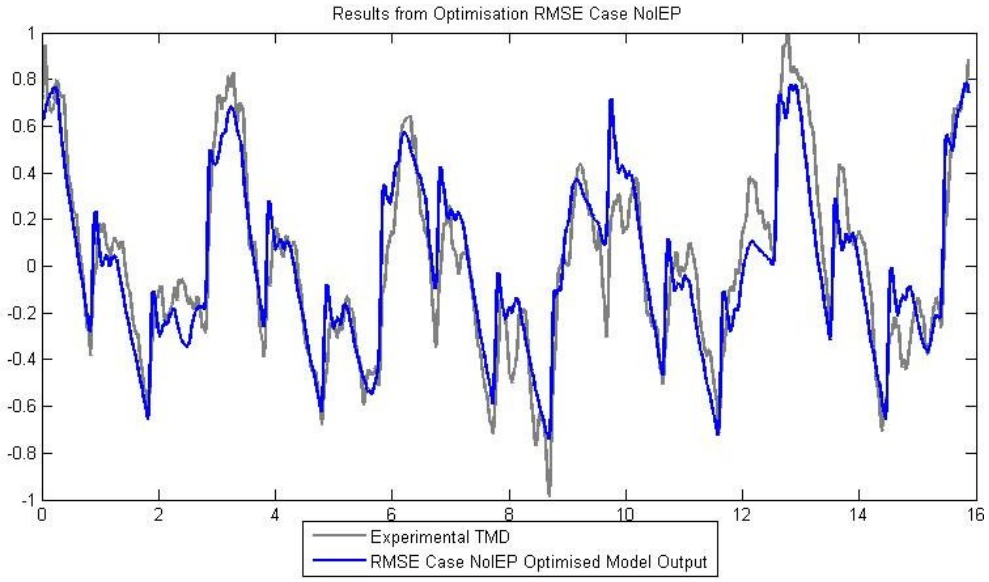

Figure 6.18: Model output from Case NoIEP using ObjRMSE.

In figures 6.11 to 6.14 VentP2 and VentM2 are presented and the gradient of the troughs in these waveform more closely match those in the TMD and in many instances the "double peak" has been retained. It should be noted that although VentM2 does not retain all instances of the "double peaks" as clearly as VentP2 the matching of the troughs is significantly improved (see figures 6.12 and 6.14). Figures 6.17 and 6.18 show the results from case NoIEP; the "double peak" is retained throughout most of the waveform from both optimisation processes and the general fit, at peaks and troughs, is superior to the other component testing cases. The waveforms from the NoIEP case clearly produce desired typical TMD characteristics whilst fitting to the sample TMD data, and thus they are deemed the best fit of the component testing cases.

The results from optimisations using either ObjFun1 or ObjRMSE both strongly support the view that the TMD waveform has direct contribution from ABP, ICP and respiration. This implies that the original removal of the ABP component from the TMDinit cases is an unintended consequence of the optimisation process being trapped in local minima during optimisation to the noisy TMD data.

Although the results obtained with ObjFun1 and ObjRMSE both strongly support the inclusion of the ABP, VentP and VentM components of the complete model they do not completely agree with each other. The TMD waveforms produced through optimisation with ObjFun1 and ObjRMSE identify different proportions of the TMD being caused by each source. When optimised with ObjFun1 case NoIEP produces a model TMD waveform with approximately 41.7% from ICP, 10% from ABP, 7.5% from VentP and 40.8% from VentM. When optimised with ObjRMSE case NoIEP produces a model TMD waveform with 42.2% from ICP, 19.8% from ABP, 13.9% from VentP and 24.1% from VentM. The validity of these differences is examined by considering more complex TMD model cases which include additional mechanisms, the NoPathICP and Global cases.

6.6 NoPathICP and Global Cases

From the results of the composite cases and the IEP only model it is reasonable to deduce that an accurate model of TMD will include influences from the ABP, VentP, VentM and IEP model components. Because it is believed that the only significant mechanism by which ICP can act on the TMD waveform is through the IEP (via the CA) the PathICP component of the complete model is not included in the general results in this section and the model case is referred to as NoPathICP. However, to examine the possibility of ICP acting directly on TMD, not via the IEP component of the complete model, one case of the complete model is considered after all the NoPathICP cases have been optimised; this case is referred to as the Global case.

The NoPathICP case is optimised to the less noisy TMD data, first using ObjFun1 and then using ObjRMSE. The starting value for each free parameter in the optimisation process is taken from the optima achieved from the earlier IEP cases and the composite NoIEP cases. The starting parameters for the optimisations using ObjFun1 are taken from the optimum achieved using ObjFun1 and vice versa for ObjRMSE. This was done so that the results from optimisations with each objective function remained separate and it could be examined which objective function produced a model TMD waveform with more "typical" characteristics.

The results from the optimisation of NoPathICP using ObjFun1 are presented in table 6.7. The case NoPathICP1 achieves an improvement on the best previous fit (case NoIEP) of 8.7% and the case NoPathICP2 improves that fit by 8.1% over case NoPathICP1. The cases NoPathICP3 and NoPathICP4 offer only marginal improvements in fit; the NoPathICP4 optimum is approximately 0.5% improvement on the fit achieved in case NoPathICP2. Case NoPathICP5 improves the fit by 1.6% compared to case NoPathICP4 or 2.1% compared to case NoPathICP2. Case NoPathICP6 offers no significant increase in fit and NoPathICP7 failed to optimise due to solvability difficulties in the numerical model. This is unexpected

Case ID	a_0	a_1	a_2	a_3	a_4	τ_v (3 s.f.)	δ	α	β	γ_1	γ_2	η_1	η_2	ObjFun1 ($\times 10^{-3}$)
NoPathICP1	0	free	free	free	free	free	free	0	0	0	10^{13}	0	0	
optimum		0.641	-0.267	0.089	0.414	100	-0.0001							16.1
NoPathICP2	0	free	free	free	free	free	free	free	0	0	10^{13}	0	0	
optimum		0.631	-0.285	0.094	0.401	100	0	0.0473						14.9
NoPathICP3	0	free	free	free	free	free	free	free	free	0	10^{13}	0	0	
optimum		0.631	-0.285	0.095	0.400	100	0.0002	0.0452	0.0094					14.830
NoPathICP4	0	free	free	free	free	free	free	free	free	free	10^{13}	0	0	
optimum		0.631	-0.285	0.096	0.400	100	0.0002	0.0454	0.0094	$\approx 10^{-9}$				14.829
NoPathICP5	0	free	free	free	free	free	free	free	free	free	free	0	0	
optimum		0.728	-0.280	0.263	0.176	100	0.0001	0.0022	0.0001	0.0516	0.389			14.692
NoPathICP6	0	free	free	free	free	free	free	free	free	free	free	free	0	
optimum		0.728	-0.280	0.263	0.176	100	-0.0024	0.0022	0.0002	0.0517	0.389	0.01		14.681

Table 6.7: Parameter Estimation - NoPathICP ObjFun1 Cases: both the parameters allowed to vary in the estimation process and the values at the optimum are shown here.

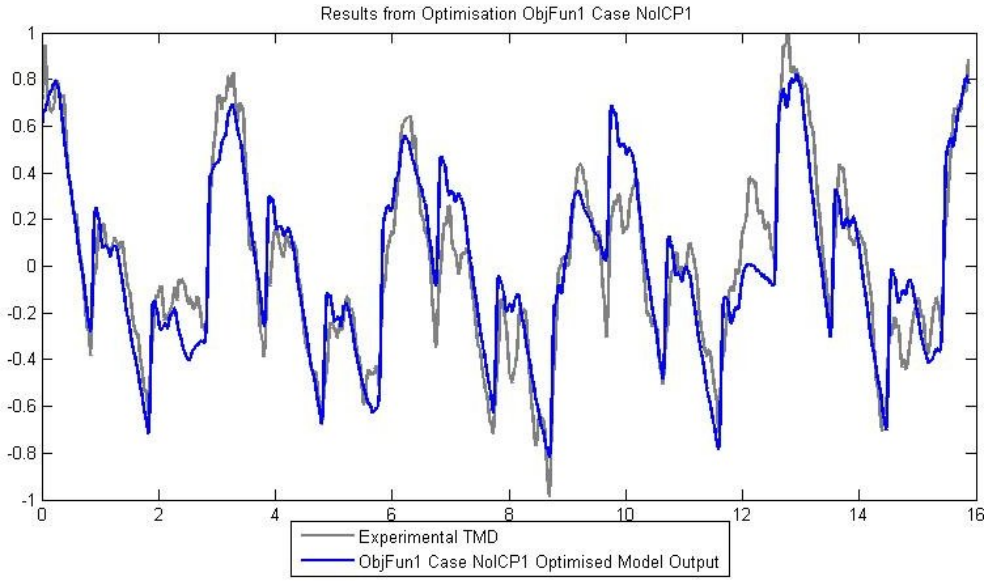

Figure 6.19: Model output from Case NoPathICP1 using ObjFun1.

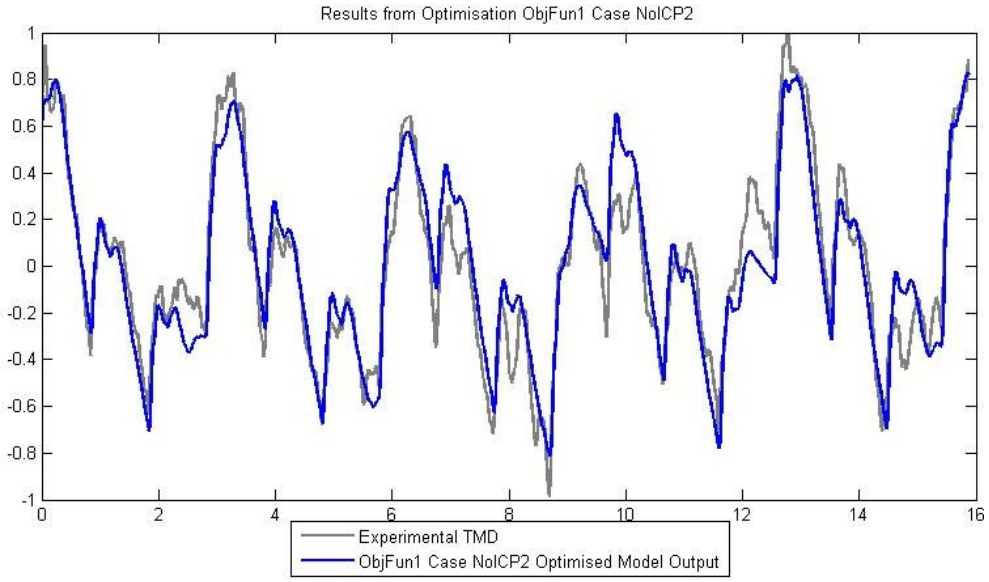

Figure 6.20: Model output from Case NoPathICP2 using ObjFun1.

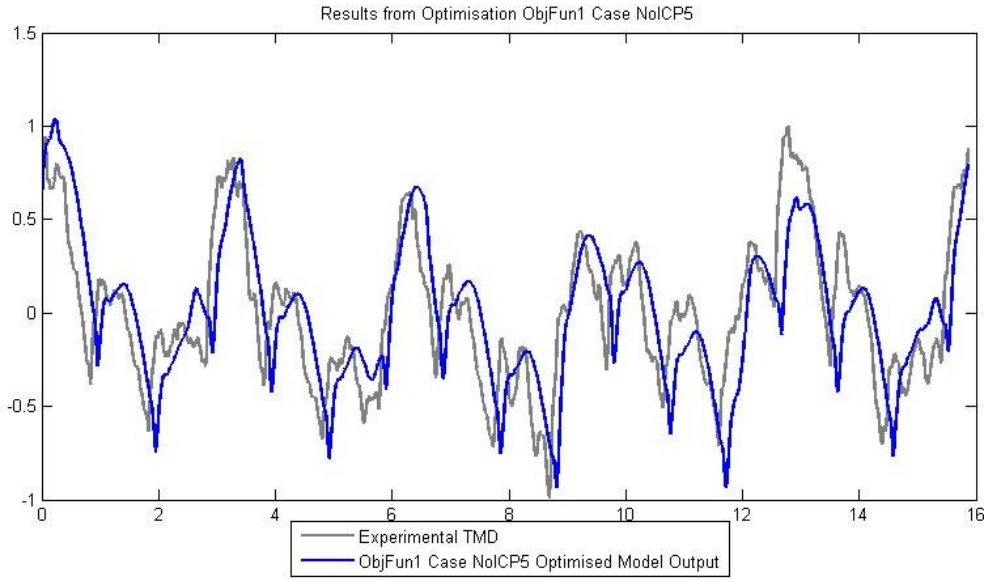

Figure 6.21: Model output from Case NoPathICP5 using ObjFun1.

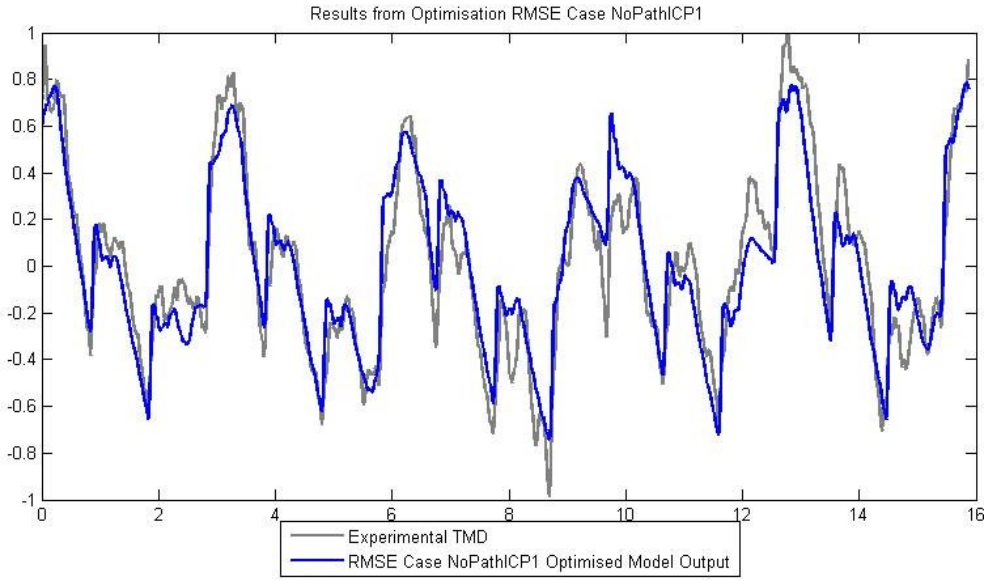

Figure 6.22: Model output from Case NoPathICP1 using ObjRMSE.

Case ID	a_0	a_1	a_2	a_3	a_4	τ_v	δ	α	β	γ_1	γ_2	η_1	η_2	ObjRMSE ($\times 10^{-3}$)
NoPathICP1	0	free	free	free	free	free	free	0	0	0	10^{13}	0	0	
optimum		0.575	-0.270	0.189	0.328	100.0017	0							3.249
NoPathICP2	0	free	free	free	free	free	free	free	0	0	10^{13}	0	0	
optimum		0.579	-0.272	0.190	0.326	100.0017	0	0.0591						2.8159
NoPathICP3	0	free	free	free	free	free	free	free	free	0	10^{13}	0	0	
optimum		0.579	-0.273	0.189	0.325	100.0017	0	0.0587	0.01					2.8095
NoPathICP4	0	free	free	free	free	free	free	free	free	free	10^{13}	0	0	
optimum		0.579	-0.273	0.189	0.325	100.0017	0.0001	0.0585	0.01	10^{-4}				2.8090

Table 6.8: Parameter Estimation - NoPathICP ObjRMSE Cases - Table 1: both the parameters allowed to vary in the estimation process and the values at the optimum are shown here.

Case ID	a_0	a_1	a_2	a_3	a_4	τ_v (3 s.f.)	δ	α	β	γ_1	γ_2	η_1	η_2	ObjRMSE ($\times 10^{-3}$)
NoPathICP5	0	free	free	free	free	free	free	free	free	free	free	0	0	
optimum		0.579	-0.273	0.189	0.324	100	0.0001	0.0584	0.01	10^{-5}	10^4			2.8087
NoPathICP6	0	free	free	free	free	free	free	free	free	free	free	free	0	
optimum		0.579	-0.274	0.189	0.324	100	0.0001	0.0583	0.01	10^{-5}	10^4	10^2		2.8083
NoPathICP7	0	free	free	free	free	free	free	free	free	free	free	free	free	
optimum		0.579	-0.274	0.189	0.323	100	0.0001	0.0583	0.01	10^{-5}	10^4	10^2	0	2.8080
Global	free	free	free	free	free	free	free	free	free	free	free	free	free	
optimum	0.064	0.543	-0.303	0.183	0.311	100	10^{-5}	0.0650	0.025	10^{-5}	10^4	10^2	0	2.7902

Table 6.9: Parameter Estimation - NoPathICP ObjRMSE Cases - Table 2: both the parameters allowed to vary in the estimation process and the values at the optimum are shown here.

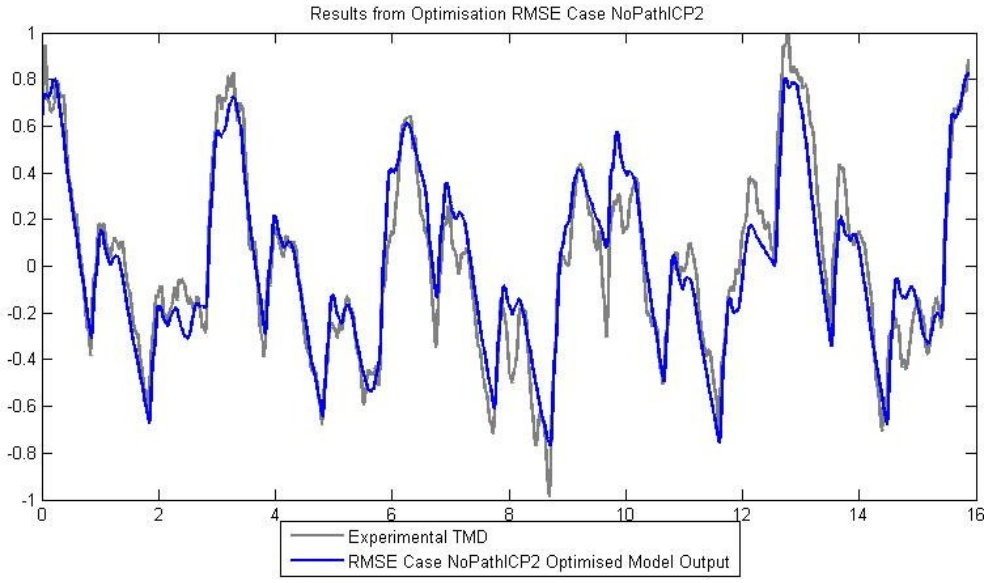

Figure 6.23: Model output from Case NoPathICP2 using ObjRMSE.

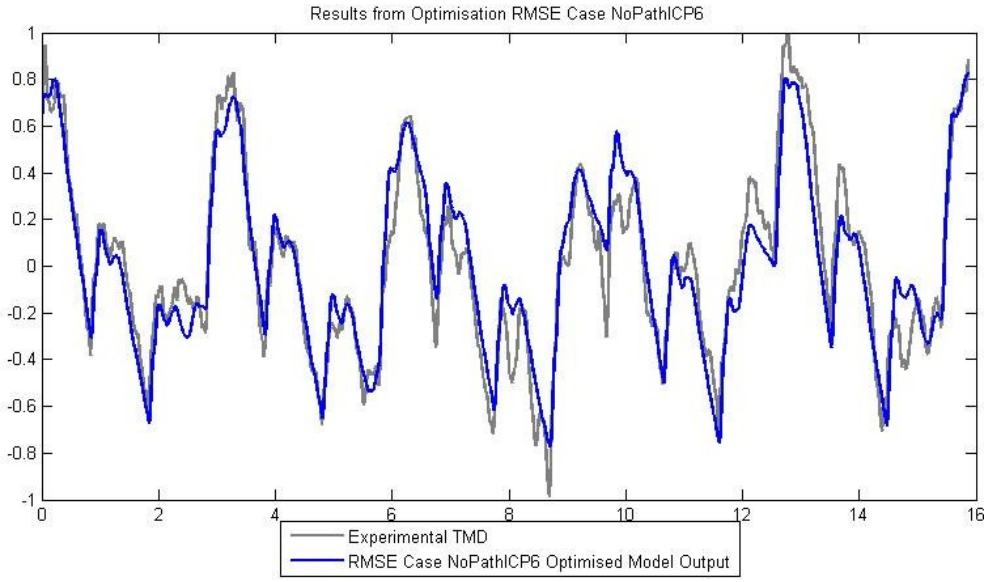

Figure 6.24: Model output from Case NoPathICP6 using ObjRMSE.

since the constraint of upper and lower bounds successfully prevented the previous cases from encountering such issues during optimisation with ObjFun1. It is unclear if the introduction of η_2 as a free parameter was the sole cause of this or if the objective function was converging on a point where inappropriate parameter combinations are more likely to occur. To help determine this the results obtained with ObjRMSE must be examined.

The results of the optimisation of the NoPathICP cases using ObjRMSE are presented in tables 6.8 and 6.9. The case NoPathICP1 achieves an improvement on the best previous fit (case NoIEP) of 8% and the case NoPathICP2 improves that fit by 15.4% over case NoPathICP1. The cases NoPathICP3 through to NoPathICP7 offer only marginal improvements in fit, the case on case improvement of fits of the order 0.01%. The fit achieved by case NoPathICP7 is a 0.3% improvement on the fit achieved by case NoPathICP2.

The most notable point of these results is that all cases of NoPathICP successfully completed the optimisation process using ObjRMSE, this supports the view that the selection of inappropriate parameter values during the optimisation of NoPathICP7 using ObjFun1 is caused primarily by ObjFun1, the objective function. Since the only differences between the two optimisation processes are the objective functions used and the starting parameters, one of these caused the selection of inappropriate parameter values. To test the objective function the optimisation process for NoPathICP can be repeated using ObjRMSE, but by starting the process with the same parameter values that caused the optimisation process to encounter numerical difficulties when optimising with the ObjFun1 objective function. The result is that no difficulties with the numerical code are encountered. This leads to the conclusion that optimisation using ObjFun1 is at a higher risk of selecting inappropriate parameter values, or combinations of parameters. However, the increased risk of numerical complication might be deemed worth while if the use of ObjFun1 in the optimisation process produces model TMD output which is more characteristic of typical TMD waveforms than those achieved with optimi-

sation processes using ObjRMSE. To determine this the waveforms produced by both optimisation procedures are analysed "by eye".

Figures 6.19 to 6.21 show the waveforms produced by the cases NoPathICP1, NoPathICP2 and NoPathICP5 when optimised using ObjFun1. The waveforms from cases NoPathICP1 and NoPathICP2 both produce reasonable fits to the data and maintain characteristics typical of a TMD waveform. However, case NoPathICP5 shows the loss of the "double peaks" and introduces a small phase shift. These are not desirable results of the optimisation process and are caused by ErrFun2 dominating the objective function. Thus, unless ObjRMSE produces data with less characteristic waveforms, it can be deduced that ObjFun1 is not an ideal objective function when refining the fit of the TMD model to experimental data. Figures 6.22 to 6.24 show the waveforms produced by cases NoPathICP1, NoPathICP2 and NoPathICP6 when optimised using ObjRMSE. All three waveforms shown here have the distinctive characteristics of a typical TMD waveform, thus it is clear that the optimisation process involving ObjRMSE rather than ObjFun1 produces a fit to the data which is more characteristic of a TMD waveform. Using ObjRMSE the fit improves from case to case, but there is very little difference between the fit of each case. The waveform produced by case NoPathICP6 shows no evidence of the nonlinear aspects of the IEP component of the complete model improving the fit to the experimental TMD waveform.

The results of the optimisation of the Global case using ObjRMSE is presented alongside the results of the NoPathICP cases optimised using ObjRMSE (table 6.9). Due to the failed optimization of case NoPathICP7 using ObjFun1 no optimisation of the Global case using ObjRMSE is performed. Optimisation of the case Global using ObjRMSE achieves an improved fit over all the NoPathICP cases. However, the level of improvement between case NoPathICP7 and Global case is small, 0.64%; and the PathICP component of the model forms less than 4.6% of the model TMD waveform. When including additional waveform sources in the TMD model it is likely that a slight improvement to fit can be obtained regardless

of whether the inclusion of such a waveform has a basis in the physical system being modelled. For this reason the small improvement in fit when the PathICP model component is introduced, combined with the small proportion of the model TMD waveform it contributes, reinforces the belief that the only significant route of ICP pressure propagation into the inner ear is via the CA as modelled in the IEP component of the complete model presented here.

Although the Global case obtains the best fit to the experimental TMD data of all the cases discussed in this work, the improvement in fit obtained through the inclusion of the PathICP component is not significant enough to justify its inclusion in a realistic TMD model based on knowledge of the physical system.

The introduction of the nonlinear aspects of the IEP model as free parameters in the optimisation process, whether using ObjFun1 or ObjRMSE, did not significantly improve the fit of the NoPathICP cases. This is an unexpected result, as a large portion of the literature on pressure transfer between the fluids of the brain and inner ear implies that the fluid propagation properties are likely to be nonlinear. This raises questions about the validity of these finding or on the validity of these aspects of the IEP model component. These questions are discussed in the next and final chapter of this thesis, Conclusions.

Chapter 7

Conclusions

In this thesis the central focus of the work has been the interpretation of TMD data in order to infer behaviour of ICP. Modelling has focused on four main mechanisms that contribute to TMD, including ICP.

Passive TMD techniques monitor volume displacements in the external ear canal; from these displacements information about IEP changes can be inferred. Because ICP is in communication with IEP via the CA it is believed that information about ICP changes can also be inferred from TMD measurements, however, the TMD waveform also has contributions from respiration and cardiovascular waves. To try and recreate these mechanisms the modelling of TMD has been broken into four main components, each focusing on a mechanism which affects TMD measurements: IEP driven by ICP, ABP, and other effects, particularly two aspects of respiration.

The results of the TMD model and those relating to specific components of the model are evaluated and conclusions drawn out and explained in the following sections.

7.1 The TMD model

The most important results of this work is that the model TMD waveform contains substantial contributions from three main sources; ICP via IEP, ABP and respiration (via direct action of ventilator-driven airway pressure and an artefact driven by body movement during respiration) are all key components of the TMD model. Although ICP acting on TMD through pathological routes, i.e. direct communication routes other than the CA, was not expected to be significant one case which included the PathICP component of the model was evaluated, case Global. The inclusion of ICP via pathological routes in Case Global did provide a slightly improved fit compared to those cases where it was not included. However, the PathICP component formed less than 5% of the model TMD output signal, which indicates that it is not a critical component of the TMD model. This result is in agreement with the conclusions drawn in many other works, as they have shown that the CA is the most important route of communication between ICP and IEP, except where patients have some pathological mechanism for ICP to TMD communication. This indicates that PathICP is not significant in the physical system being modelled and thus case Global is not discussed further.

Case NoPathICP7 is believed to be the most accurate representation of the physical system being modelled in this work and thus the focus on the remainder of this chapter focus on the results of this case and the NoPathICP case group.

In the results of case NoPathICP7 (the best fitting case of the most appropriate TMD model cases) the model output signal is formed of the following proportions; IEP driven by ICP forms 42.4%, VentP forms 13.8%, VentM forms 23.7%, and ABP forms 20.1%. This is an interesting result because when this research started the presiding school of thought was that the two largest contributions to the TMD waveform were from IEP (driven by ICP) and ABP through vasculature in the inner and outer ear, but this result shows that ICP and respiration are the two largest contributors to the TMD waveform. This particular result is discussed in

detail in section 7.3, but first the general results are discussed.

7.2 Contribution of ICP via IEP

As outlined above IEP, driven by ICP, forms 42.4% of the model TMD signal; this is slightly less than was anticipated when this research commenced. However, this may be related to the unexpected contribution from respiratory waves in this sample data which may not be a normal occurrence. Regardless, ICP via IEP is clearly an integral part of the TMD waveform in this data.

The IEP component of the TMD model represents the fluid interaction, and communication of pressure, between the ICP and the IEP via the CA; it is then assumed a linear relationship between IEP and its contribution to TMD. The main features accounted for in the IEP model include a long thin fluid-filled tube, lined with linear elastic tissue, representing the CA and the tissue which lines it; a compliant fluid-filled chamber, representing the main inner ear chambers (the cochlear and the labyrinths); and a mechanical valve arm, representing a structure connected to the RWM which forms an interface between the CA and the main fluid-filled chamber of the inner ear.

The key objective of including the IEP component of the model was to attempt to replicate nonlinear effects expected to occur during fluid pressure communication between ICP and IEP. The importance of these nonlinear effects is indicated by the improvement in fit obtained when moving from cases where the nonlinear effects were not included to those where they were. The parameters related to the nonlinear effects in the IEP model are β (coefficient for the lining of the CA), and η_1 and η_2 (coefficients for the properties of the valve arm).

Many cases involving the IEP component of the model were considered: TMDinit3 to 8, TMDwVentP5 and 6, IEP3 to 7, NoPathICP3 to 7, and Global, but results from the NoPathICP and Global cases provide the most insight into the roles

of these nonlinear effects. The introduction of the nonlinear effects between the optimisation of parameter estimation for each case, provided little or no significant improvement in fit in all cases. This result shows that for the data analysed including the nonlinear effects in the IEP component of the model provided no significant benefit, thus indicating that these nonlinear effects were not exhibited in the communication between ICP and IEP.

The lack of significance of the nonlinear effects is contrary to what was anticipated at the commencement of this research, and thus the causes for these unexpected results were investigated. The conclusions drawn from the investigation of each nonlinear effect are outlined in the following paragraphs.

The introduction into the optimisation process for parameter estimation related to the nonlinear effect produced by the tissue lining the CA, β, provided very little improvement in fit for all cases. This can be partially explained by examining the nature of the nonlinear effect and comparing it to other linear effects already exhibited in the model. The compliances of the tissue lining the CA adds a nonlinear damping and phase shift to the IEP waveform, however, there are several other aspects of the IEP component of the model which also provide damping and phase shift to the system. Thus unless an accurate fit to the TMD data can only be achieved using the nonlinear damping generated by the CA tissue component of the IEP model - opposed to the linear damping effects - then the nonlinear effects of the tissue lining the CA are not a significant component of the IEP model. So the results in this work suggest that, for the patient data examined here, the compliant tissue lining the CA is either not present or its nonlinear effects are negligible compared to those produced by the linear aspects of the IEP model and are not required to obtain an accurate fit to the data.

When allowed to vary in the optimisation of parameter estimation process the nonlinear effects within the RWM valve component of the IEP model, related to parameters η_1 and η_2, provided very little improvement in fit. Since the effects of the

valve arm within the IEP component of the model are not similar to those produced by any of the linear aspects of the model it implies that the nonlinear aspects provided by the valve arm are not required to effectively model the experimental TMD sample used in this work.

This result would lead to the conclusion that the communication route between ICP and IEP does not have nonlinear effects, however, investigation of the cause of this result identified several key pieces of information regarding the data sample used. The importance of this information had not being clear before the modelling process had been conducted, but it is likely that these factors affected the behaviour of the underlying physical system being modelled. The two key pieces of information were that the patient from which the sample data was taken had abnormally low middle ear pressure (MEP), and abnormally high baseline ICP (the mean pressure around which dynamic pressure changes occur). When considered in light of this additional information it is questionable whether the conclusion that communication routes between ICP and IEP are linear in nature can be extended beyond this data sample; this is because both MEP and baseline ICP affect the RWM valve system and might cause it to enter a state where nonlinear characteristics are not exhibited. A brief explanation of how these effects might impact on the results presented here now follows.

The RWM valve model assumes that the difference between IEP and MEP is sufficiently small for the RWM to be held at a tension where is can move with the dynamic changes in IEP, thus also allowing the RWM valve to open and close with the dynamic changes in IEP. It is acceptable to assume that if baseline ICP is high then baseline IEP will be a similarly high level, as it is believed that baseline pressure is directly transmitted from ICP to IEP. Assuming normal levels of MEP, the raised IEP may cause the typical difference between IEP and MEP to be sufficiently high for the tension in the RWM to hold the RWM valve in an open position throughout the entire cycle of dynamic changes in ICP and IEP. Similarly, assuming normal levels of baseline ICP and hence normal levels of baseline IEP,

if the MEP is sufficiently low the difference between IEP and MEP may again be sufficiently high to hold the RWM valve open throughout the dynamic changes in ICP and IEP. Because, for the data analysed in this work, the patient had both raised baseline ICP (and hence raised baseline IEP) and abnormally low MEP the likelihood of the RWM valve being held open by the pressure difference across the RWM is increased. Thus, although nonlinear valve effects were not required to obtain a reasonable fit to the sample data used in this work, nonlinear effects may be required to suitably model other data samples with the physical system in a different state (i.e. different values of baseline ICP, baseline IEP and MEP). In the model presented here the RWM tension, and the angle at which the tension acts, is assumed to remain constant over the period being modelled, so a possible extension to the RWM valve model might have the tension of the RWM and the angle at which it acts depend on IEP and the difference between baseline IEP and MEP.

7.3 Contribution of Respiration

The large proportion of TMD which comes from the ventilator-driven airway pressure and the associated body movement artefact means that, for this sample, the contribution to TMD from respiration forms approximately 37.5% of the model TMD waveform. The fact that respiration primarily acts on the TMD waveform through the ventilator-driven movement artefact, and an unknown mechanism directly proportional to ventilator-driven airway pressure, is of particular interest; a discussion of this now follows.

There are two likely reasons for respiration to act on TMD through both of these model components. The first is that the pressures imposed on an artificially ventilated patient are sufficient for the airway pressure to act on the TMD through the middle ear; or the second is that the model component attempting to repre-

sent ventilator-driven body movement (VentM) does not account sufficiently for the complexities of the physical system and cannot produce a reasonable fit on its own. It is unlikely that respiration is acting through the middle ear in this patient for two reasons. Firstly, in a normal individual the ME is only in direct communication with the airways - via the Eustachian tube - when the patient swallows or a sudden increase in airway pressure occurs - such as sneezing. Secondly, this patient has an abnormally low MEP which is indicatives that the Eustachian tube, which connects the middle ear to the airways, is closed and has remained closed for a prolonged period (hours). Since the middle ear, via the Eustachian tube, was considered the most likely potential route of direct communication between TMD and ventilation driven airway pressure, evidence on this route being closed indicates that such direct communication does not exist. Thus the inclusion of both respiration driven model components indicates that not all significant aspects of the respiration driven body movement are accounted for by the VentM model component. The respiration driven body movement is now discussed in an attempt to establish where effective improvements in the model component might be achieved.

The respiration driven body movement artefact is modelled based on a series of relationships and simple assumptions. It is known that the relationship between lung volume and artificially imposed airway pressure can modelled with reasonable accuracy by an equation of the following form.

$$P_{vent} = F(V_{lung}) + \tau_v \dot{V}_{lung} \tag{7.1}$$

The relationship between lung volume and chest wall displacement has been shown to be linear, and thus in this work it is assumed that body movement related to respiration is also linearly related to lung volume. The last stage of the model assumes that body movement caused by respiration affects TMD through a linear mechanism. For the model considered in this work it was assumed that the function of lung volume was equal to lung volume with a coefficient (i.e. $F(V_{lung}) = C_0 V_{lung}$) and that the function of lung volume to body movement was directly proportional

(i.e. $V_{lung} = C_1 M_{vent}$); with the two coefficients, C_0 and C_1 being absorbed into the existing parameters a_3 and τ_v respectively. Thus the equation for the ventilator-driven movement artefact (M_{vent}) is

$$P_{vent} = M_{vent} + \tau_v \dot{M}_{vent} \tag{7.2}$$

The detailed formulation of the model for respiratory-driven body movement artefact is contained in section 2.4 of chapter 2. This model has a number of shortcomings. The first aspect of the model which could be improved is the choice function of lung volume, $F(V_{lung})$, in the equation defining the relationship between lung volume and airway pressure; as alternative functions might more accurately model the relationship. Another significant shortcoming relates to the assumption that the respiration driven body movement affects the TMD waveform in a linear manner; this model is used because there is no data relating to such a problem with TMD before. The final shortcoming recognised in this work is connected to the relationship between chest displacement and body movement. It is clear that the relationship between lung volume and chest displacement is linear[29], however, it is not clear that the relationship between chest displacement and movement artefact in the TMD is linear.

It must be noted that despite the shortcomings in the respiration driven body movement artefact model the inclusion of both of the ventilator related model components enables the TMD model to obtain a very accurate fit.

7.4 Contribution of ABP

The proportion of the model TMD waveform generated by ABP is 20.1%. At first inspection this seems a reasonable result and agrees with the theory that ABP contributes to TMD. However, care must be taken when examining this result because the contribution from ABP is inverted relative to the other components. This implies that an increase in ABP has the opposite effect on TMD measurements to

that of an increase in ICP (or another component). Though this is possible if either the dominant mechanism through which ABP contributes to TMD measurements inverts the ABP pressure waveform or the other sources of TMD are inverted relative to the contribution from ABP by some other mechanism; however, this result may be indicative that there are aspects in the physical system not accounted for in the model. One such aspect which has been identified through the analysis of the data is that ABP is sampled from the radial artery, which is located in the forearm, and this might mean that there may be a slight delay between ABP affecting the head (and driving ICP) and it being recorded by the transducer located in the forearm (despite ABP being recorded simultaneously with the other data streams). It was originally thought that this delay was not significant, but the results from this work indicate that this may not be the case.

If the delay introduced by measuring ABP at the radial artery is shown to be negligible then the results of the modelling are of particular interest. This is because it provides insight into the mechanics of how ABP acts on TMD, specifically, evidence that ABP affects TMD inversely to ICP. Because it is unclear if the delay is negligible the implications of such a result are summarised in short here. One possible mechanism by which ABP might act on TMD inversely to ICP is if the ossicles invert the displacement caused by IEP (driven by ICP): i.e. an increase in IEP would cause the TM to move medially (inward) decreasing the TMD reading, while vasculature in the external ear canal might expand as pressure and volume increased within them. Thus if the TM were stationary, and IEP and ABP acted by this mechanism, an increase in ABP would appear to cause the TMD measurement to respond as if the IEP had decreased (and the TM had moved laterally).

Thus, if the results relating to ABP are not due to a delay introduced through the sampling method then more detailed study of the low-frequency properties of the ossicles should be considered, in order to model and investigate how passive TMD measurements are driven by IEP.

7.5 Future work

The material presented in this work highlights areas which require further research to obtain additional insight. This section contains a brief discussion of how the work presented in this work might be extended and new research to be considered in light of the results presented.

It is clear that within the IEP component of the TMD model there are many aspects which affect the transmission of the ICP waveform into the TMD waveform; many of these aspects cause similar effects in the output waveform even if the physical mechanisms by which they occur are different. For this reason it may suitable in future work to investigate removing unnecessary components which may duplicate the effects of other aspects of the model. Considering such limits of the current model may be beneficial particularly as they may highlight the importance either of the aspects remaining or of those that have been removed. There are many such limits, but one of particular interest is the limit where the CA is considered to be fully open and ICP is in direct communication with the RWM valve at the interface with the inner ear. Such a limit of the model would highlight the nonlinear effects of the valve mechanic within the IEP component of the model and provide insight into the relevance of its effects on the model.

Specifically, the limit assumes that the CA is fully open and there is no compliant tissue lining it, thus $\alpha \to 0$ and $\beta \to 0$. There is no need to resolve the N-S equations governing the fluid flow in the CA in this limit; instead it is taken that $\tilde{P}_{ca} = \tilde{P}_{icp}$, thus the IEP system of PDE's, (3.2) - (3.5), simplifies to the following ODE.

$$\frac{\partial \tilde{P}_{cc}}{\partial \tilde{t}} = \gamma_2 \tilde{H}^{5/2}(\tilde{P}_{icp} - \tilde{P}_{cc}) \tag{7.3}$$

where

$$\tilde{H} = \max\left\{0\ ,\ 1 + \eta_1(\tilde{P}_{icp} - \tilde{P}_{cc}) + \sqrt{1 - \eta_2(\tilde{P}_{icp} - \tilde{P}_{cc})^2}\right\} \tag{7.4}$$

This ODE preserves the main nonlinear "valve" mechanism affecting propagation of ICP waves into the inner ear and preserves the damping and phase-shift properties introduced through the compliant inner ear aspect of the IEP model component. Further analysis of this limit would likely provide useful insight in the characteristics of ICP to TMD waveform propagation properties.

Some other extensions to the IEP component of the model which should be considered are extending the RWM valve aspect to vary directly with baseline IEP and MEP, thus enabling the effect of the valve to be varied according to another mechanism; although it should be noted that this may not prove to be necessary if the model is applied to a sufficient number of data sets.

Investigation of the respiration component of the TMD waveform should be continued, this should first take the form of attempting to remove the respiration movement artefact by refining the data acquisition process and then if this fails the extending the respiration driven components of the model should be considered. Extending the respiration related movement artefact component is a sensible action to be taken as it may be possible to improve the level of fit achieved by the model without significantly increasing the complexity of the model component. There are two key aspects of the respiration driven components of the model where extension would be possible. Firstly, the relationship between the airway pressure and lung volume; currently only a simple model is used for this which assumes a linear static-pressure volume relationship which could easily be substituted for a more accurate relationship. Secondly, the relationship between respiration driven body movement and the TMD measurement process has been assumed linear; little data was available when the basis of the model for this mechanic was formed, thus appropriate investigation may lead to an effective model being formed.

The results presented in this work relating to ABP should be investigated in any future work. Firstly the possible delay introduced by measuring ABP in the radial artery must be investigated to establish the nature of the results presented here.

If any delay introduced to ABP through the data acquisition process is found to be significant then resolution is straightforward; the delay introduced to the ABP data can be approximated through comparison with the direct ICP data and then removed from the ABP data sample before being used in the modelling process. If any delay introduced through the data acquisition process is found to be insignificant then investigation of the mechanisms by which ABP affects TMD should be considered. Particular attention should be given to the possible role of the ossicles inverting the TMD waveform relative to IEP, as they may provide greater insight than previously thought on how TMD measurements are driven by, and may be indicative of, ICP waveforms.

The final and most important point to note is that all the work presented in this thesis is conducted on one data set, sampled from one ear of one patient; this is due to limitations on time and the availability of data. It is not possible to establish from analysis of this single data set whether the conclusions drawn can be extended to the broader population. Particularly with regard to the parameter values used to obtain best fit to the patient's data, it is impossible to establish where within a spread across the general population these parameter values lie. For this reason the main focus of any future work should be to test the model outlined in this work, and variations of it as outlined above, on multiple data samples from a spectrum of the population. This would likely provide the greater insight than any work conducted on a limited source of data.

Glossary

ABP arterial blood pressure; also used as the label for the arterial blood pressure component of the complete TMD model. 19, 44, 48–51, 61, 63–66, 70–73, 76, 100, 101, 103–105, 107, 115, 125, 126, 136, 137, 143, 144, 146, 147

CA cochlear aqueduct; a tubular hollow that connects the inside of the skull to the inner ear. 6–10, 14, 16, 18–33, 35–44, 47, 49, 50, 52–54, 57, 64, 65, 90, 91, 103, 105, 115, 126, 135–139, 145, 149

CC cochlea; one of the chambers within the inner ear (referred to as the cochlea chamber (CC) in this work). 6–8, 21, 22, 32, 33, 91

compliance compliance is defined to be the rate of change of volume (ΔV) per unit change in pressure (ΔP). 11, 12, 17, 18, 30, 31, 34, 53, 54, 90, 91, 105, 139

Crank-Nicolson Crank-Nicolson; an implicit FD method for numerically approximating the solutions to differential equations. 56–58, 60

CSF cerebral spinal fluid. 2, 6–9, 11, 13, 24

FD finite difference methods; a family of methods used for numerically approximating the solution to differential equations. 56–60, 148

ICP intracranial pressure; the pressure of the fluid within the cranium (brain pressure). 2–4, 8–14, 16–19, 21, 22, 26–28, 30–32, 35, 43, 44, 46–53, 55, 57,

61–67, 70–73, 76, 90, 91, 100–104, 115, 116, 125, 126, 135–141, 144–147, 149

IEP inner ear pressure; the fluid pressure within the inner-most compartment of the ear. 4, 8, 10, 11, 13–15, 18, 22, 24, 31, 43, 44, 48–51, 53, 55, 57, 60, 61, 90, 92, 96, 103, 104, 107, 108, 111, 114–116, 126, 134–141, 144–147

MatLab numerical computing environment and programming language developed by MathWorks. 55, 68, 81–83, 86

NS Navier-Stokes equations; a set of equations used in fluid dynamics. 24–27, 29, 30

ossicle the bones which communicate sound waves into the inner ear, from the tympanic membrane to the OWM. 5, 6, 13, 18–21, 32, 144, 147

OWM oval window membrane; one of two membranes which separates the inner and middle ear (the other is the RWM). 5, 21, 149

patent patent - open ; patency is the degree to which the CA is open and allows fluid pressure communication between ICP and the inner ear. 7–10, 14, 16, 24, 30

Reynolds Reynolds number or reduced Reynolds number; a number which indicates the balance of viscous and inertial forces in non-oscillatory fluid flow. 25–30

RWM round window membrane; one of two membranes which separates the inner and middle ear; the CA exits into the inner ear next to the RWM. 7, 8, 19, 21, 32, 34–39, 41, 47, 52–54, 57, 91, 138–141, 145, 146, 149

TCCS Transcranial and Cerebral Sonography Techniques; a family of techniques used for noninvasively monitoring brain pressure. 4, 19, 150

TMD tympanic membrane displacement; the group of techniques which measure displacement of the tympanic membrane either spontaneously or in response to a tone stimulus. Part of the TCCS family of techniques. 1, 4, 5, 12, 14, 16–22, 32, 43–46, 48–51, 55, 60–67, 72–77, 79–82, 84, 86–88, 90, 93, 99–101, 103–109, 111, 114–116, 125, 126, 133–148

tympanic membrane Commonly known as the ear drum. 5, 6, 13, 14, 19, 149, 150

Womersley Womersley parameter; a number which indicates the balance of viscous and inertial forces in oscillatory fluid flow. 25, 26, 29, 30

Bibliography

[1] D.J. Acheson. *Elementary Fluid Dynamics*. OXFORD UNIVERSITY PRESS, 2003.

[2] D.J. Acheson. *Elementary Fluid Dynamics*, page 248. OXFORD UNIVERSITY PRESS, 2003.

[3] C.J. Avezaat, H.M. Van Eijndhoven, and D.J. Wyper. Cerebrospinal fluid pressure and intracranial volume-pressure relationships. *J. Neurology, Neurosurgery, and Psychiatry*, 42:687–700, 1979.

[4] E. Bachor, S. Byahatti, and C.S. Karmody. New aspect in the histopathology of the cochlear aqueduct in children. *Amer. J. Otology*, 20:612–620, 1999.

[5] B.I.J. Beentjes. The cochlear aqueduct and the pressure of cerebrospinal and endolabyrinthine fluids. *Acta Otolaryngol*, 73:112–120, 1972.

[6] M.C. Biggs. Constrained minimization using recursive quadratic programming. *Towards Global Optimization*, pages 341–349, 1975.

[7] A.A. Birch. Communicated in person or provided by Dr Anthony Birch. Medical Physics, Southampton General Hospital, 2004-2008.

[8] I.G. Bloomfield, I.H. Johnston, and L.E. Bilston. Effects of proteins, blood cells and glucose on the viscosity of cerebrospinal fluid. *Pediatric Neurosurgery*, 28:246–251, 1998.

[9] C.G. Broyden. The convergence of a class of double-rank minimization algorithms. *J. Inst. Math. Appl.*, 6:76–90, 1970.

[10] B. Carlborg. Hydromechanics of the intracranial and labyrinthine fluids - experimental study in cats. In A.Reid R.J. Marchbanks and A.Ernst, editors, *Intracranial and inner ear physiology and pathophysiology*, chapter 2, pages 16–34. Whurr Publishers Ltd, 1998.

[11] B. Carlborg, K.S. Konradsson, A.H. Carlborg, J.C. Farmer, and O. Densert. Pressure transfer between the perilymph and the cerebrospinal fluid compartments in cats. *Amer. J. Otology*, 13(1):41–48, 1992.

[12] B. Carlborg, K.S. Konradsson, and J.C. Farmer. Pressure relation between the labyrinthine and intracranial fluids: experimental study in cats. In A.Ernst & R.J.Marchbanks, editor, *Intracranial and Intralabyrinthine Fluids: Basic Aspect and Clinical Applications.*, pages 63–72. Springer Verlag, 1996.

[13] Y. Censor. Pareto optimality in multi-objective problems. *Appl. Math. Optimiz.*, 4:41–59, 1977.

[14] A.R. Conn, N.I.M. Gould, and P.L Toint. *Trust-Region Methods*. SIAM and MPS, 2000.

[15] N.O. Da Cunha and E. Polak. Constrained minimazation under vector-valued criteria inn finite dimensional spaces. *J. Math. Anal. Appl.*, 19:103–124, 1967.

[16] G. Dantzig. *Linear Programming and Extensions*. Princeton University Press, 1963.

[17] G. Dantzig, A. Orden, and P. Wolfe. Generalized simplex method for minimizing a linear form under linear inequality restraints. *Pacific J. Math.*, 5:183–195, 1955.

[18] H. Davson, K. Welch, and M.B. Segal. *Physiology and Pathophysiology of the Cerebrospinal Fluid*, pages 731–758. Churchill Livingstone, 1986.

[19] R.A. Feijen, J.M. Segenhout, F.W.J. Albers, and H.P. Wit. Cochlear aqueduct flow resistance depends on round window membrane position in guinea pigs. *J. Ass. Res. Otolaryngology*, 5:404–410, 2004.

[20] R. Fletcher. A new approach to variable metric algorithms. *Computer Journal*, 13:317–322, 1970.

[21] R. Fletcher. *Practical methods of optimization*. John Wiley and Sons, 1987.

[22] P.E. Gill, W. Murray, and M.H. Wright. *Practical Optimization*. London Academic Press, 1981.

[23] D. Goldfarb. A family of variable metric updates derived by variational means. *Mathematics of Computing*, 24:23–26, 1970.

[24] Q. Gopen, J.J. Rosowski, and S.N. Merchant. Anatomy of the normal human cochlear aqueduct with functional implication. *Hearing Research*, 107:9–22, 1997.

[25] S.P. Han. A globally convenient method for nonlinear programming. *J. Optimization Theory and Applications*, 22:297, 1977.

[26] W. Hock and K. Schittkowski. A comparative performance evaluation of 27 nonlinear programming codes. *Computing*, 30:335, 1983.

[27] R. Hofman, J.M. Segenhout, F.W.J. Albers, and H.P. Wit. The relationship of the round window membrane to the cochlear aqueduct shown in three-dimensional imaging. *Hearing Research*, 209:19–23, 2005.

[28] M.P. Hughes and R.J. Marchbanks. Characteristics of infrasonic otoacoustic emmissions generated by the cardiovascular system. In A.Reid R.J. Marchbanks and A.Ernst, editors, *Intracranial and inner ear physiology and pathophysiology*, chapter 21, pages 197–206. Whurr Publishers Ltd, 1998.

[29] T. Kondo, T. Uhlig, P. Pemboerton, and P.D. Sly. Laser monitoring of chest wall displacement. *European Respiratory Journal*, 10:1865–69, 1997.

[30] E.W. Lang, K. Paulat, C. Witte, J. Zolondz, and H.M. Mehdorn. Noninvasive intracranial compliance monitoring. *J. Neurosurgery*, 98:214–218, 2003.

[31] J. Lang. Communication routes between intracranial and intralabyrinthine fluid-filled spaces. In A.Ernst & R.J.Marchbanks, editor, *Intracranial and Intralabyrinthine Fluids: Basic Aspect and Clinical Applications.*, pages 45–50. Springer Verlag, 1996.

[32] J.A. Langlois, W. Rutherland-Brown, and K.E. Thomas. Traumatic brain injury in the united states: Emergency department visits, hospitalizations, and deaths, 2004. `http://www.cdc.gov/ncipc/tbi/TBI.htm`.

[33] E.O. Laurens-Thalen, H.P. Wit, J.M. Segenhout, and F.W.J. Albers. Direct measurement flow resistance of cochlear aqueduct in guinea pigs. *Acta Oto-laryngol*, 124:670–674, 2004.

[34] K.W. Lindsay and I. Bone. *Neurology and Neurosurgery Illustrated*, pages 51–52 and 79. Churchill Livingstone, 2004.

[35] F.H. Linthicum. Temporal bone slices provided by Dr Fred Linthicum. House Ear Institute, 2100 W. 3rd Street, Los Angeles, CA 90057. Website `http://www.hei.org/research/scientists/flinthicum.html`, 2005.

[36] R.J. Marchbanks. *A study of tympanic membrane displacement*. PhD thesis, Brunel University, 1980.

[37] R.J. Marchbanks. Measurements of inner ear fluid pressure and clinical applications. In E.L. Luxon, editor, *Textbook of Audiological Medicine: Clinical aspects of hearing and balance.*, pages 289–307. Martin Dunitz Ltd, 2002.

[38] R.J. Marchbanks. Communicated in person or provided by Dr Robert J. Marchbanks. Medical Physics, Southampton General Hospital, 2004-2008.

[39] A. Marmarou, K. Shulman, and J. LaMorgese. Compartmental analysis of compliance and outflow resistance of the cerebrospinal fluid system. *J. Neurosurgery*, 43:523–534, 1975.

[40] R. Mills, M. Szymanski, and E. Abel. Movements of the intact and reconstructed ossicular chain during changes in static pressure. *Acta Otolaryngol*, 124:26–29, 2004.

[41] P.G. Morton. *Critical Care Nursing: A Holistic Approach*, chapter Instructor's Resource CD-ROM. Lippincott Williams and Wilkins, 8th edition, 2004.

[42] J.A. Nelder and R. Mead. A simplex method for function minimization. *Computing J.*, 7:308–313, 1965.

[43] A.J. Phillips and R.J. Marchbanks. Effects of posture and age on tympanic membrane displacement measurements. *Brit. J. Audiology*, 23:279–284, 1989.

[44] M.J.D. Powell. The convergence of variable metric methods for nonlinearly constrained optimization calculations. In *Nonlinear Programming 3*. Academic Press, 1978.

[45] M.J.D. Powell. A fast algorithm for nonlinearly constrained optimization calculations. In *Numerical Analysis*, volume 630. Springer Verlag, 1978.

[46] M.J.D. Powell. *Variable Metric Methods for Constrained Optimization*, pages 288–311. Lecture notes in Mathematics. Springer Verlag, 1983.

[47] A. Reid, R.J. Marchbanks, D.M. Burge, A.M. Martin, D.E. Bateman, J.D. Pickard, and A.P. Brightwell. The relationship between intracranial pressure and tympanic membrane displacement. *Brit. J. Audiology*, 24:123–129, 1990.

[48] P. Reilly. *Head Injury*, chapter Management of intracranial pressure and cerebral perfusion, pages 385–401. Chapman and Hall, 1997.

[49] A.Ernst & R.J.Marchbanks. *Intracranial and Intralabyrinthine Fluids: Basic Aspect and Clinical Applications.* Springer Verlag, 1996.

[50] M. Samuel, D.M. Burge, and R.J. Marchbanks. Tympanic membrane displacement testing in regular assessment of intracranial pressure in eight children with shunted hydrocephalus. *J. Neurosurgery*, 88:983–995, 1998.

[51] Sarosh Kapadia. Private communication. 2005.

[52] E. Schiffer, E. Van Gessel, and Z. Gamulin. Influence of sex on cerebrospinal fluid density in adults. *British Journal of Anaesthesia*, 83:943–944, 1999.

[53] D.F. Shanno. Conditioning of quasi-newton methods for function minimization. *Mathematics of Computing*, 24:647–656, 1970.

[54] G.D. Smith. *Numerical Solutions of Partial Differential Equations: Finite Difference Methods.* Clarendon Press: Oxford, 3rd edition, 1986.

[55] V. Tamburrelli, S. Silvestri, and S. A. Sciuto. Reliable procedure to switch from volume controlled to pressure controlled ventilation assuring tidal volume during anesthesia. In *EMBS*, pages 415–418, 2003.

[56] E. Thalen, H. Wit, and H. Sagenhout. Inner ear pressure changes following square wave intracranial or ear canal pressure manipulation in the same guinea pig. *Eur. Arch. Otolaryngology*, 259:174–179, 2002.

[57] E.O. Thalen, H.P. Wit, J.M. Segenhout, and F.W.J. Albers. Dynamics on inner ear pressure change caused by intracranial pressure manipulation in the guinea pig. *Acta Otolaryngol*, 121:470–476, 2001.

[58] Epidemiology U.S. National Cancer Institute's Surveillance and End Results (SEER) Program Development Team. The meninges. `http://training.seer.cancer.gov/brain/tumors/anatomy/meninges.html`, 2007.

[59] N. Wagner and A. Walsted. Postural-induced changes in intracranial pressure evaluated non-invasivley using the mms-10 tympanic displacement analyser in healthy volunteers. *Acta Otolaryngol Suppl.*, 543:44–47, 2000.

[60] H.P. Witt, R.A. Feijen, and W.J. Albers. Cochlear aqueduct flow resistance is not constant during evoked inner ear pressure change in the guinea pig. *Hearing Research*, 175:190–199, 2003.

[61] J. Wlodyka. Studies on cochlear aqueduct patency. *Acta Otolaryngol*, 87:22–27, 1978.

[62] J.R. Womersley. Method for the calculation of velocity, rate of flow and viscous drag in arteries when the pressure gradient is known. *J. Physiol*, 127:553–563, 1955.

Experimental project documentation from hereon

Project Protocol: Assessment of Correlation between Direct ICP and TMD Measurements.

Date: 12/08/05 Version 2

Background

Currently there are no methods of directly measuring intracranial pressure which are not highly invasive. However, due to the connection between the inner ear and the intracranial region by the cochlear aqueduct, intracranial pressure signals can be obtained using a technique which measures the Tympanic Membrane Displacement (TMD) in the middle ear. The signals measured by the TMD technique show pressure waves which are thought to be related to the respiratory and cardio-vascular systems and are almost certainly of intracranial origin.

This work should increase our understanding of the relationship between intracranial pressure and tympanic membrane displacement and take a further step towards reliable assessment of intracranial pressure non-invasively via the ear.

Aims & Objectives

1. To determine the level of correlation between ICP and TMD measurements.
2. To obtain data for developing and testing mathematical models of fluid dynamics within the cochlear aqueduct.
3. To develop a transfer function relating ICP to TMD and the appropriate inverse function to obtain ICP readings from TMD measurements.
4. To investigate the impact of Cardiovascular and Respiratory signals on TMD analysis compared to direct ICP measurement.
5. To determine which background signals of ICP will be transmitted through the cochlear aqueduct to be read by TMD analysis.
6. To determine how close the relationship between patients with low ICP-TMD correlation are to pathological abnormalities or age dependant loss of patency in the cochlear aqueduct.

Patient Recruitment

Unconscious, ventilated patients whose intracranial pressure is being measured invasively will be recruited, 15 from paediatric and 15 from adult intensive care units. The children are included because previous work indicates that the coupling between intracranial pressure and the tympanic membrane is much clearer in children.

When a suitable patient is admitted, the patient's parent, guardian or nearest relative will be approached. This will initially be done by the consultant in charge of the patient's management. If the relatives are willing to hear more details then a clinical scientist or the consultant in charge will provide full details of the study and leave them with an information sheet for at least one hour before returning to answer any further questions, and ask for assent.

Inclusion Criteria

- Aged between 4 and 18, being treated in the Paediatrics Intensive Care Unit or between 16 and 70, being treated in the Neuroscience Intensive Care Unit (there is some overlap between wards).
- Having their intracranial pressure monitored by means of a direct pressure access device as part of their clinical management.
- On a ventilator as part of their clinical management.

Exclusion Criteria

- Aged over 70. Reduced or no communication between intracranial and inner ear fluids is common in the elderly (i.e. patency of the cochlear aqueduct is thought to be negatively correlated to age)
- Aged under 4. (equipment specification)
- Any middle ear abnormalities, otitis media or excessive ear wax, (they distort TMD measurements).
- Any Physiological conditions that may effect the TMD measurements such as base of skull fracture or leakage of bloody or CSF from the ear.
- Lack of an acoustic reflex threshold at or below 90dB SPL. (unable to acquire measurements of TMD response to a stimulus)
- Non accidental injuries.

Timing

- Measurements are expected to take approximately 1 hour and will be performed at a time that is convenient for the clinical staff, relatives and researcher team. After the measurements the patient's ICP and ventilatory status will be checked daily. If there has been a significant change (Greater than10 mmHg change in ICP or new ventilation protocol) then the measurements will be repeated. Measurements will not be repeated more than once for any patient.

A few words on nomenclature: -

ICP is the abbreviated form for 'Intracranial Pressure' and TMD is 'Tympanic Membrane Displacement'. Tympanic Membrane Displacement (TMD) measurements are the means by which Intracranial Pressure (ICP) may be assessed non-invasively. The 'CCFP (Cerebral and Cochlear Fluid Pressure) Test' is the clinical procedure by which TMD is used to assess ICP.

Measurement Procedure

Total test time: -

	Time (min)
Impedance Audiometry:	
Left Ear	3
Right Ear:	3
Patient position assessment:	2
CCFP Test:	
Left Ear	21
Right Ear:	21
Total	50 mins
(Total for only one ear only	26 mins)

Physiological measurements to be recorded in parallel with TMD:-

Connect physiological data acquisition recording equipment to obtain:

- Direct ICP
- Arterial Blood Pressure
- Airway Pressure
- ET-CO_2 levels

Position:- Nurses will be asked if the patient can be repositioned to enable testing of both ears. If this is not possible then only the ear accessible will be tested.

CSF Drain:- Patients whose ICP is monitored via an intraventricular pressure access device with drainage system will be tested once with the drainage system open and once with the drainage system closed. Time spent with the drain closed is to be kept to a minimum. In the unlikely event that ICP is seen to rise due to closure of the drain then the drain is to be opened and no further measurements attempted with the drain closed.

Test order: The index number of the subject should be registered in a sequential numerical order starting from '1'. Subjects should have their (L) ear tested first and then if possible their (R) ear tested. The following procedure is for (L) ear test.

1 Tympanometry

Apparatus: GSI-33 Middle Ear Analyser (Acoustic Immittance Meter).

1.1.1 Tympanometry: (L) - *with speed of sweep set to default* (50 daPa/s)
1.1.2 Reflex: Ipsilateral @ 1000Hz (L)
1.1.3 Background acoustic Immittance: Select 10s recording of acoustic Immittance to determine if this is varying with respiration (repeat once)

Selection Criteria: Proceed to CCFP measurements section 1.2 if:
a) MEP (middle ear pressure) between +50 daPa and -100 daPa
b) Compliance 0.3 to 1.5 ml

c) Reflex thresholds at 1000Hz ipsilateral is 90 dB or better

2 CCFP Testing

Apparatus: MMS-11 CCFP Analyser (TMD) – Software update to be implemented to enable longer period/continuous pressure measurements.

Settings for acoustic reflex Measurements

IMPORTANT NOTE: - The test parameters are not the default settings -

Remember to check and reset these values throughout the test.

Stimulus duration = 1.0s,
Stimulus switch off = 0.3s,
Interstimulus duration = 4.0s,
Number of records per average = 10 for 100dB SPL, 10 for ART + 20dB,
Artefact rejection = 20 - but increase to 40 (and then 60) if TMD amplitude is large and records are being rejected.

Stimulus intensity to be first at 100dB SPL and then at acoustic reflex threshold (ART) + 20 dB (to a maximum of 110dB SPL)

2.1 Measure and note position of patient.
2.2 Place CCFP Analyser headset across forehead of subject and seal into (L) ear and test seal. Ensure that tubing is not touching the bed, any pillow or other tubing etc.
2.3 Test seal and obtain 'good' fitting before proceeding.
2.4 (L) ear at 100 dB SPL
2.5 Pause if required
2.6 (L) ear at ART +20dB, write down mean ICP measurement as indicated by the direct pressure monitor.
2.7 Repeat measurement - (L) ear at ART +20dB
2.8 Select 'Heartbeat' icon and measure background intra-aural pressure waves.
2.9 Record nominally four minutes of spontaneous TMD, i.e. in 10, 20 second or longer epochs.
2.10 Deselect 'Heartbeat' icon
2.11 Remove CCFP Analyser headset.
2.12 If possible return to step 1.1.1 then repeat for the (R) ear instead of (L).

Analysis

Purpose: To assess intracranial-cochlear fluid communication (via cochlear aqueduct, which may or may not be patent) by post processing and comparing the cross-correlations of direct ICP measurements with TMD measurements. Obtain both the time constant of the intracranial-cochlear communication and an invertible transfer function, or its nonlinear equivalent, which uses ICP values to obtain TMD values and vice versa.

- Compare the cross-correlation of direct ICP and TMD measurements with the cross-correlation of direct ICP with cardiovascular and respiratory measurements.

- Obtain a function that accurately reproduces the observed relationships between ICP and TMD, for individual relationships and if possible collectively.

Stimulus Exposure time

The exact stimulus exposure level that an individual receives is dependent on his/her ipsilateral ART at 1000kz. The following is for the worst possible case.

Calculation of this level of stimulus exposure is according to:-

$$\text{Leq (60 mins)} = 10 \log \frac{1}{T} (t_1 \times 10^{SPL1/10} + t_2 \times 10^{SPL2/10} + t_3 \times 10^{SPL3/10} + ...)$$

Where T = Total time = 3600s for Leq (60 mins)

SPLX = sound pressure level of stimulus

t_x = duration of the stimulus

Worst case

This is for the CCFP test at 100dB SPL and a repeated test at 110dB SPL -- the highest stimulus level is for a subject with ipsilateral ARTs of 90 dB HL and therefore the test intensity is 110 dB SPL. Each test comprises 10 stimuli of 0.3s duration. The resulting stimulus exposure is multiplied by 2 as a safety margin to allow for rejected measurements. .

Stim dB SPL	Exposure t s	$t \times 10^{SPL/10}$
100	$2 \times 10 \times 0.3 = 6$	6×10^{10}
110	$2 \times 2 \times 10 \times 0.3 = 12$	1.200×10^{12}

$$\text{Leq (60 mins) at the ear drum} = 10 \log \frac{1}{3600} (6 \times 10^{10} + 1.200 \times 10^{12})$$

$$= 85.4 \text{ dB SPL}$$

This figure falls well within the Internationally accepted level for noise exposure in industry.

PATIENT/RELATIVES INFORMATION SHEET

Department of Medical Physics & Bioengineering
Mail Point 29
D Level, Centre Block
Southampton General Hospital
Tremona Road
SOUTHAMPTON
Hampshire
SO16 6YD

Tel: 023 8079 6335
General Fax: 023 8079 4117
Email tony.birch@suht.swest.nhs.uk

Study into the relationship between direct measurements of intracranial pressure (ICP) and simultaneous measurements of tympanic membrane displacement (TMD).

(Investigation of a non-surgical method for measuring intracranial pressure)

Date: 01/06/2005 Version 1

Invitation

You are being asked to allow your relative to take part in a research study. Before you decide it is important for you to understand why the research is being done and what it will involve. Please take time to read the following information carefully and discuss it with others if you wish. Ask us if there is anything that is not clear or if you would like more information. Take time to decide whether or not you wish to allow your relative to take part.

Thank you for reading this.

What is the purpose of the study?

The purpose of this study is to obtain measurements of eardrum movement from groups of children and adults. Simultaneous to the eardrum movement measurements we will be recording the pressure within the brain. This information will then be used to aid development of a non-invasive technique for continuous brain pressure monitoring by measuring eardrum movement.

Why has my relative been chosen?

Your relative has been chosen because they are already undergoing continuous brain pressure monitoring as a part of their clinical management.

Do I have to allow my relative to take part?

You are under no obligation to allow your relative to take part, it is up to you to decide whether or not they will take part. If you do decide that they are to take part then you will be given this information sheet to keep and be asked to sign a consent form. If you decide that they are to take part you are still free to withdraw them at any time and without giving a reason. A decision to withdraw at any time, or a decision not to take part, will not affect the standard of care they receive.

What will happen to my relative if I agree for them to take part?

The care your relative receives will be unaffected by taking part in this study. Staff associated with the study will make two visits, each one hour long. During these visits a record will be made of brain pressure, breathing, heart rate, blood pressure and carbon dioxide levels; all of these measurements are already being made as part of their normal clinical care. In addition to these measurements, we will make measurements of eardrum movement and middle ear pressure. These involve placing a small tube with a rubber ear seal into the outer ear. The eardrum is then stimulated using a short burst of sound. After the two visits nothing further is required of the patient, and your relative's care will continue unaffected.

What is the procedure that is being tested?

The only common way of continuously measuring brain pressure is by an invasive surgical procedure. This study is an investigation into the possibility of using non-invasive measurements of eardrum movement to continuously monitor brain pressure through a natural connection between the brain and the ear.

Currently the technique can be used to make single estimates of brain pressure when used regularly over long periods on the same individual. The technique can also be used to "listen" to the movements of the eardrum continuously. This investigation hopes to gain a greater understanding into the connection between the eardrum and the brain pressure so that continuous monitoring of brain pressure can be done without invasive surgery.

What are the side effects of any treatment received when taking part?

It is highly unlikely, but after the tests a conscious patient may experience a maximum of 24 hours of hearing fatigue. Your relative will be unconscious when we take our measurements and this further reduces the risk of the suffering the 24 hours of hearing fatigue.

What are the possible disadvantages and risks of taking part?

There are no significant disadvantages or risks of taking part.

What are the possible benefits of taking part?

There is no intended clinical benefit to the patient from taking part in the trial.

The purpose of this trial is to gather data to help in the treatment of future patients.

Because measurements are being taken of the eardrum, there is a small chance some disorders of the ear, independent of the study, may be noticed. In this case the clinician treating your relative will be informed then they in turn will discuss it with you.

What happens when the research study stops?

The patients clinical management is unaffected by this study. When the study stops it will have no impact on patients.

What if something goes wrong?

If your relative is harmed due to someone's negligence, then there may be grounds for a legal action but you or your relative may have to pay for it. Regardless of this, if you wish to complain, or have any concerns about any aspect of the way you or your relative have been approached or treated during the course of this study, the normal National Health Service complaints mechanisms should be available to you and your relative.

Will my taking part in this study be kept confidential?

All information which is collected about your relative during the course of the research will be kept strictly confidential. Any information about your relative which leaves the hospital will have their name and address removed so that they cannot be recognised from it.

What will happen to the results of the research study?

The results of the study may be published in a peer reviewed paper, alternatively they may be released as part of a PhD Thesis. Although publication is likely, it cannot be guaranteed at this time. There will be no opportunity to inform you which group of the study your relative was in as all data is made anonymous before use.

Who is organising and funding the research?

This project is being jointly funded by the Engineering and Physical Sciences Research Council in collaboration with Marchbanks Measurements Systems Ltd. and Southampton University Hospitals NHS Trust.

The doctors treating your relative are receiving no extra payment for including them in our study.

Who has reviewed the study?

This research project has been approved as valuable and scientifically valid by an independent peer review panel within the hospital.

It has been approved as ethical by Southampton and South West Hampshire local regional ethics committee.

Thank you for taking the time to read this sheet and potentially being a part of this study

Contact for Further Information

Mr Tony Birch
Medical Physics & Bioengineering Department
D-Level, Centre Block
Southampton General Hospital
Tremona Road,
Southampton
SO16 6YD
email: tony.birch@suht.swest.nhs.uk
tel: 023 8079 6335

The patient/relative will be given a copy of the information sheet and a signed consent form to keep.

Patient Identification Number for this trial:

Department of Medical Physics &
Bioengineering
Southampton University Hospitals NHS
Trust
D Level, Centre Block
Southampton General Hospital
Tremona Road
SOUTHAMPTON
Hampshire
SO16 6YD

ASSENT FORM

12/08/2005 Version 1

Title of Project:

Assessment of the correlation between direct measurements of intracranial pressure (ICP) and simultaneous measurements of tympanic membrane displacement (TMD).

Name of Researcher: Tony Birch

Please initial box

I confirm that I have read and understand the information sheet

dated ..... version .....

for the above study and have had the opportunity to ask questions. ☐

I understand that the participation of my relative is voluntary and that I am free to withdraw at any time, without giving any reason, without their medical care or legal rights being affected. ☐

I agree for my relative to take part in the above study. ☐

_____	_____	_____
Name of Patient	Date	Signature
_____	_____	_____
Name of Person taking assent (if different from researcher)	Date	Signature
_____	_____	_____
Researcher	Date	Signature

1 for patient; 1 for researcher; 1 to be kept with hospital notes